

Copyright  
by  
Arjang Gandomkar  
2015

**The Thesis Committee for Arjang Gandomkar  
Certifies that this is the approved version of the following thesis:**

**LEAK-OFF TEST (LOT) MODELS COMBINING WELLBORE AND  
NEAR-WELLBORE MECHANICAL AND THERMAL BEHAVIORS**

**APPROVED BY  
SUPERVISING COMMITTEE:**

**Supervisor:**

---

Kenneth E. Gray

---

Hugh C. Daigle

**LEAK-OFF TEST (LOT) MODELS COMBINING WELLBORE AND  
NEAR-WELLBORE MECHANICAL AND THERMAL BEHAVIORS**

**by**

**Arjang Gandomkar, B.S. P.E.**

**Thesis**

Presented to the Faculty of the Graduate School of

The University of Texas at Austin

in Partial Fulfillment

of the Requirements

for the Degree of

**Master of Science in Engineering**

**The University of Texas at Austin**

**August 2015**

## **Dedication**

To my family

## **Acknowledgements**

I am very grateful for the opportunity to conduct research under Dr. Kenneth E. Gray. I appreciated his efforts, support, and invaluable guidance throughout my research.. His profound and vast knowledge has taught me a lot of priceless lessons.

Special thanks are due to my colleagues and friends in our research group, Taylor Adams, Lucas Barros, Yongcun Feng, Joseph Fu, Chiranth Hegde, Anthony Ho, Xiaorong Li, Cesar Soares, Scott Wallace, Peidong Zhao, and many other friends who are not mentioned for all their technical discussions and moral support.

I am grateful for the financial support provided by British Petroleum, Chevron, ConocoPhillips, Marathon, National Oilwell Varco, Occidental Oil and Gas, and Shell in Wider Windows Joint Industry Program.

I acknowledge the staff of PGE department at The University of Texas at Austin: Frankie Hart, Mary Pettengil, Dr. Ewegen Podnos, and Dr. Kamy Sephernoori for their technical and administrative support.

I would like to thank, John Jones and Fernando Ziegler from Marathon Oil Company for their assistance throughout the research and providing field data.

Finally, I express my sincere appreciation to my beloved family for their endless love and their incredible support through my entire life.

## **Abstract**

### **LEAK-OFF TEST (LOT) MODELS COMBINING WELLBORE AND NEAR-WELLBORE MECHANICAL AND THERMAL BEHAVIORS**

Arjang Gandomkar, M.S.E.

The University of Texas at Austin, 2015

Supervisor: Kenneth E. Gray

Considerable efforts to model leak-off test (LOT) and leak-off behaviors have been carried out in the past. Altun presented a model to estimate leak-off volume by dividing the wellbore system into four sub-systems: mud compression, casing expansion, fluid leakage, and borehole expansion (Altun 2001). The volume response from each sub-system is then combined to represent the total volume pumped during a LOT.

Most existing leak-off models do not account for mechanical behavior of cement and rock formations around the wellbore. While their compressibilities are small, the cement and rock formation volume changes can be significant. In this research, a mechanical expansion model has been developed, based on a linearly elastic, concentric cylinder theory developed by Norris (Norris 2003). The model is an extension of Lamé equations for multi concentric cylinders and assumes the horizontal stresses on the system's boundary are applied equally in all directions, i.e., the horizontal, far-field stresses around the system are isotropic.

The resulting model simulates the compound radial displacements of casing, cement, and formation along the cased hole, based on pressures inside the wellbore and in the far-field stress region. The volume generated from concentric cylinder expansion is then combined with Altun's model to simulate the total volume pumped during a LOT. One use of the model is the estimation of minimum horizontal far field stress. Since the model consists of concentric cylinders, the pressure on the outside boundary can approximate the minimum horizontal far field stress, which in turn is related to overburden pressure. The pressure inside the most inner cylinder is calculated from known mud weight. With an initial estimation for the far field stress and iterative methods, the minimum horizontal stress can be estimated.

The developed models were then applied to field LOT data from Gulf of Mexico. The results show that leak-off volume along the cased hole should be analyzed as a compound expansion of casing, cement, and formation.

## Table of Contents

List of Tables .....	xi
List of Figures .....	xii
Chapter 1: Introduction .....	1
1.1 Description .....	1
1.2 Objective .....	1
1.3 Thesis Organization .....	3
Chapter 2: Literature Review .....	4
2.1 Leak-Off Test (LOT) .....	4
2.2 Factors Affecting Leak-Off Trend .....	10
2.2.1 Wellbore Condition .....	10
2.2.2 Mud Type .....	11
2.2.3 Mud Viscosity .....	12
2.2.4 Temperature Effect .....	13
2.2.4 Pump Rate .....	14
2.2.5 Special Formation's LOT .....	15
2.2.6 Mud Penetration .....	17
2.2.7 Trapped Air or Gas .....	18
2.2.8 Cement Channel .....	19
2.2.8.1 Large Channel .....	19
2.2.8.2 Small Channel .....	20
2.2.8.3 Plugged Channel .....	21
Chapter 3: Altun's LOT Model .....	22
3.1 Inception .....	22
3.1.2 Altun's Model .....	22
3.1.3 Altun's Model Formulation .....	23
3.1.3.1 Mud Compression .....	23
3.1.3.2 Casing Expansion .....	23
3.1.3.3 Borehole Expansion .....	25



3.1.3.4 Fluid Leak .....	26
3.1.3.5 General Solution .....	27
Chapter 4: Wider Windows Leak-Off Test Model .....	30
4.1 Introduction.....	30
4.2 Wider Windows Model.....	32
4.2.1 Norris Solution.....	33
4.2.1 Multi-Cylinder Solution by Norris.....	37
Chapter 5: Mechanical and Thermal Effects on Radial Displacements .....	40
5.1 Case Study .....	40
5.1.1 Case Study I.....	40
5.1.3 Case Study II.....	48
5.2 Thermal Effect on Displacement .....	54
5.3 Thermal Effect on Pressure Profile.....	55
5.4 Analytical Thermal Model.....	56
Chapter 6: Thermal Effect on Fracture Gradient and Initiation.....	60
6.1 Background .....	60
6.2 Objective .....	62
6.3 Model .....	63
Chapter 7: Compressibility .....	68
7.1 Compressibility Effect .....	68
7.1.1 Rock Matrix Compressibility.....	68
7.1.2 Pore Compressibility.....	69
7.1.3 Bulk Compressibility .....	69
7.1.4 Compressibility Formulations.....	70
7.2 Compressibility Outcome .....	71
7.2.1 Volume Change Due to Compressibility .....	72
Chapter 8: Software Development.....	82
8.1 Horizontal Stress Estimation.....	82
8.1.1 Procedures and Assumptions .....	83

8.2 Matlab Software.....	83
8.3 Results.....	87
8.3.1. Model Advantages .....	92
8.2.2 Model Disadvantages.....	94
8.4 PKN Model Formulation .....	95
Chapter 9: Conclusion and Recommendation.....	97
9.1 Wider Windows Model.....	97
9.1.1 Sub-Systems.....	97
9.2 Non-Linearity.....	98
9.3 Fracture Profile .....	98
9.4 Future Work Recommendation.....	98
Nomenclature .....	100
References.....	102

## **List of Tables**

Table 5.1:	Assumed data used for case study I .....	42
Table 5.2:	Data used by Altun for GOM U-2 (Altun, 2001).....	48
Table 5.3:	Assumptions for Altun’s model .....	49
Table 5.4:	Models comparison based on quadratic fit .....	52
Table 6.2:	Wellbore strengthening methods (Salehi and Nygaard, 2011) .....	61
Tables 8.1:	Wellbore data from program sponsor .....	87

## List of Figures

Figure 2.1: Idealized XLOT plot (Modified after Lee, 2004, developed originally in API RP 66 work group) .....	4
Figure 2.2: Schematic LOT records for two classes of FIP. (a) is class 1 and (b) is class 2 (Modified after Edwards et al., 1998) .....	6
Figure 2.3: FIP and FPP comparison (Zoback, 2007, from Fu, 2014) .....	6
Figure 2.4: Typical LOT plot (Postler, 1997).....	8
Figure 2.5: Procedure for reading FCP point on a LOT plot (Modified after van Oort, 2007).....	9
Figure 2.6: XLOT with 2 pumping cycles. (Modified after Edwards, 1998).....	9
Figure 2.7: Effect of wellbore conditions on interpretation of LOT measurement (Naygaard and Salehi, 2011).....	11
Figure 2.8: External and Internal mud cake depending on mud type. A is the case for WBM and B is the case for OBM and SBM.....	12
Figure 2.9: Offshore and onshore mud density profiles with temperature rigs (Rezmer and Cooper, 2000, from Fu, 2014) .....	14
Figure 2.10: Effect of mud pump rate on LOT data (Modified after Postler, 1997, from Fu, 2014) .....	15
Figure 2.11: Non-linear LOT of SMS (Modified after Paknejad 2007, from Fu, 2014) .....	16
Figure 2.12: LOT log-log plot (Modified after Paknejad 2007, from Fu, 2014) ..	16
Figure 2.13: Possible distribution of pore pressure for penetrating mud vs. non-penetrating mud (Modified after Haimson and Fairhurst, 1967).....	17

Figure 2.14: Leak-off test with trapped gas inside the wellbore (Modified after Raaen and Brudy, 2001, from Allerstofer, 2011) .....	18
Figure 2.15: Cement channel classifications (Postler, 1977, from Allerstofer, 2011) .....	19
Figure 2.16: Effect of cement channels (Postler, 1997) .....	20
Figure 3.1: Altun’s sub-systems solution (Modified after Altun, 2001) .....	22
Figure 3.2: Stress acting on casing (Modified after Altun, 2001) .....	24
Figure 3.3: Altun’s model general solution by adding each step (Gray and Fu, 2013) .....	28
Figure 4.1: Wider Windows U-Tube System incorporation near wellbore cement and rock formation to 5-8 wellbore radii (Gray, 2011) .....	31
Figure 4.2: Concentric Cylinder and Interface Numbering Scheme (Norris, 2003) Cylinders Shown Schematically - Thicknesses Not Scaled.....	33
Figure 4.3: Single Cylinder Solution (Norris, 2003), (taken from Norris’ personal website) .....	34
Figure 4.4: Multi-Cylinder System (Norris, 2003).....	38
Figure 5.1: Wellbore schematic used for case study I. It is assumed to be an offshore wellbore. (Modified after Gonzalez et al., 2004). Formations’ Poisson’s ratio values are kept constant and the same in order to minimize its effect on the displacements.....	41
Figure 5.2: Steady state temperature profile of case study I based on Holmes and Swift model developed in MATLAB .....	42
Figure 5.3: Displacement for <i>zone one</i> as shown in Figure 5.1 .....	44
Figure 5.4: Displacement for casing 13 5/8” at <i>zone two</i> .....	45

Figure 5.5: Displacement for 13 5/8" at <i>zone three</i> . After some depth the thermo-mechanical changes seems smaller compared to only mechanical effect since the wellbore is cooling down and shrinking.....	46
Figure 5.6: Displacement for <i>zone four</i> .....	46
Figure 5.7: Displacement for <i>zone four</i> (horizontal stress is 60% of vertical stress).....	47
Figure 5.8: Wellbore temperature profile for GOM U-2 wellbore used in Altun's SPE paper.....	50
Figure 5.9: Wellbore temperature profile for GOM U-2.....	51
Figure 5.10: Volume change for GOM U-2.....	51
Figure 5.11: LOT prediction by Wider Windows and Altun models.....	53
Figure 5.12: Radial change in cement in <i>case study I</i> .....	54
Figure 5.13: Pressure profile for 13 5/8" casing in <i>case study I</i> .....	55
Figure 5.14: Controlled volume used for energy balance (Holmes and Swift, 1970).....	56
Table 6.1: Lost circulation classification and remedies (Ghalambor et al. 2014).....	60
Figure 6.1: Leak of test at different bottom hole temperature (Pepin et. al. 2004).....	63
Figure 6.2: ABAQUS three layer model and formations properties.....	64
Figure 6.3: Result predictions of the block by ABAQUS.....	65
Figure 6.4: Stress distribution around the sub model after cooling the system by 25 degrees. Magnitude of tensile stress has increased around the wellbore compared to Figure 6.3, meaning fracture initiation and propagation are more likely to occur. ....	66

Figure 6.5: Fracture development using XFEM on the sub model analysis .....	66
Figure 7.1: Approach adapting Altun’s model to include cement and formation (Adapted from Atlun, 2001) copied from (Gray, 2013) .....	71
Figure 7.2: Volume calculation including compressibility effect (Gray, 2013)..	72
Figure 7.3: Volume change response to pressure change for 5 times the radius.	74
Figure 7.4: Volume change response to compressibility change for 5 times the radius.....	75
Figure 7.5: Volume change response to height change for 5 times the radius....	75
Figure 7.6: Volume change response to pressure change for 6 times the radius.	76
Figure 7.7: Volume change response to compressibility change for 6 times the radius.....	76
Figure 7.8: Volume change response to height change for 6 times the radius....	77
Figure 7.9: Volume change response to pressure change for 7 times the radius.	77
Figure 7.10: Volume change response to compressibility change for 7 times the radius.....	78
Figure 7.11: Volume change response to height change for 7 times the radius....	78
Figure 7.12: Volume change response to pressure change for 8 times the radius.	79
Figure 7.13: Volume change response to compressibility change for 8 times the radius.....	79
Figure 7.14: Volume change response to height change for 8 times the radius....	80
Figure 7.15: Lateral distance effect on volume gain with varying height for 10-100ft, and constant pressure difference and formation compressibility.....	81
Figure 8.1: Horizontal stress schematic (Adapted from Altun, 2001) .....	82
Figure 8.2: MATLAB GUI startup menu.....	84
Figure 8.3: Wider Windows GUI layout .....	85

Figure 8.4: Wider Windows LOT software menu .....	86
Figure 8.5: LOT example .....	88
Figure 8.6: LOT curve match by Wider Windows and Altun models .....	89
Figure 8.7: Shmin trend based on the Shmin gradient predicted by the software shown in Figure 8.6.....	91
Figure 8.8: Fracture profile calculated based on PKN model .....	92
Figure 8.9: Erroneous FIT data due to trapped air or gas inside the wellbore ....	93
Figure 8.10: Corrected FIT data after subtracting the trapped air or gas from the system .....	94
Figure 8.11: PKN fracture design (modified after Gidley et al., 1989, from Abousleiman et al., 1996) H is the height of the fracture and W stands for width of the fracture. ....	95



## **Chapter 1: Introduction**

This chapter will discuss the description and objective of the thesis. Also, a brief description of each chapter in this thesis is given.

### **1.1 DESCRIPTION**

When an operator decides to drill into a new formation, a mud weight window which is an operating pressure limit must be defined. This can be done by geological data, empirical formula, or the use of nearby wellbore data. These techniques are indirect methods. After indirect method estimation, the operator can alter or confirm the mud weight window using direct method. In direct method the exposed or newly drilled formation will be tested physically. For instance, the operator may choose to perform leak-off test (LOT), extended leak-off test (XLOT), or mini fracturing test.

Whether it is an offshore or onshore wellbore, a leak-off test (LOT) is an industry standard and sometimes a government's requirement to estimate the operating pressure of the wellbore in a newly drilled formation.

### **1.2 OBJECTIVE**

The operating pressure is very important since it constitutes the mud weight window used for drilling the formation. The mud weight window of any wellbore is defined by its pore pressure gradient as minimum pressure and its formation fracture gradient as maximum pressure. If pressure inside the wellbore is below the pore pressure the pressure of the formation will kick into the wellbore causing the mud in the borehole to rise up. In some cases, this pressure is very high that will cause the mud to gush out of the wellbore and causing a wellbore "blow out". Of course, this is why a blow out preventer (BOP) is required by federal law or state law to avoid such catastrophe. On the

other hand, if the wellbore pressure is greater than the formation pressure (fracture gradient), the formation will be fractured, and mud will be lost into the formation. This scenario is known as “lost circulation.” This notorious event has been very costly to operators for decades.

It becomes obvious that it’s very important to interpret leak-off test correctly to avoid costly mistakes. There are different models to help understand leak-off test better. One that is very comprehensive is Altun’s model (Altun, 1999). The model is divided into four sub-systems: mud compression, casing expansion, borehole expansion, and fluid leakage. However, Altun’s model neglects the volumes and compressibilities of the cement sheaths and rock formations outside the casing. Also, none of the current LOT models include thermal effects on any sub-system or material near the wellbore.

Therefore, the main goal of this research in Wider Windows JIP was to incorporate the volumes generated by the displacement of cement sheath and rock formation beyond casing string as well as thermal effect on leak-off test interpretation.

### **1.3 THESIS ORGANIZATION**

Chapter 2 provides the literature review on leak-off test along with its nomenclatures and influencing factors.

Chapter 3 discusses the derivation of sub-systems of Altun's LOT model. The model's shortcomings are also pointed out.

Chapter 4 shows the new approach that was developed in Wider Windows JIP for LOT model enhancement to provide a better leak-off test data interpretation.

Chapter 5 studies the effects of the new sub-systems introduced in chapter 4 based on mechanical and thermal effects using case studies.

Chapter 6 covers the effect of temperature on fracture initiation of a formation and in lost circulation. Due to complex nature of temperature, finite element method has been employed for analysis.

Chapter 7 provides a basic understanding about the effect of compressibility on volume change during a pressure change.

Chapter 8 is a software development based the findings in the previous chapters. It is a MATLAB program that receives volume and pressure data from field data along with rock, wellbore, and mud properties to produce a leak-off test.

Finally, chapter 9 presents the conclusion of the thesis. A few recommendations are also suggested for future work at end of the chapter.

## Chapter 2: Literature Review

This chapter is an overview of some literatures available on leak-off test models. Factors that will affect leak-off test are also discussed in this chapter.

### 2.1 LEAK-OFF TEST (LOT)

One of the advantages of LOT is to establish the minimum horizontal stress of a newly drilled formation. A classic example of LOT trend that has been used in many papers is the idealized XLOT, developed originally in *API RP 66 work group*, shown in Figure 2.1. XLOT stands for extended leak-off test. It is a series of LOT's that are done on a formation for accurate prediction of minimum horizontal stress.

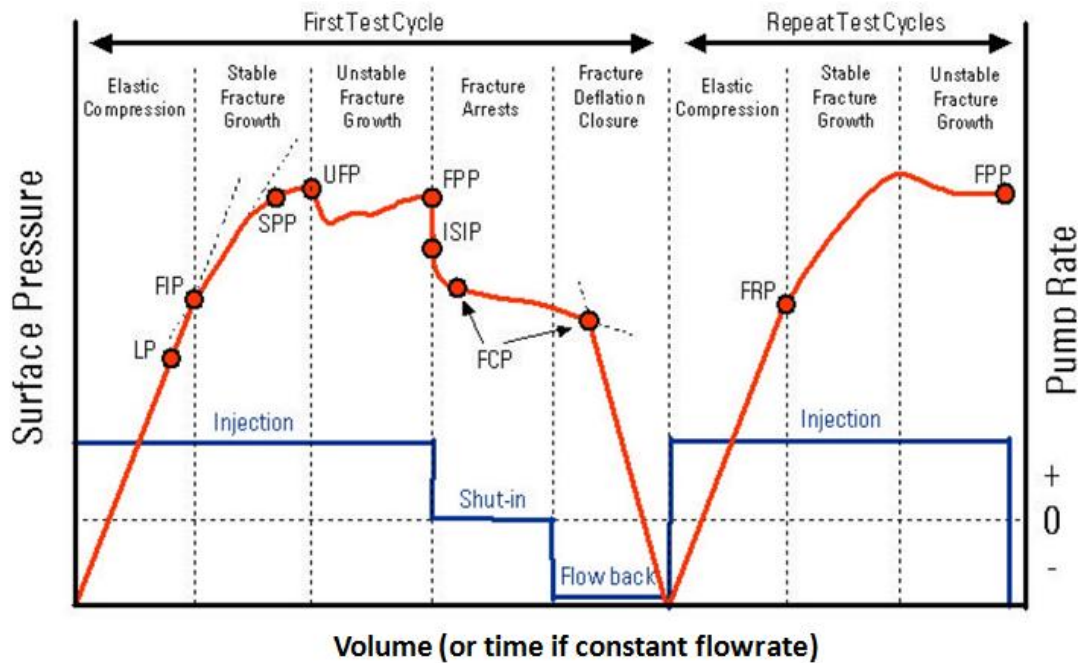


Figure 2.1: Idealized XLOT plot (Modified after Lee, 2004, developed originally in API RP 66 work group)

As shown in Figure 2.1, the first part of the graph, from the origin to FIP, also known as Leak-Off Pressure (LOP), is linear. The line from origin to LP point is called Formation Integrity Test (FIT), and used to measure the pressure rating and integrity of casing shoe. This linearity is due to mud compression inside the wellbore. From LP to fracture initiation pressure (FIP), the formation will develop mini fractures if the formation is intact. If the formation has pre-existing fracture, the fracture will just be reopened. After FIP, the mud will seep into the fractures and cause a pressure buildup as mud pump pressure (surface pressure) increases. This pressure buildup causes the fractures to propagate into the formation. The non-linear trend of this zone is due to effects of the mud leak coefficient as well as the compressibility of the formation as shown in chapter 7. When more mud is pumped, the mud discharge rate varies which cause a non-linear trend (Postler, 1997). After FIP, the compressibility of the system is changed since the formation's compressibility is added to the system. This compressibility change causes the pressure to decline. This is why the slope of the curve decreases after FIP (Addis, 1998).

FIP can be classified into two fracture classes: a) class 1 b) class 2 as shown in Figure 2.2. In class 1, the wellbore wall is intact and fractures are induced from the first time during LOT. Therefore, FIP is almost the same as breakdown pressure (Edwards et al., 1998). In class 2, preexisting fractures are reopened. In this case, FIP is a good estimation of in situ minimum horizontal stress (Edwards et al., 1998). After first phases of XLOT, case 2 occurs. This is why some operators choose to do XLOT for a better accuracy of minimum horizontal estimation.

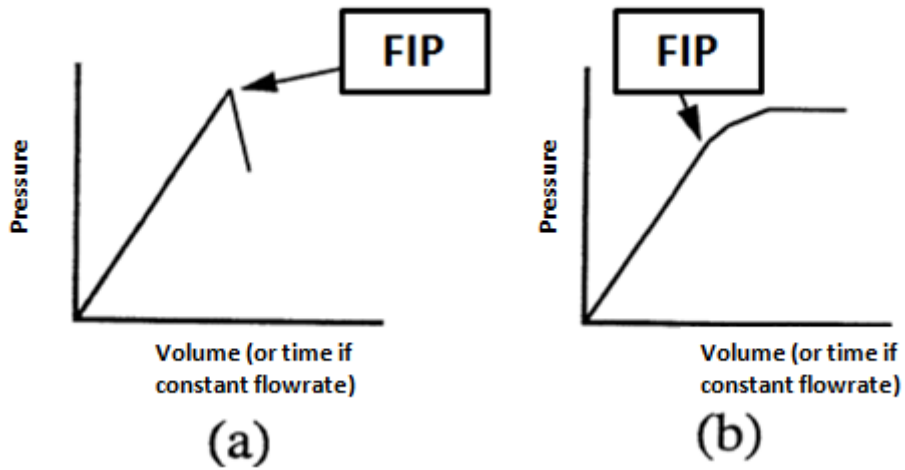


Figure 2.2: Schematic LOT records for two classes of FIP. (a) is class 1 and (b) is class 2 (Modified after Edwards et al., 1998)

FIP should be equal to FPP when the volume of the pressurized system increases due to fracturing (Zoback, 2007) as shown in Figure 2.3.

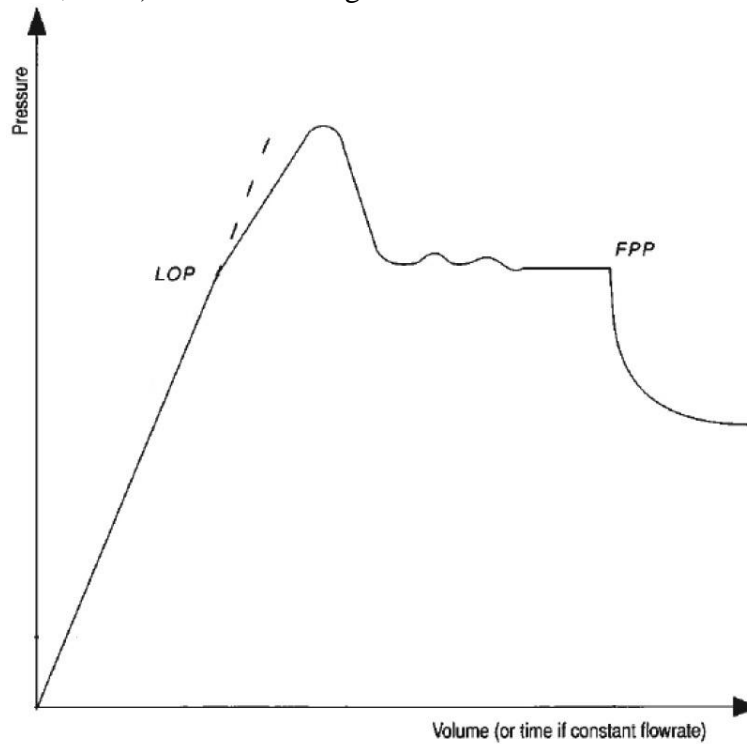


Figure 2.3: FIP and FPP comparison (Zoback, 2007, from Fu, 2014)

Up to stop pump pressure (SPP), the pressure in the fracture is stable, meaning fluid is lost along the length of the fracture (Postler, 1997). After SPP, the fracture becomes unstable since it has passed the confining pressure (hoop stress). The pressure at this point is known as unstable fracture pressure (UFP). At UFP, the wellbore pressure overcomes the hoop stress of the wellbore, and this value is higher than minimum horizontal stress. The horizontal stress is estimated to be between FIP and SPP. Massive loss occurs at UFP due to the fracture being extended away from the wellbore (Alberty, 1999). The extension of the fracture into the formation could be tens to thousands of feet (Van Oort, 2007). If UFP is observed, it is classified as lost circulation event. A cement squeeze job is required to repair the damage.

For better estimation of horizontal stress, the pumps are shut down at SPP, the pump is stopped at this point, and a rapid drop in pressure may be observed because of fluid loss in the open fracture and the loss of pump friction pressure (Postler, 1997). Then the wellbore is bleed off to observe fracture closure known as FCP. After the pump stops, the fracture may still grows (FPP) or instantaneously be shut in (ISIP). This depends on the formation characteristics. When mud pump stops, a drop in pressure occurs in the trend which is caused by the loss of pump friction pressure and the loss of fluids to the fractures (Postler, 1997). If the ISIP is lower than half of the LOP, it is likely that a leak channel exists in the surface equipment, casing, or cement (Postler, 1997). ISIP value depends on the length of the fracture. If the fracture is extended beyond hoop stress, ISIP is a good estimation for minimum horizontal stress (Postler, 1997).

FCP occurs when pressure levels off after shut-in as shown in Figure 2.4. Point D in Figure 2.4 represents the FCP since there pressure is leveling off. However, it is usually not easy to identify the FCP on a LOT. Slope technique can be used to overcome this

issue. There are slope changes before and after FCP point on a LOT plot as shown in Figure 2.5. The intersection of dashed lines A and B in Figure 2.5 represents the FCP (van Oort, 2007).

Fracture reopening pressure (FRP) happens during XLOT's second pumping schedule. Usually, the magnitude of FRP is lower than the first cycle's FIP since the tensile strength of the rock has been greatly reduced due to induced fractures in the first cycle as shown in Figure 2.6 (Edwards, 1998).

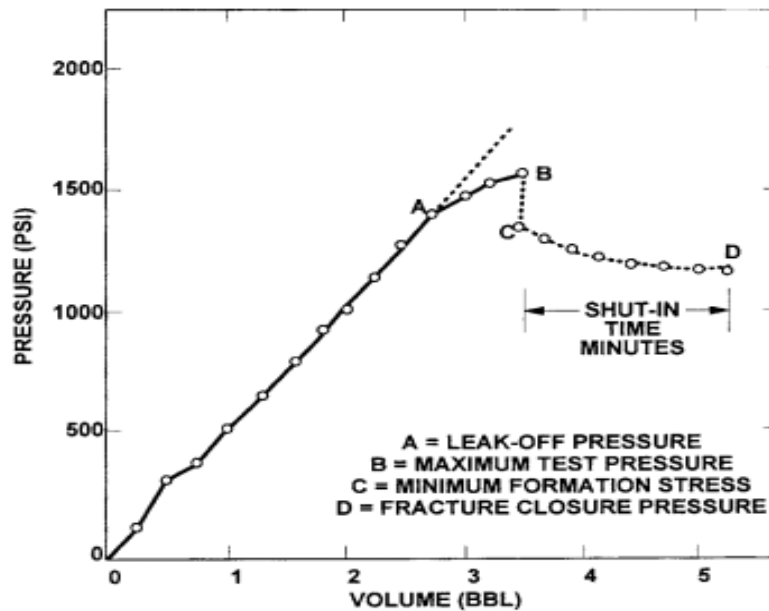


Figure 2.4: Typical LOT plot (Postler, 1997)



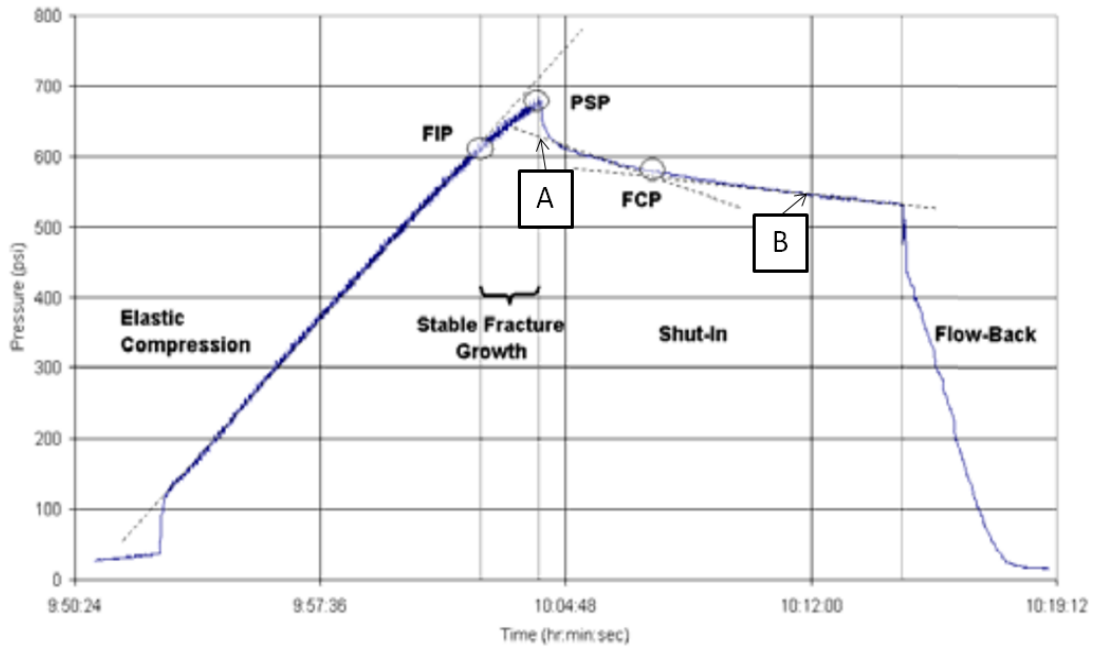


Figure 2.5: Procedure for reading FCP point on a LOT plot (Modified after van Oort, 2007)

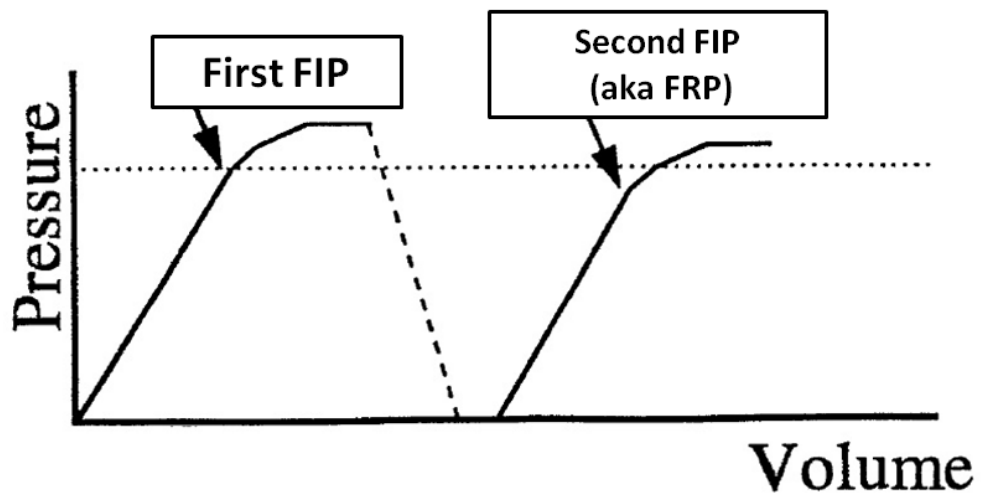


Figure 2.6: XLOT with 2 pumping cycles. (Modified after Edwards, 1998)

## **2.2 FACTORS AFFECTING LEAK-OFF TREND**

Factors such as mud properties, wellbore conditions, and temperature that will influence leak-off test are discussed here.

### **2.2.1 Wellbore Condition**

A wellbore can have four different conditions prior to a LOT or XLOT as shown in Figure 2.7. For example, the borehole can be intact meaning that there are no fractures on the wellbore walls. In this case, the fracture initiation pressure and propagation must overcome not only the hoop stress, but also the tensile strength of the formation. The tensile strength doesn't exist anymore if a fracture appears on the wall of the wellbore, so the propagation must overcome the hoop stress only. However, when a large fracture exists, the hoop and tensile strength have been greatly reduced. In this situation LOT is measuring minimum horizontal stress. The last wellbore condition is when a fracture is propagated and intersects vugs or natural fractures (Nygaard and Salehi, 2011). In this case, LOT or XLOT is measuring pore pressure of the formation.




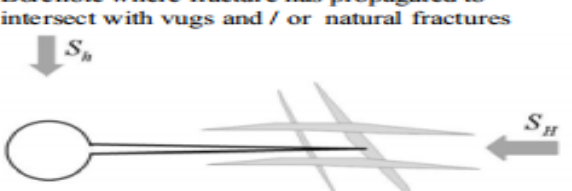
Wellbore Condition	Leak Off Test Measurement
<p>Intact Borehole</p> 	$S_{\theta} - PP + T_0$
<p>Borehole with a very small fracture</p> 	$S_{\theta} - PP$
<p>Borehole with a large propagated fracture in far field zone</p> 	$S_h$
<p>Borehole where fracture has propagated to intersect with vugs and / or natural fractures</p> 	$PP$

Figure 2.7: Effect of wellbore conditions on interpretation of LOT measurement (Naygaard and Salehi, 2011)

### 2.2.2 Mud Type

Type of the mud will influence the trend of the LOT and XLOT especially during propagation stage. Water based mud (WBM) tends to be less compressible compared to oil based mud (OBM) or synthetic based mud (SBM). The value for WBM compressibility is between 2 to 3 x 10<sup>-6</sup> psi<sup>-1</sup>, whereas, OBM's compressibility is usually between 3 to 4 x 10<sup>-6</sup> psi<sup>-1</sup> (Alberty and McLean, 2014). WBM tends to build an external

filter cake on the wellbore wall which isolates the fracture tip as shown in Figure 2.8A. This isolation causes resistant to propagation, therefore, a higher fracture propagation pressure is required. However, the filter cake in OMB and SBM is built internally as shown in Figure 2.8B. There is no external cake due to wettability contrast between the formation and the mud (Aadnoy, 2009). This characteristic of OBM and SBM cannot isolate the tip of the fracture, so there is less pressure required for propagation compared to WBM (Aadnoy, 2009).

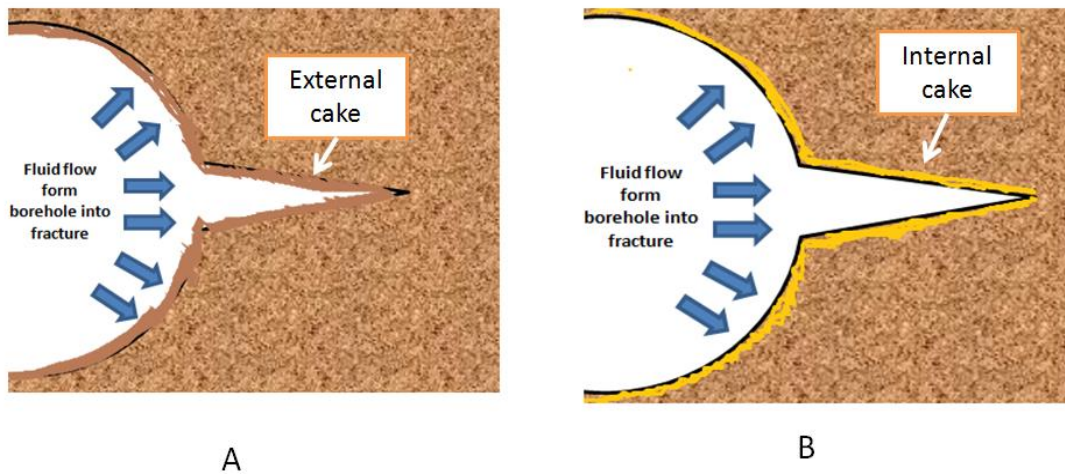


Figure 2.8: External and Internal mud cake depending on mud type. A is the case for WBM and B is the case for OBM and SBM

### 2.2.3 Mud Viscosity

Viscosity is an important factor in fracture propagation (Postler, 1997 and Ishijima and Roegiers, 1983). Most of the mud loss takes place on the fracture walls. If the viscosity of the mud is high, the pressure required for fracture propagation is higher. A higher propagation pressure is expected when pumping using viscous fluid (Ishijima and Roegiers, 1983).

#### **2.2.4 Temperature Effect**

Change in temperature influences the stress around the wellbore. Since the compressibility and thermal coefficients of formations are low, any change in them can result in a large volume change. Since the wellbore and formation temperatures are not the same, the wellbore can experience a wellbore cooling or heating at the same time. Thermal effect has been discussed in chapter 5 and 6 of this thesis. A thermal cool down can bring the stress of the rock down and causes a lower FIP and FPP during a LOT. Previous studies have shown that thermal effects in sandstone ranges from 2.5 psi/°C to 52.2 psi/°C (Van Oort, 2007) and 5 psi/°C to 15 psi/°C in water injection wells in sandstones (Van Oort, 2007).

Temperature can also influence mud properties like viscosity, density, and compressibility. They both increase as the mud cools down and decrease as the mud warms up. The cooling effect makes it possible to have a higher effective mud density at a casing shoe than the recorded mud density at the drill floor. This effect can lead to miscalculation of leak-off gradients if the change in mud density is not recognized (Rezmer and Cooper, 2000). Figure 2.9 shows the mud density profiles corresponding to temperature profiles for both deepwater wells and land rigs.

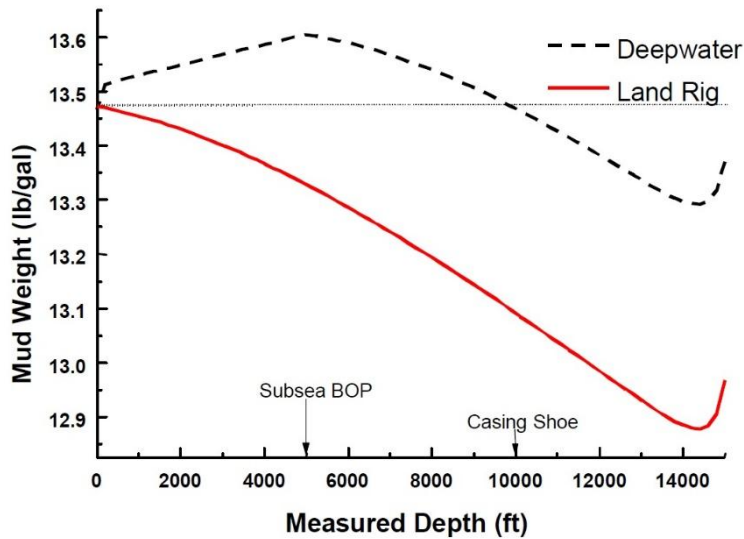


Figure 2.9: Offshore and onshore mud density profiles with temperature rigs (Rezmer and Cooper, 2000, from Fu, 2014)

#### 2.2.4 Pump Rate

Postler and Ishijima suggest that both FIP and FPP increase as the pump rate increases (Postler, 1997 and Ishijima and Roegiers, 1983). As shown in Figure 2.10, the magnitude of FIP and FPP has increased when the pump rate is doubled from 0.75 bbl/min to 1.25 bbl/min. An increase in FIP and FPP doesn't necessary measure the true strength of the formation. Since these data are recorded by gauges on surface, they may acutely measure the friction increase of the pump by an increase in the rate. Therefore, it is suggest that the lowest possible rate be performed for a LOT (Postler, 1997).

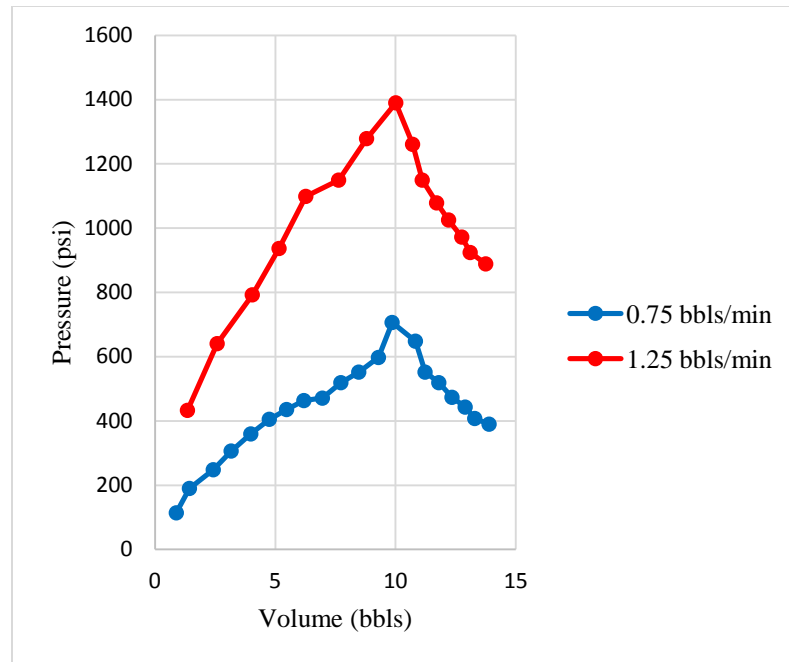


Figure 2.10: Effect of mud pump rate on LOT data (Modified after Postler, 1997, from Fu, 2014)

### 2.2.5 Special Formation's LOT

Most LOT's will start with a linear trend first, then the non-linear part will be developed afterward. However, in some formations the trend will be non-linear from the beginning. For example, shallow marine sediment (SMS) will exhibit such LOT. This non-linear trend makes it harder to interpret the LP and FIPP points on the LOT plot. SMS are deposits below the sea floor to a depth of 3,000 ft (Wojtanowicz, 2001), but some have been found as deep as 3,500 ft (Rezmer-Cooper, 2000). The four identified mechanisms are induced fractures, induced storage, geo-pressured sands in conductor intervals, and transmission of geo-pressure through cement channels (Fu, 2014). To understand SMS LOT's, LOT is transferred into a log-log graph (Paknejad et al, 2007). Figure 2.11 and Figure 2.12 shows an example of using log-log plot done by Paknejad.

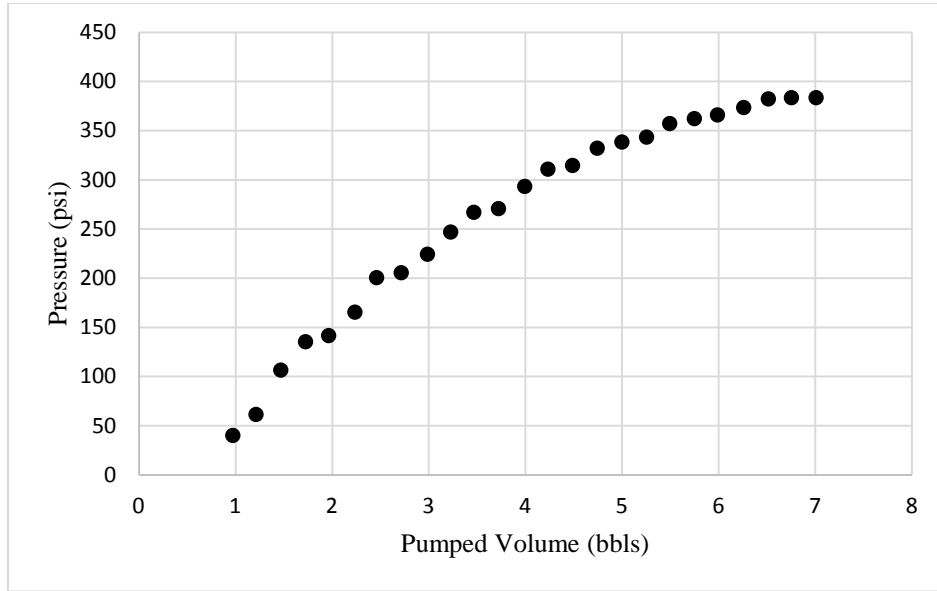


Figure 2.11: Non-linear LOT of SMS (Modified after Paknejad 2007, from Fu, 2014)

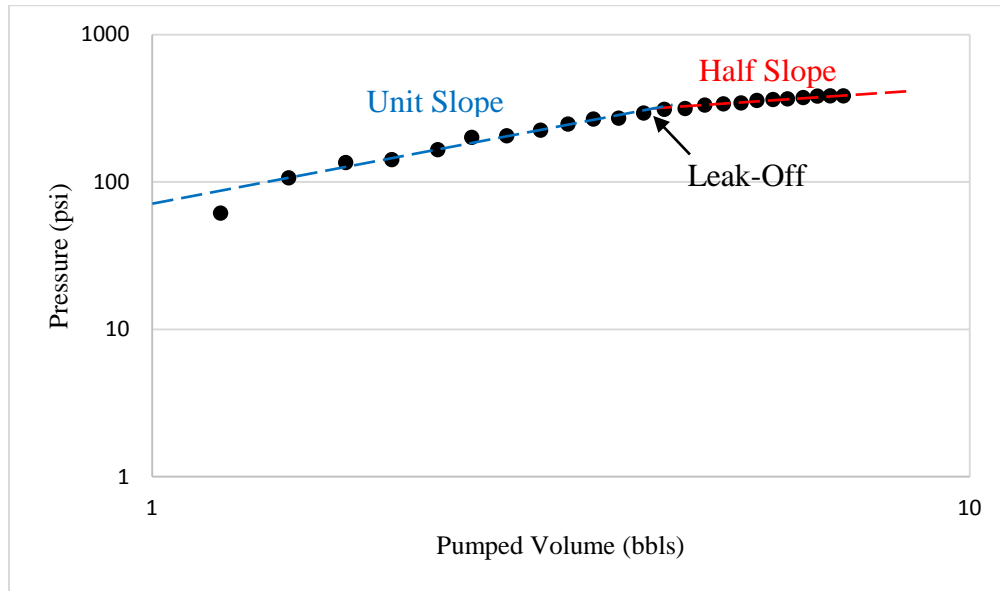


Figure 2.12: LOT log-log plot (Modified after Paknejad 2007, from Fu, 2014)

Using a log-log plot, a clear deflection point can be identified as the slope changes from unit slope to half slope.



## 2.2.6 Mud Penetration

WBM, OBM, and SBM are the most commonly used mud types used in the industry. WBM is classified as non-penetrating fluid, while, OBM and SBM are penetrating mud (Altun, 1999). LOT's with penetrating fluid like WBM will exhibit higher FIP, while OBM and SBM LOT's tend to have lower FIP since the mud can penetrate easier (Postler, 1997). When penetrating fluid is invading into a formation, the pore pressure increases, therefore, the formation strength decreases (Altun, 1999). Figure 2.13 shows the difference in pore fluid distributions for a penetrating fluid and a non-penetrating fluid.

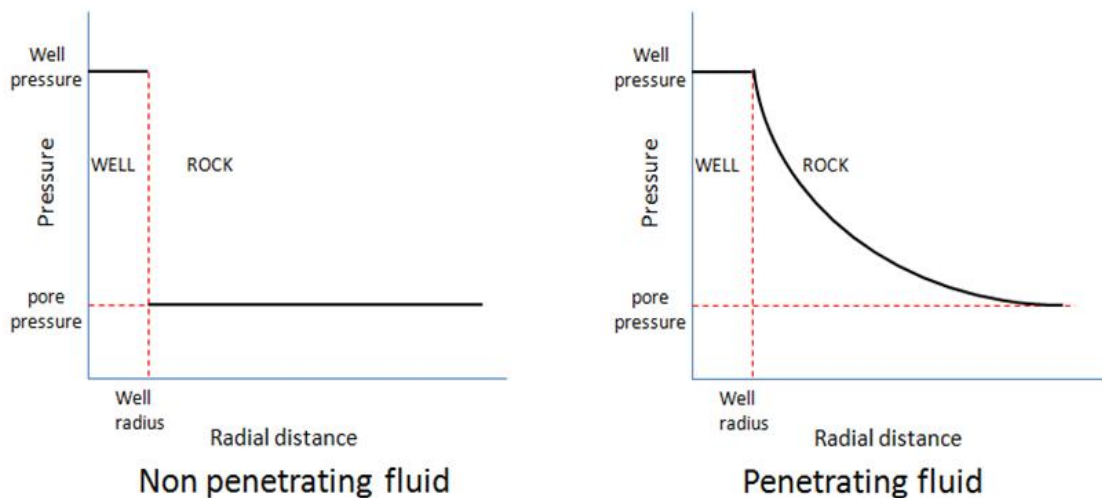


Figure 2.13: Possible distribution of pore pressure for penetrating mud vs. non-penetrating mud (Modified after Haimson and Fairhurst, 1967)

Fluid penetration is also a function of permeability of the formation too. If the permeability is low i.e. in shale formations, the penetration is low. In fact, mud filtrate is barely made on walls of this type formation. Since there is not much penetration allowed, a higher initiation and propagation pressures are required. This is why FIP and FPP are

higher in impermeable formation compared to permeable formations such as unconsolidated sandstone formations.

### 2.2.7 Trapped Air or Gas

A wellbore must be conditioned properly to avoid any cutting or trapped gas in the mud system before a LOT. The objective is to condition the mud inside the wellbore to obtain a uniform density and circulate out any gas in the system prior to any tests (Postler, 1997). If a LOT with trapped gas is performed, a non-linear trend will be introduced in the beginning of the plot as shown in Figure 2.14. This non-linear trend always looks concave up.

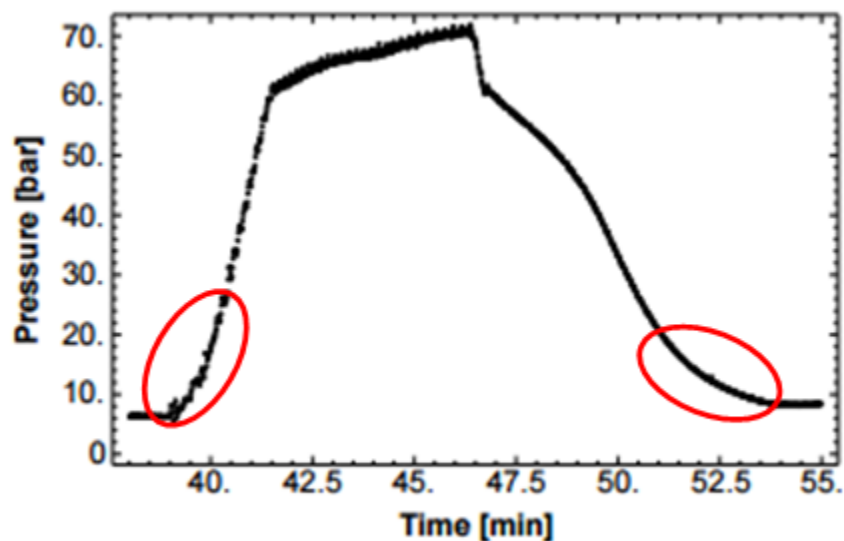


Figure 2.14: Leak-off test with trapped gas inside the wellbore (Modified after Raaen and Brudy, 2001, from Allerstofer, 2011)

The wellbore must be conditioned and equipment must be rigged up properly since the trapped gas can introduce error in the readings. Since the deviation from straight line isn't very significant, trapped gas will not introduce a sudden change in the elasticity of the system (Raaen and Brudy, 2001).

## 2.2.8 Cement Channel

Cement channel happens when the cement is not bonding with either the formation or the wellbore's casing. The channel causes an annulus that mud can escape through during any drilling operation such as LOT. This seepage of mud will affect the trend and curviness of the LOT plot. Cement channels are classified into three groups: large, small, and plugged channels (Postler, 1997) as shown in Figure 2.15.

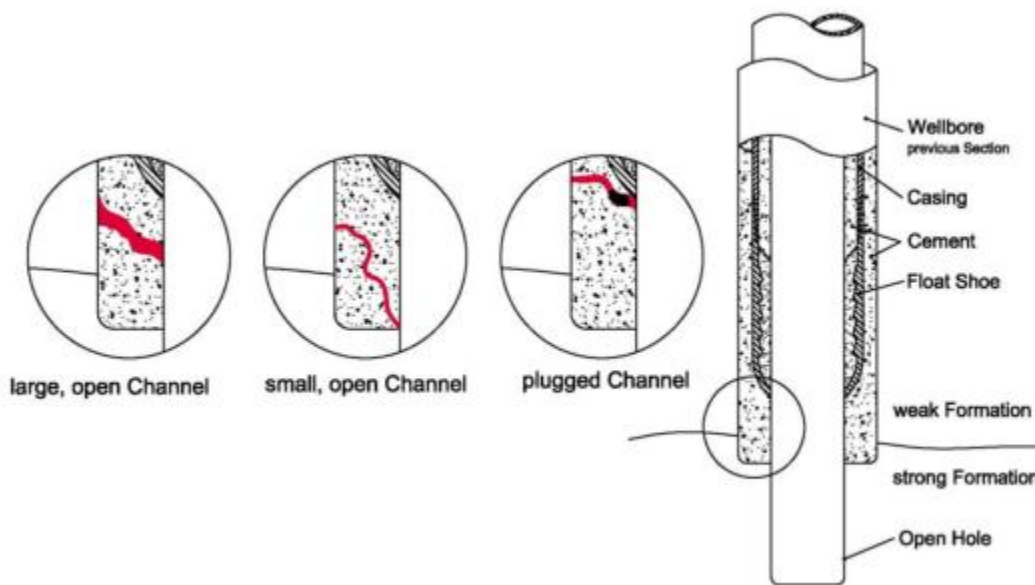


Figure 2.15: Cement channel classifications (Postler, 1977, from Allerstofer, 2011)

### 2.2.8.1 Large Channel

Due to the large size channel the integrity of the wellbore is lowered, and immediate communication with a weaker zone that is not isolated is allowed. Therefore, the measured FIP and FPP will be from the weaker zone as shown in Figure 2.16A. Leak-off occurs at a value lower than the expected value.

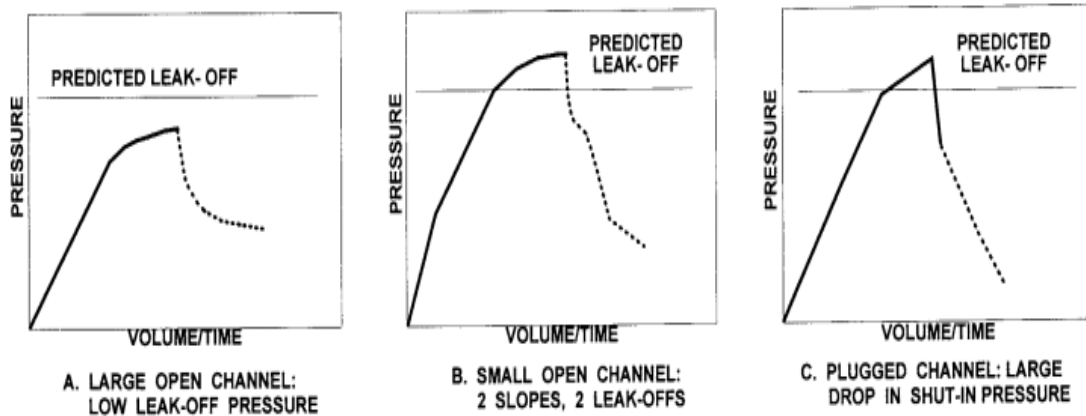


Figure 2.16: Effect of cement channels (Postler, 1997)

If case A happens, the existing channels must be plugged by a cement squeeze job to repair the faulty cement (Postler, 1997).

### 2.2.8.2 Small Channel

There is no immediate communication between the weaker zone and only a small amount of mud seeps into the weaker formation in a small cement channel scenario. Since only a portion of diverted fluid acting against the weaker zone initiates fractures, pressure is still built up in the borehole at a slower rate until the leak off pressure is met (Postler, 1997). As shown in Figure 2.16B, there are two slopes since two fracture zones are initiated: one for the weaker zone and the other one for the stronger formation during the test. Sometimes the slope change can be very hard to observe on the graph. The deflection in slope may not even be from small cement channel. Performing cement bond logging or a cement remedial job will verify if the cement is the cause of the problem.

### ***2.2.8.3 Plugged Channel***

A cement channel can be plugged either by gelled mud or drilling cuttings. However, during a LOT, this plug can be removed or distorted. A direct communication with weaker formation happens when the channel is unplugged. When this happens, the shut-in pressure drops significantly due to a large pressure difference between mud pump pressure and break down pressure as shown in Figure 2.16C. When the test is repeated after the plug is completely removed, either a plot similar to large or small cement channel will happen. Cement channels cause a lower recorded break down pressure during LOT or XLOT, but suspecting that the cement channel is the definite problem in a LOT seems to be the hardest task.

## Chapter 3: Altun's LOT Model

### 3.1 INCEPTION

Altun's model was developed in 1999 to assist in analyzing nonlinear LOT behavior. It has been used for non-linear behavior of field data prediction. In case of a non-linear trend, the model is used to predict the fracture pressure of the formation which constitutes the maximum gradient of mud weight window (Altun, 2001).

#### 3.1.2 Altun's Model

The model consists of four superimposed sub-systems: mud compression, casing expansion, borehole expansion, and fluid leak. Each sub-system's solution is added to the others in order to predict the LOT trend. In other words, the model uses four sub-systems to history match the LOT data. Figure 3.1 shows the schematic of sub-systems of Altun's model.

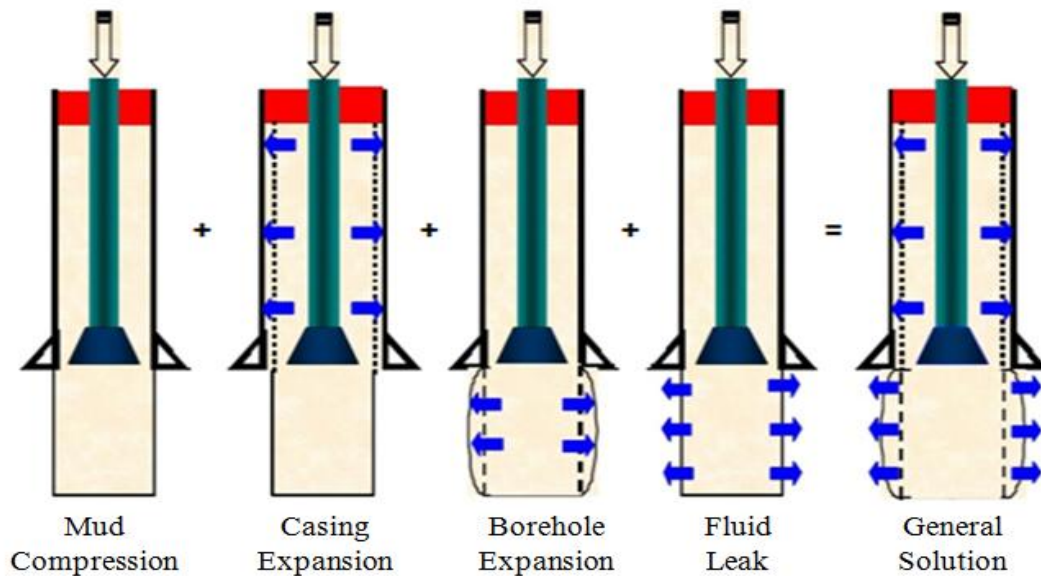


Figure 3.1: Altun's sub-systems solution (Modified after Altun, 2001)

### 3.1.3 Altun's Model Formulation

Altun considered solely the mechanical effect of the sub-systems. In the following section the mathematical formulation of each sub-system is discussed.

#### 3.1.3.1 Mud Compression

This sub-system is assumed to be rigid and fixed throughout the leak-off test. This means that the wellbore is closed or isolated (Altun, 2001). The pressure change inside the wellbore is caused by slow and steady pump rate. With this assumption, only fluid compression can be considered in the wellbore (Altun, 2001). The pumped volume to compress mud is then derived to be:

$$V_m = c_{mud} V_o P \quad (3.1)$$

Where,

$V_m$  = volume required to compress mud

$c_{mud}$  = mud compressibility

$V_o$  = original volume of mud in the system

$P$  = pump pressure

#### 3.1.3.2 Casing Expansion

Altun called this sub-system casing expansion even though he only takes into account the displacement of the casing, not the compressibility of the casing. Therefore, it makes more sense if this sub-system is called casing displacement. Figure 3.2 shows the casing expansion modeled by Altun.  $R_i$  and  $R_o$  are casing's inner and outer radius respectively.  $P_i$  is the wellbore pressure that is pushing against outside pressure  $P_o$ . Two volumes are considered: 1. due to expansion of the casing itself, and 2. Mud compression due to additional volume expansion of the casing in 1 (Altun, 2001).

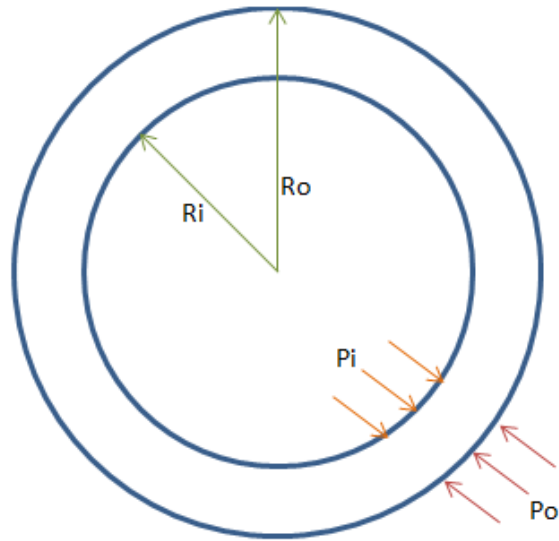


Figure 3.2: Stress acting on casing (Modified after Altun, 2001)

The equation for the volume pumped to expand the casing is:

$$V_{ce} = 2\pi h_{csg} R_i^2 \frac{P}{E_{csg}} \left[ -\frac{(R_o^2 + R_i^2)}{R_o^2 - R_i^2} (1 - \nu^2) - (\nu + \nu^2) \right] \quad (3.2)$$

Where,

$V_{ce}$  = volume pumped to expand casing

$h_{csg}$  = length of the casing string

$R_i$  = inner radius of the casing string

$E_{csg}$  = casing Young's modulus

$P$  = pump pressure

$R_o$  = outer radius of the casing string

$\nu$  = casing Poisson's ratio

and the volume pumped to compress the casing expansion volume can be described as:



$$V_{cce} = 2\pi h_{csg} c_{mud} R_i^2 \frac{P^2}{E_{csg}} \left[ -\frac{(R_o^2 + R_i^2)}{R_o^2 - R_i^2} (1 - \nu^2) - (\nu + \nu^2) \right] \quad (3.3)$$

Where,

$V_{cce}$  = mud volume change due expansion of the casing

$c_{mud}$  = compressibility of drilling mud

### 3.1.3.3 Borehole Expansion

Borehole expansion's volume change is calculated very similar to casing expansion sub-system volume calculation. However, the boundary is not constant since the borehole expands (Altun, 2001). This is because the original or total mud volume,  $V_o$ , inside the wellbore is varying by time. If we assume that the volume increment,  $V_e$ , is the volume increment or the variable volume of the system due to borehole expansion caused by pump pressure. The new total volume of the wellbore is  $V_o + V_e$ .

The volume pumped to expand the borehole is:

$$V_{be} = 2\pi h_{fmn} r_o^2 \left[ \frac{P}{E_{fmn}} + \left( \frac{P}{E_{fmn}} \right)^2 \right] \quad (3.4)$$

And the volume pumped to compress the borehole expansion volume is:

$$V_{cbe} = 2\pi h_{fmn} r_o^2 c_{mud} P \left[ \frac{P}{E_{fmn}} + \left( \frac{P}{E_{fmn}} \right)^2 \right] \quad (3.5)$$

Where,

$V_{be}$  = volume pumped to expand the borehole

$h_{fmn}$  = length of Open-hole

$r_o$  = radius of borehole

$E_{fmm}$  = formation Young's Modulus

$P$  = pump pressure

$V_{cbe}$  = volume pumped to compress the borehole expansion volume

$c_{mud}$  = mud compressibility

### **3.1.3.4 Fluid Leak**

The leak or discharge of mud into the formation is estimated as Poiseuille's flow in Altun's model. The general relationship for the leak volume is given as:

$$V_l = D\Delta Pt \quad (3.6)$$

Where,

$V_l$  = leak volume

$D$  = leak constant

$\Delta P$  = the pressure difference between the tip of the channel and the bottom of the channel

$t$  = time

If the channel shape is assumed to have a rectangular shape, then the leak constant  $D$  becomes:

$$D = \frac{W^2 A_{x-s}}{\mu L} \quad (3.7)$$

Where,

$D$  = leak constant (Length<sup>4</sup> Time/Mass)

$W$  = channel width (Length)

$A_{x-s}$  = cross-sectional area of the fracture (Length<sup>2</sup>)

$\mu$  = mud viscosity (Mass/Length/Time)

$L$  = channel length (Length)

Since the time can be expressed as the ratio of volume over rate, the volume pumped to compress the leak volume becomes:

$$V = DP \frac{V}{q} + c_{mud} V_o P \quad (3.8)$$

$\Delta P$  is replaced by  $P$  only. Equation 3.8 represents the pumped volume if the system allows leak and fluid compression only. If solve for  $V$  Equation 3.8 becomes:

$$V = \frac{c_{mud} V_o P}{1 - \frac{D}{q} P} \quad (3.9)$$

Equation (3.9) can be solved using series expansion since  $\frac{D}{q} P$  is less than one.

$$\frac{1}{1-x} = \sum_0^{\infty} x^n = 1 + x + x^2 + x^3 + \dots \quad (3.10)$$

Using the relationship in Equation 3.10, Equation 3.8 approximates to:

$$V = c_{mud} V_o P + [c_{mud} V_o \left(\frac{D}{q}\right) P^2 + c_{mud} V_o \left(\frac{D}{q}\right)^2 P^3 + \dots] \quad (3.11)$$

### 3.1.3.5 General Solution

Each sub-system is calculated individually and the solution of each system is added in order to produce the general solution. Figure 3.3 summarizes this procedure.

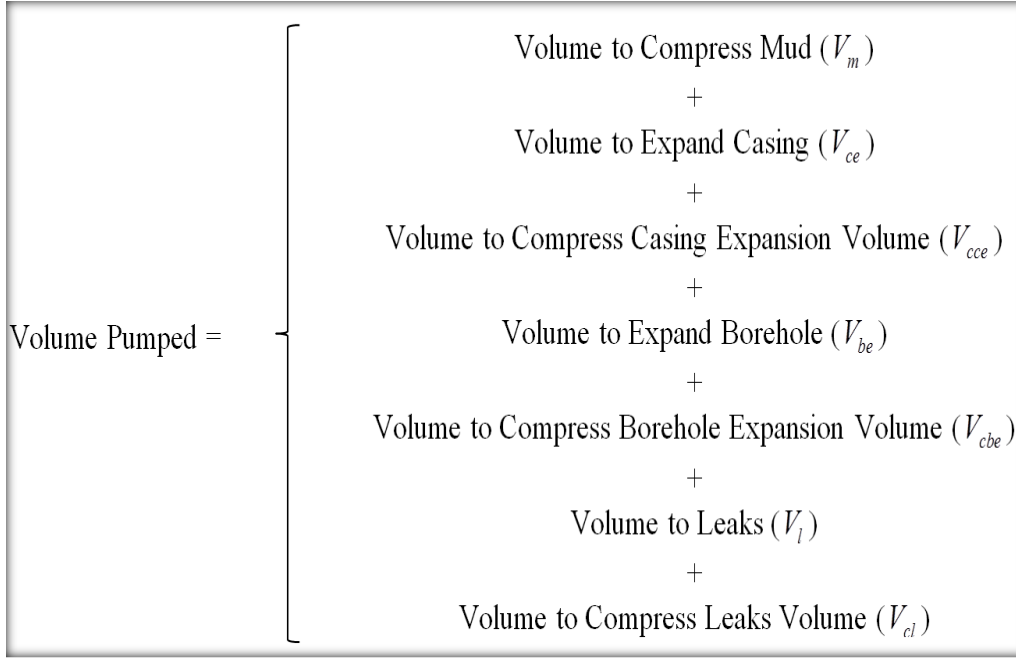


Figure 3.3: Altun's model general solution by adding each step (Gray and Fu, 2013)

and the total system equation is:

$$\begin{aligned}
 V = & c_{mud} V_o P + 2\pi h_{csg} R_i^2 \frac{P}{E} \left[ -\frac{R_o^2 + R_i^2}{R_o^2 - R_i^2} (1 - \nu^2) - (\nu + \nu^2) \right] \\
 & + c_{mud} P \left( \pi h_{csg} R_i^2 \frac{P}{E_{csg}} \left[ \frac{R_o^2 + R_i^2}{R_o^2 - R_i^2} (1 - \nu^2) + (\nu + \nu^2) \right] \right)^2 \\
 & + 2\pi h_{fnn} r_o^2 \frac{P}{E_{fnn}} \left[ 1 + \frac{P}{E_{fnn}} \right] + c_{mud} P \left[ 2\pi h_{fnn} r_o^2 \left( \frac{P}{E_{fnn}} \right) \left( 1 + \frac{P}{E_{fnn}} \right) \right] \\
 & + \left[ c_{mud} V_o \left( \frac{D}{q} \right) P^2 + c_{mud} V_o \left( \frac{D}{q} \right)^2 P^3 + c_{mud} V_o \left( \frac{D}{q} \right)^3 P^4 + \dots \right]
 \end{aligned} \tag{3.12}$$

However, Altun concluded that the following types of volume are negligible after sensitivity analysis: the volume to expand casing expansion volume, volume to expand

borehole, volume to compress borehole expansion volume, and volume to compress leaks volume. Therefore, the total system behavior becomes:

$$V = \frac{V_o(e^{c_{mud}P} - 1)}{1 - \frac{D}{q}P} + 2\pi h_{csg} R_i^2 \frac{P}{E_{csg}} \left[ \frac{R_o^2 + R_i^2}{R_o^2 - R_i^2} (1 - \nu^2) - (\nu + \nu^2) \right] \quad (0.1)$$

## Chapter 4: Wider Windows Leak-Off Test Model

### 4.1 INTRODUCTION

The Wider Windows project, “*Leak-Off Test Models Combining Wellbore and Near-Wellbore Fluid, Mechanical, and Thermal Behavior*”, seeks quantitative, thermo-elastic models for the interpretation of routine leak-off tests. Superposition of drilling fluid; casing-cement-rock, formation sequences, volumes, and associated compressibilities; and down-hole thermal behavior are developed in both analytical and numerical (finite element) models (Gray, 2013). The analyses of field examples are included.

Both modeling approaches incorporate the U-Tube elements illustrated in Figure 4.1 (Gray, 2013). Figure 4.1 shows a vertical cross section of a well, schematically illustrating the drilled open hole and casing, mud, cement, and formation intervals of various rock types, with commonly encountered operational situations noted, for which intermediate casing strings are utilized. In addition to fluid and mechanical behaviors, the thermal behavior of each element or part of the system can result in consequential volume changes of fluid, casing, cement, and formation from thermal expansion/contraction (Gray, 2013).

In Figure 4.1, a horizontal cross section (CS-1 to CS-5) is shown through each casing string, to depict the sequence of concentric mud or cement and previous casing strings. The openhole section is represented in CS-5. The heavy dotted line indicates the variable lateral extent or “boundary” at which pressure and stress changes in the wellbore system will have essentially died out. The stresses at this outer boundary, approximately

5-8 wellbore radii, will essentially equal the minimum horizontal in-situ stress (Gray, 2013).

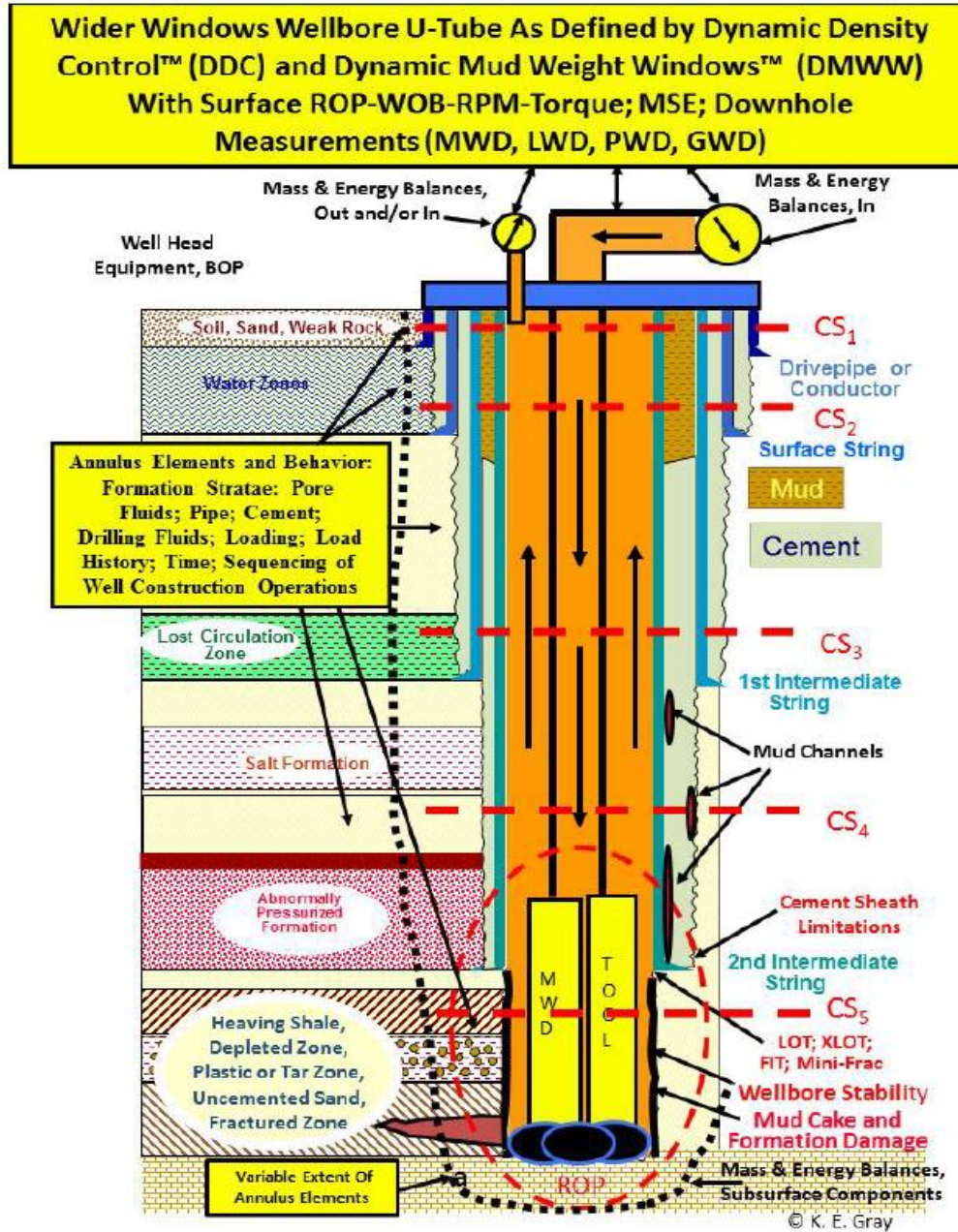


Figure 4.1: Wider Windows U-Tube System incorporation near wellbore cement and rock formation to 5-8 wellbore radii (Gray, 2011)

Additional cross sections could be incorporated, so as to pass through and include some particular rock zone of interest or a particular area of interest. Some examples would include a suspected mud channel or fractured zone, an over pressured horizon, a salt zone, a pressure depleted zone, a plastic or tar zone, a sub-salt formation, or a highly friable hole section (Gray, 2013)

#### **4.2 WIDER WINDOWS MODEL**

The analytical model utilizes linearly elastic, concentric cylinders to represent the casing, mud or cement, additional sequences, outward into the surrounding rock formation at that CS depth for a specified wellbore pressure and outer boundary pressure, i. e., the estimated minimum horizontal stress at that depth level (Gray, 2013). The analytical model is very much simplified relative to the complex U-Tube system depicted in Figure 4.1. But it provides a base case for preliminary sensitivity analyses of constituents of the physical system and provides a comparison with and calibration of the numerical model for known results.

Figure 4.2 shows the cylinder and interface numbering scheme for five concentric cylinders to represent the casing, cement, additional sequences, outward into the surrounding rock formation at that cross-sectional depth for a specified wellbore pressure and outer boundary pressure, i. e., the minimum horizontal stress at that level.



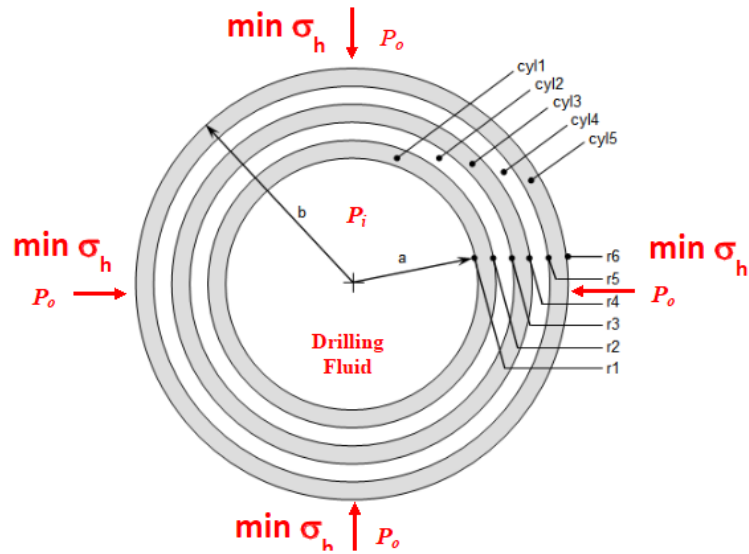


Figure 4.2: Concentric Cylinder and Interface Numbering Scheme (Norris, 2003)  
Cylinders Shown Schematically - Thicknesses Not Scaled

The displacements and stresses of each cylinder or zone are calculated using Norris model which has been derived from Lamé equations.

#### 4.2.1 Norris Solution

The stress distribution for a single unconstrained thick-walled cylinder under pressure loading from both inside and outside is shown below. The linear solution to this problem is known as the Lamé equations. Figure 4.3 shows a single cylinder with external pressure and internal pressure.

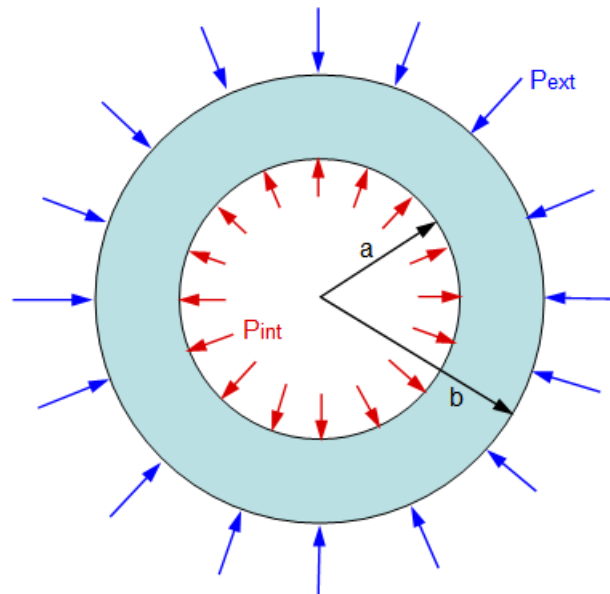


Figure 4.3: Single Cylinder Solution (Norris, 2003), (taken from Norris' personal website)

According to Lamé equations, the radial and hoop stresses at any radial location,  $r$ , are given by the following formulas:

$$\sigma_r = \frac{P_i a^2 - P_o b^2 - (P_i - P_o)(a^2 b^2 / r^2)}{b^2 - a^2} \quad (0.2)$$

$$\sigma_\theta = \frac{P_i a^2 - P_o b^2 + (P_i - P_o)(a^2 b^2 / r^2)}{b^2 - a^2} \quad (0.3)$$

Where,

$\sigma_r$  = radial stress

$\sigma_\theta$  = hoop stress

$a$  = inner radius of the cylinder

$b$  = outer radius of the cylinder

$P_i$  = internal pressure

$P_o$  = external pressure

$r$  = any radial location

And if the cylinder is fully or partially constrained axially then a uniform axial stress also develops which is given by:

$$\sigma_z = E\varepsilon_z + \nu(\sigma_r + \sigma_\theta) \quad (0.4)$$

Where,

$\nu$  = cylinder Poisson's ratio

$\sigma_z$  = axial stress

$\varepsilon_z$  = axial strain

$E$  = cylinder Young's modulus

If the cylinder is unconstrained then Equation 4.3 equals to zero (Norris, 2003), and the induced axial strain can be defined as:

$$\varepsilon_z = \frac{-\nu(\sigma_r + \sigma_\theta)}{E} \quad (0.5)$$

The linear strain displacement relations in polar coordinates for a generalized plain strain axisymmetric problem are:

$$\varepsilon_r = \frac{\partial u}{\partial r} \quad (0.6)$$

$$\varepsilon_r = \frac{u}{r} \quad (0.7)$$

$$\varepsilon_z = \text{const.} \quad (0.8)$$

$$\frac{\partial u}{\partial z} = \frac{\partial v}{\partial z} = \frac{\partial w}{\partial z} = 0 \quad (0.9)$$

$$\frac{\partial u}{\partial \theta} = \frac{\partial v}{\partial \theta} = \frac{\partial w}{\partial \theta} = 0 \quad (0.10)$$

Where,

$\varepsilon_r$  = radial strain

$u$  = radial deflection

$v$  = hoop deflection

$w$  = axial deflection

$r$  = radial direction

$\theta$  = hoop direction

$z$  = axial direction

The 3D constitutive relations for an isotropic Hookean material can be expressed as:

$$\varepsilon_r = \frac{1}{E} [\sigma_r - \nu(\sigma_\theta + \sigma_z)] + \alpha T \quad (0.11)$$

$$\varepsilon_\theta = \frac{1}{E} [\sigma_\theta - \nu(\sigma_r + \sigma_z)] + \alpha T \quad (0.12)$$

$$\varepsilon_z = \frac{1}{E} [\sigma_z - \nu(\sigma_r + \sigma_\theta)] + \alpha T \quad (0.13)$$

Where,

$\alpha$  = coefficient of thermal expansion

$T$  = temperature difference relative to  $T_0$

$T_0$  = stress-free temperature

Equation 4.12 can be rearranged as

$$\sigma_z = E\varepsilon_z + \nu(\sigma_r + \sigma_\theta) - E\alpha T \quad (0.14)$$

The radial displacement can be expressed as:

$$u = r\varepsilon_\theta = \frac{1}{E} [\sigma_\theta - \nu(\sigma_r + \sigma_\theta)] + r\alpha T \quad (0.15)$$

$$u = \frac{r}{E} [\sigma_\theta(1-\nu^2) - \nu\sigma_r(1+\nu) - \nu E\varepsilon_z] + r(1+\nu)\alpha T \quad (0.16)$$

The radial displacements at the inner and outer surfaces of the cylinder are:

$$u_a = \frac{a}{E} \left\{ \frac{2P_o b^2 (\nu^2 - 1) + P_i [a^2 (1 - \nu - 2\nu^2) + b^2 (1 + \nu)]}{b^2 - a^2} - \nu E \varepsilon_z \right\} + a(1 + \nu)\alpha T \quad (0.17)$$

$$u_b = \frac{b}{E} \left\{ \frac{2P_i a^2 (\nu^2 - 1) - P_o [b^2 (1 - \nu - 2\nu^2) + a^2 (1 + \nu)]}{b^2 - a^2} - \nu E \varepsilon_z \right\} + b(1 + \nu)\alpha T \quad (0.18)$$

Where,

$u_a$  = inner radial deflection

$u_b$  = outer radial deflection

#### 4.2.1 Multi-Cylinder Solution by Norris

Extension of the single cylinder solution to a system of concentric cylinders begins by enforcing the kinematic compatibility constraint at the interface between each cylinder (Norris, 2003). The outer radial deflection of any cylinder must equal the inner radial deflection of the cylinder that is bonded to its outer surface (Norris, 2003). This statement can be expressed in the following equation:

$$u_b^i = u_a^{i+1} \quad (0.19)$$

Where,

$i=1:N-1$

For each pair of bonded cylinders,  $i$  is the cylinder number, starting at 1 for the innermost cylinder and ending at  $N$  for the outermost cylinder. Figure 4.4 shows the cylinder and interface numbering scheme for a system of 5 cylinders.

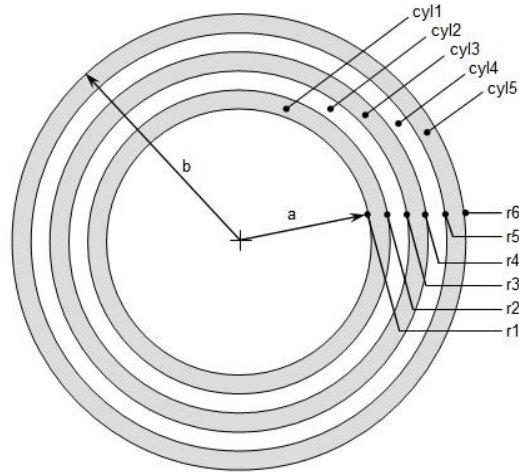


Figure 4.4: Multi-Cylinder System (Norris, 2003)

Consider a system with only two bonded cylinders. The interfaces will then be numbered from 1 to 3, and the cylinders numbered from 1 to 2. The system of cylinders can be represented with only 1 single equation. Substituting Equation 4.16 and 4.17 into Equation 4.18 and collecting similar terms, the resulting equation can be expressed in terms of:

$$Ap_1 + Bp_2 + Cp_3 = D \quad (0.20)$$

The subscripts denote the interface numbers. Since the interface pressures on interface 1 and 3 are known, only  $p_2$  is unknown. Therefore, Equation 4.19 can be readily solved. The values of A, B, C, and D in Equation 4.19 are as follows:

$$A_i = \frac{2r_{i-1}^2(v_{i-1}^2 - 1)}{E_{i-1}(r_i^2 - r_{i-1}^2)} \quad (0.21)$$

$$B_i = \frac{r_i^2(1 - v_i - 2v_i^2) + r_{i+1}^2(1 + v_i)}{E_i(r_{i+1}^2 - r_i^2)} + \frac{r_i^2(1 - v_{i-1} - 2v_{i-1}^2) + r_{i-1}^2(1 + v_{i-1})}{E_{i-1}(r_i^2 - r_{i-1}^2)} \quad (0.22)$$

$$C_i = \frac{2r_{i+1}^2(v_i^2 - 1)}{E_i(r_{i+1}^2 - r_i^2)} \quad (0.23)$$

$$D_i = (v_i - v_{i-1})\varepsilon_z + (1 + v_{i-1})\alpha_{i-1}T_{i-1} - (1 + v_i)\alpha_i T_i \quad (0.24)$$

with  $i$  ranging from 2 to  $N$ , where  $N$  is the total number of cylinders. The  $i$  subscript on the radius denotes the radial interface number, and the  $i$  on the material properties denotes the cylinder number.

Extending the solution to an arbitrary number of cylinders results in the following system of equations with one row for each interface:

$$\begin{bmatrix} 1 & 0 & 0 & 0 & 0 & 0 \\ A & B & C & 0 & 0 & 0 \\ 0 & A & B & C & 0 & 0 \\ 0 & 0 & A & B & C & 0 \\ 0 & 0 & 0 & A & B & C \\ 0 & 0 & 0 & 0 & 0 & 1 \end{bmatrix} \begin{bmatrix} p_1 \\ p_2 \\ p_3 \\ p_4 \\ p_5 \\ p_N \end{bmatrix} = \begin{bmatrix} D_1 = p_{\text{int}} \\ D_2 \\ D_3 \\ D_4 \\ D_5 \\ D_N = p_{\text{ext}} \end{bmatrix} \quad (0.25)$$

The first and last rows have the internal and external pressure boundary conditions. This system of equations can be solved using Gauss Elimination to obtain all of the unknown interface pressures between the cylinders. Once the interface pressures are solved, then they can be substituted back into Lamé equation 4.15 to determine the corresponding radial displacements.

Note that all the procedures and equations from this chapter are from Norris' personal website. Modification of some of the equations were done by Gray (2012)

## **Chapter 5: Mechanical and Thermal Effects on Radial Displacements**

In this chapter effects of mechanical and thermal behaviors on displacement of materials near the wellbore such as casing, cement, and formation are studied in different case studies.

### **5.1 CASE STUDY**

Two different case studies are done. First case study is the comparison between mechanical and thermo-mechanical effects. The second case study is the addition of thermal effects to Altun's model over an actual LOT test from Altun's SPE paper in 2001. Both Cases studies are done in a plane strain condition meaning that there is no displacement in vertical/upward direction. Both scenarios assume equal horizontal stresses ( $\sigma_{\min}=\sigma_{\max}$ ). Suggested Poisson's ratio values for casing's and cement's from literature are used. Formations' Poisson's ratio values are selected to be the same for all formations in order to minimize their effects on displacements. A Poisson's ratio of 0.3 was used since it is a typical value assumed for many rock formations.

#### **5.1.1 Case Study I**

Figure 5.1 Shows a replica wellbore schematic used for this case study that was originally developed in Gonzalez paper (2004). Table 5.1 lists the other assumptions. In order to estimate the thermal effects, a temperature profile inside the wellbore must be established. The temperature inside the wellbore, shown in Figure 5.2, is estimated using a steady state approach developed by Holmes and Swift as discussed in *Section 5.4*. In



Figure 5.2, maximum fluid temperature in the system occurs one-fourth to one-third of the way up in the annulus (Raymond, 1969).

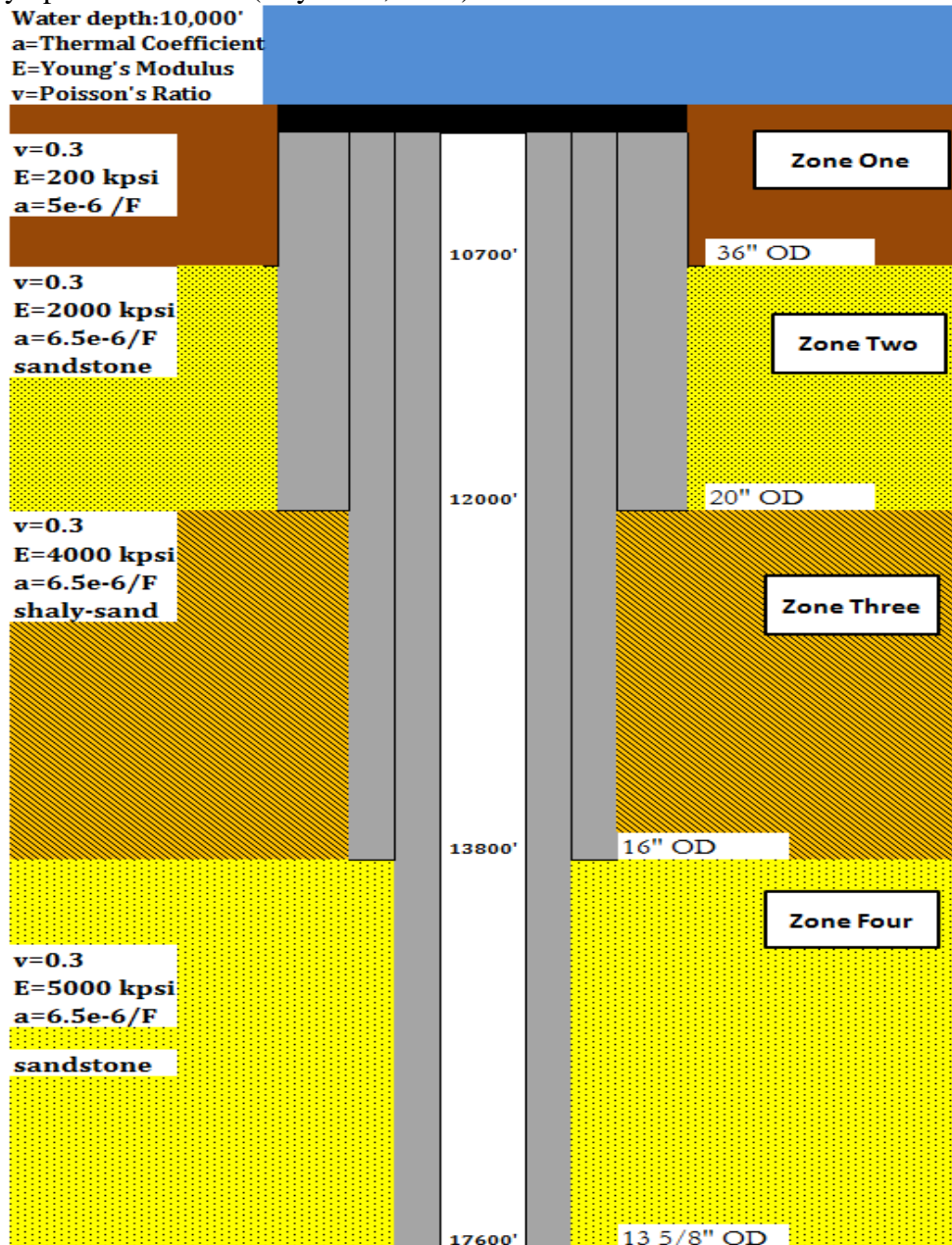


Figure 5.1: Wellbore schematic used for case study I. It is assumed to be an offshore wellbore. (Modified after Gonzalez et al., 2004). Formations' Poisson's ratio values are kept constant and the same in order to minimize its effect on the displacements.

Table 5.1: Assumed data used for case study I

<b>Temperature Gradient</b>	0.013	deg F/ft
<b>Temperature at Mud-line</b>	35	deg F
<b>Vertical stress (<math>\sigma_v</math>)</b>	1	psi/ft
<b>Horizontal stress (<math>\sigma_h</math>)</b>	$0.3 \cdot \sigma_v$	psi/ft
<b><math>\alpha_{t\text{-steel}}</math></b>	6.50E-06	/degF
<b><math>\alpha_{t\text{-cement}}</math></b>	1.00E-05	/degF
<b>E-steel</b>	30000	Kpsi
<b>E-cement</b>	3000	Kpsi
<b>v-steel</b>	0.3	
<b>v-cement</b>	0.25	
<b>Linearly elastic, Isotropic</b>		

Formations' Poisson's ratio values are arbitrary selected and kept constant during this study.

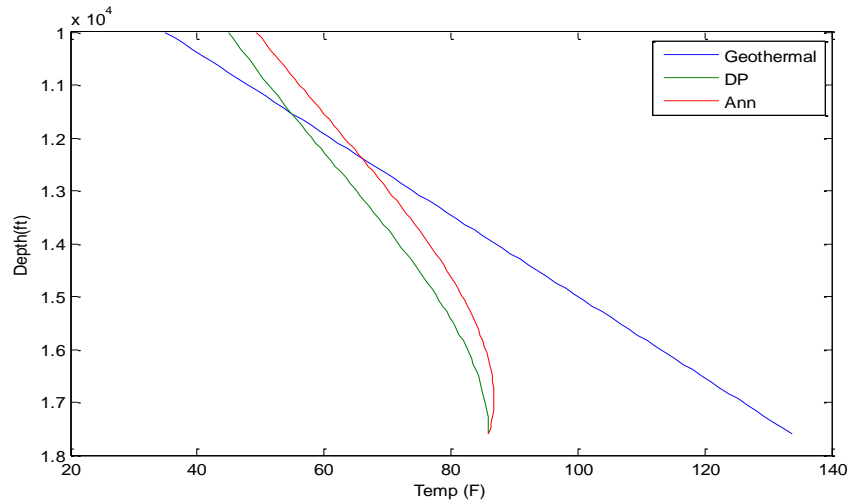


Figure 5.2: Steady state temperature profile of case study I based on Holmes and Swift model developed in MATLAB

The beginning of the graph represents the mud line, not the surface. The total water depth is ignored since the strings of casing start at the mud line. The temperature inside the wellbore is increasing with depth. However, at some depth, the geo-thermal temperature exceeds the wellbore temperature, causing the wellbore to feel a cooling effect. This can be seen in Figure 5.2 at any depth beyond 12,400 ft. After the analysis was done over the wellbore, the mechanical and thermo-mechanical displacements for internal diameter of 13 5/8" casing were compared for each zone. As shown in Figure 5.3, thermo-mechanical displacements are larger than the mechanical ones, because at this zone the wellbore temperature is larger than the formation temperature. However, the change in temperature becomes smaller with increasing depth, so this is why the slope for thermo-mechanical trend is almost unity. Note that, the mechanical trend has negative values. This is because the far field stresses overtakes the inside pressure of the wellbore. However, it has a positive slope, meaning the pressure inside the wellbore will overcome the far field stresses eventually.

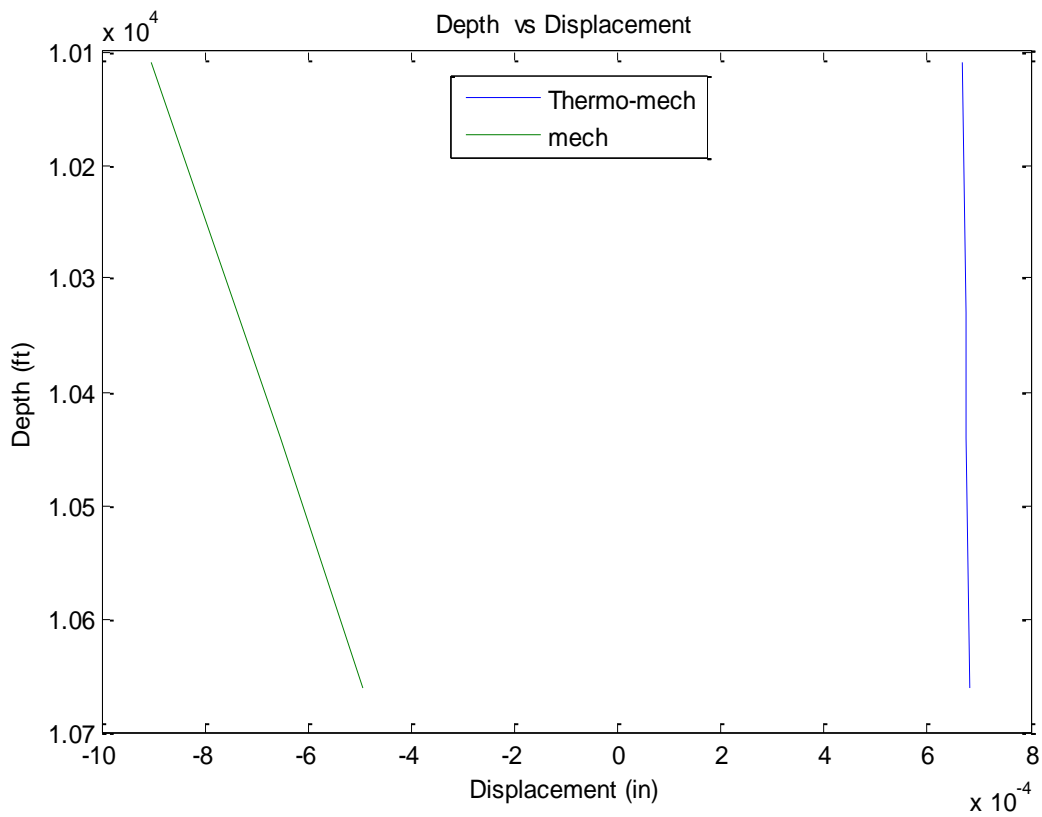


Figure 5.3: Displacement for *zone one* as shown in Figure 5.1

The trends in zone two looks similar to zone one, as shown in Figure 5.4. However, the thermo-mechanical displacements are smaller compared to zone one because the temperature difference between the wellbore and the zone is getting smaller.

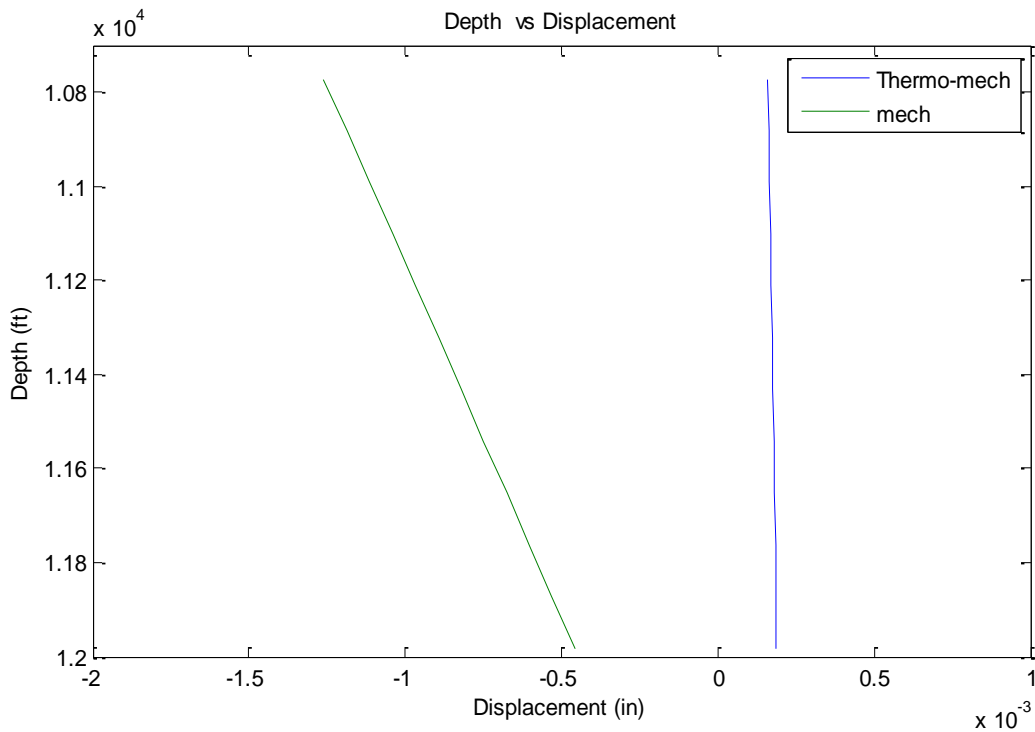


Figure 5.4: Displacement for casing 13 5/8” at *zone two*

When moving further into zone three, it can be seen in Figure 5.5 that mechanical displacements are larger than the thermo-mechanical displacements after 12,400 ft (cross-over point). After 2,400 ft the wellbore temperature is lower than the formation temperature, causing a wellbore thermal contraction. However, the values are still positive because: 1. the temperature difference is small, so the thermal shrinkage doesn’t contribute very much. 2. the wellbore pressure is overcoming the far field stress making the wellbore to expand and overcoming the thermal contraction.

The formation depth increases with increasing depth, causing greater temperature difference. The greater the temperature difference, the larger the thermo-mechanical displacement. Sometimes, the thermal displacements can overcome the mechanical

displacements, as shown in Figure 5.5 and 5.6. As depth increases thermo-mechanical model tends to approach negative values causing the wellbore to shrink.

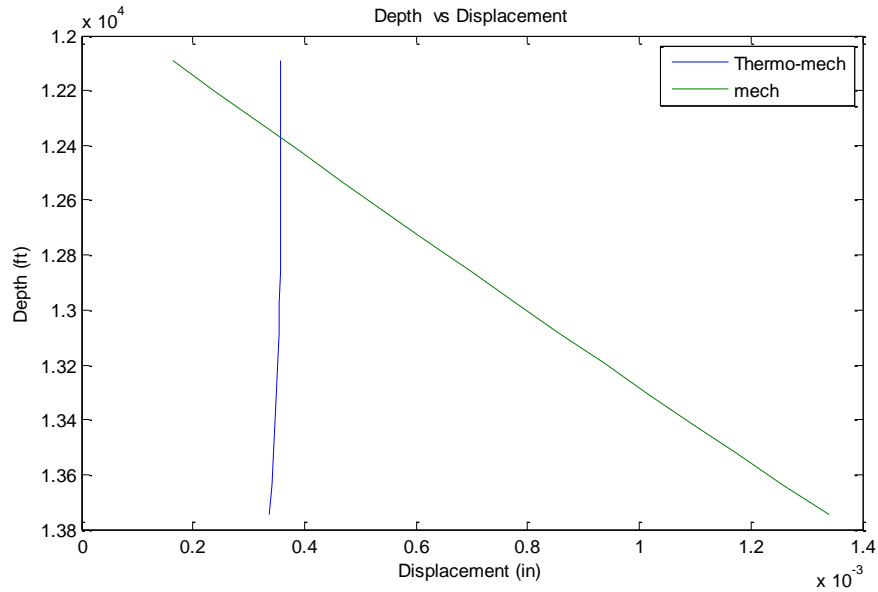


Figure 5.5: Displacement for 13 5/8" at *zone three*. After some depth the thermo-mechanical changes seems smaller compared to only mechanical effect since the wellbore is cooling down and shrinking

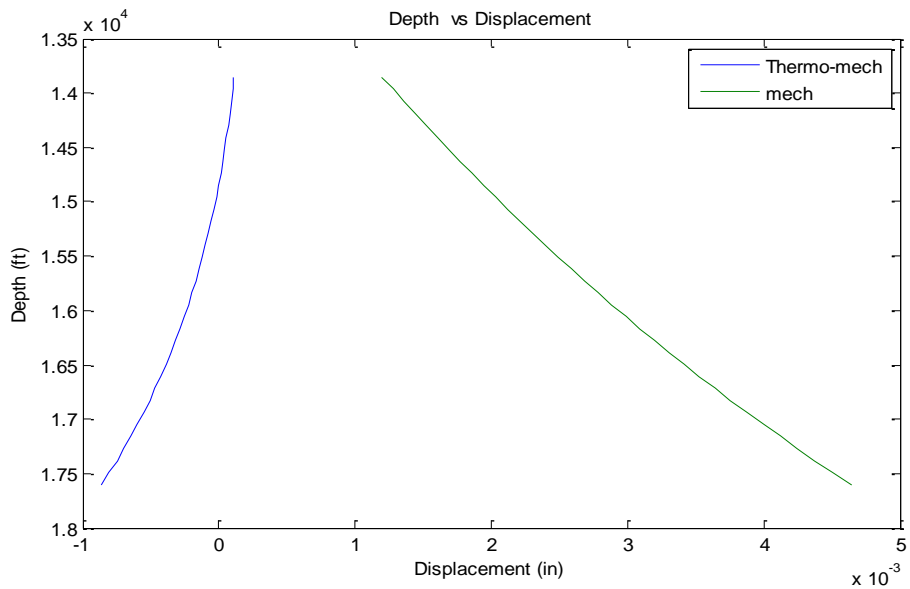


Figure 5.6: Displacement for *zone four*

The displacement is a function of many parameters: far field stresses, geothermal gradient, flow rate, mud density and temperature, etc. For instance, Figure 5.7 shows the displacement for zone four with one exception that the far field stresses are now 60% of the vertical stress.

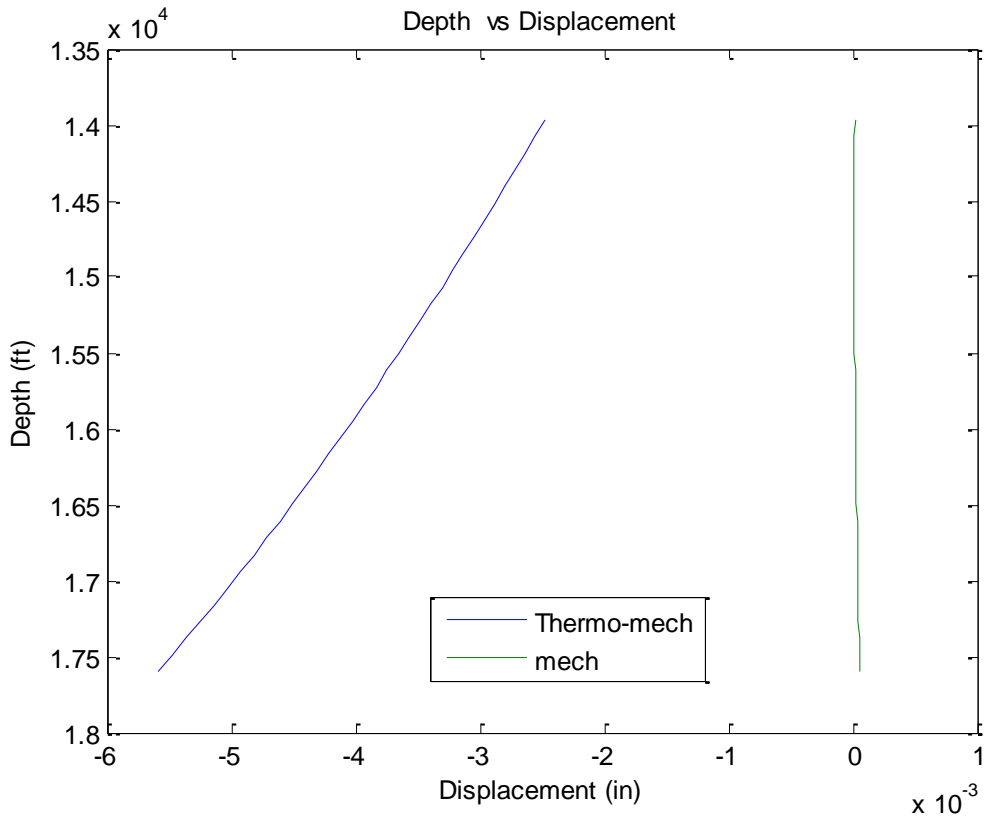


Figure 5.7: Displacement for *zone four* (horizontal stress is 60% of vertical stress)

These displacement changes affect the volume of the system. Since the studied wellbore depth was only 7,600 ft from the mud line, volume changes were very small. In fact, the calculated volume with respect to mechanical changes was very close to volume of the system volume, and the volume with thermo-mechanical effect was only half a barrel less than the volume of the system. However, when the far field stresses doubled, the volume calculated based on thermo-mechanical effect is one barrel less than the

volume of the system. These changes become more consequential as the depth of the wellbore increases or the geothermal gradient increases.

### 5.1.3 Case Study II

This case study shows the result from Altun’s model coupled with thermo-mechanical effect. Altun model is solely based on mechanical changes of the casing and formation. The Wider Windows LOT model adds the thermal effects of formation and casing to Altun’s model. The case study was done over the same data used by Altun on GOM U-2 wellbore as shown in Figure 3.3. Table 5.2 and 5.3 list the data and assumptions respectively.

Table 5.2: Data used by Altun for GOM U-2 (Altun, 2001)

<b>Location</b>	GOM	
<b>Water depth (assumed)</b>	65	ft
<b>Depth</b>	8,782	ft
<b>TVD casing</b>	8,773	ft
<b>Casing OD</b>	9 5/8	in
<b>Pump rate</b>	0.25	bbl/min
<b>Volume pumped</b>	6.75	bbl



Table 5.3: Assumptions for Altun's model

<b>Casing ID</b>	8 6/8	in
<b>Temperature Gradient</b>	0.013	deg F/ft
<b>Temperature at Sea-bed</b>	65	deg F
<b>Vertical stress (<math>\sigma_v</math>)</b>	1	psi/ft
<b>Horizontal stress (<math>\sigma_h</math>)</b>	$0.4 \cdot \sigma_v$	psi/ft
<b><math>\alpha_{t\text{-steel}}</math></b>	6.50E-06	/degF
<b><math>\alpha_{t\text{-cement}}</math></b>	1.00E-05	/degF
<b>E-steel</b>	30000	Kpsi
<b>E-cement</b>	3000	Kpsi
<b>v-steel</b>	0.3	
<b>v-cement</b>	0.25	
<b>Leak-off rate coefficient into formation</b>	8e-5	
<b>Linearly elastic, Isotropic</b>		

A temperature profile inside the wellbore was estimated using steady state condition. Figure 5.8 shows the temperature profile inside the wellbore. Beyond 2,500 ft the wellbore temperature is lower than the formation temperature, causing the wellbore to feel thermal contraction. Figure 5.9 shows the comparison between radial displacements between two models. The first graph on top is the model including thermal and mechanical effects while the other one takes into account the mechanical effect. As temperature increases with depth, the effect of thermal expansion on displacement becomes more important. In fact, after 7,000 ft, the wellbore starts to shrink since the thermal contraction effect is greater than mechanical effect. Changes in displacement will

affect the wellbore volume. Figure 5.10 shows the volume difference between mechanical and thermal for the wellbore. A little volume expansion due to thermal expansion is seen up to 2,500 ft. After that point, the mechanical effect suppresses the thermal effect, causing the wellbore to expand.

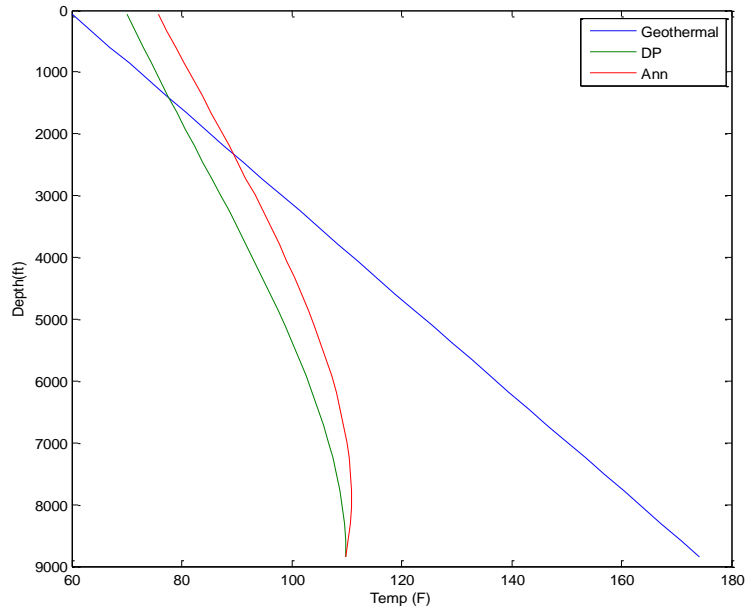


Figure 5.8: Wellbore temperature profile for GOM U-2 wellbore used in Altun’s SPE paper

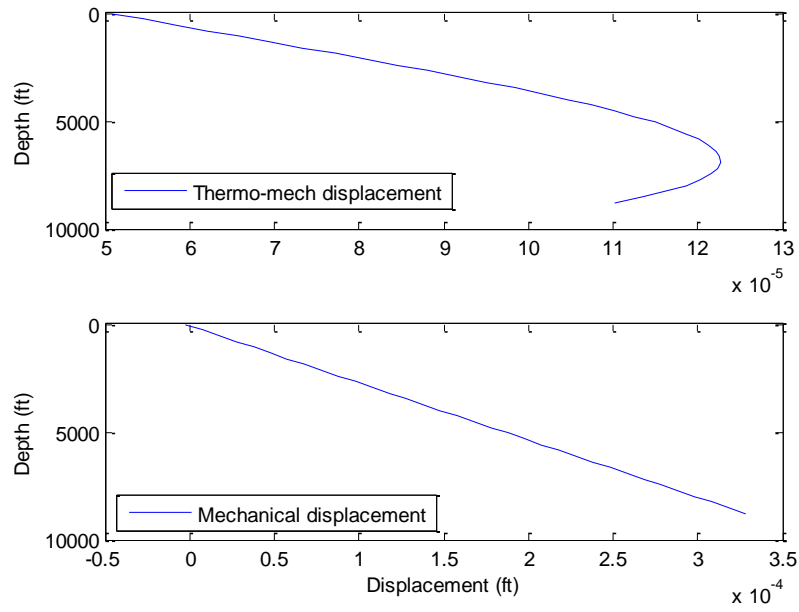


Figure 5.9: Wellbore temperature profile for GOM U-2

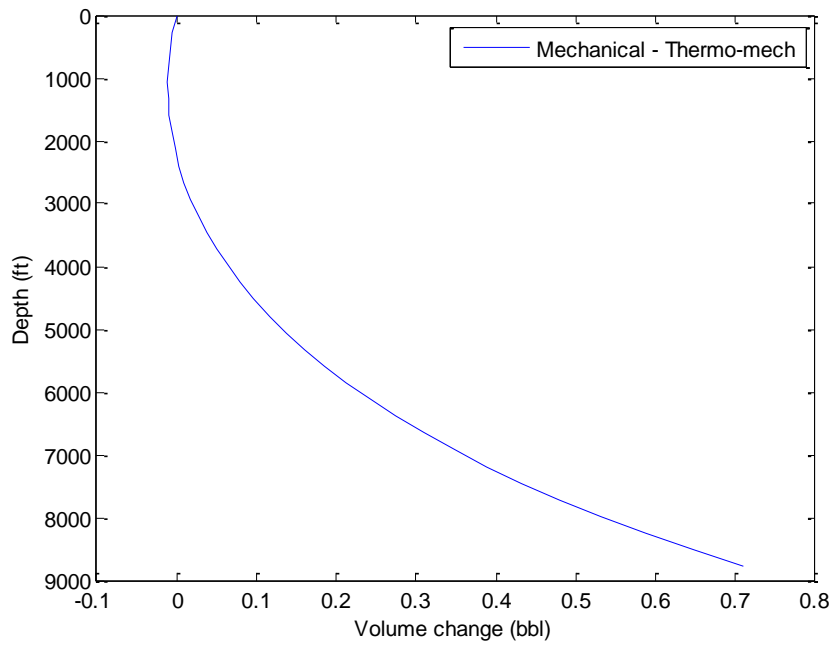


Figure 5.10: Volume change for GOM U-2

After comparing the two scenarios, it becomes obvious that the thermal effect on the pressure analysis and displacement becomes important and cannot be ignored. As temperature increases with depth, the effect of thermal expansion on displacement becomes more important. Figure 5.11 shows the comparison between Altun and The Wider Windows models. The Wider Windows is using same procedure as Altun's model except it incorporates thermal effects on the system's total volume calculation.

Table 5.4: Models comparison based on quadratic fit

	Quadratic fit (MATLAB)
Actaul data	$P = -28.69V^2 + 438.5V - 24.26$
Altun's Model	$P = -34.29V^2 + 475.9V + 37.3$
Wider Windows Model	$P = -28.15V^2 + 423.9V - 30.4$

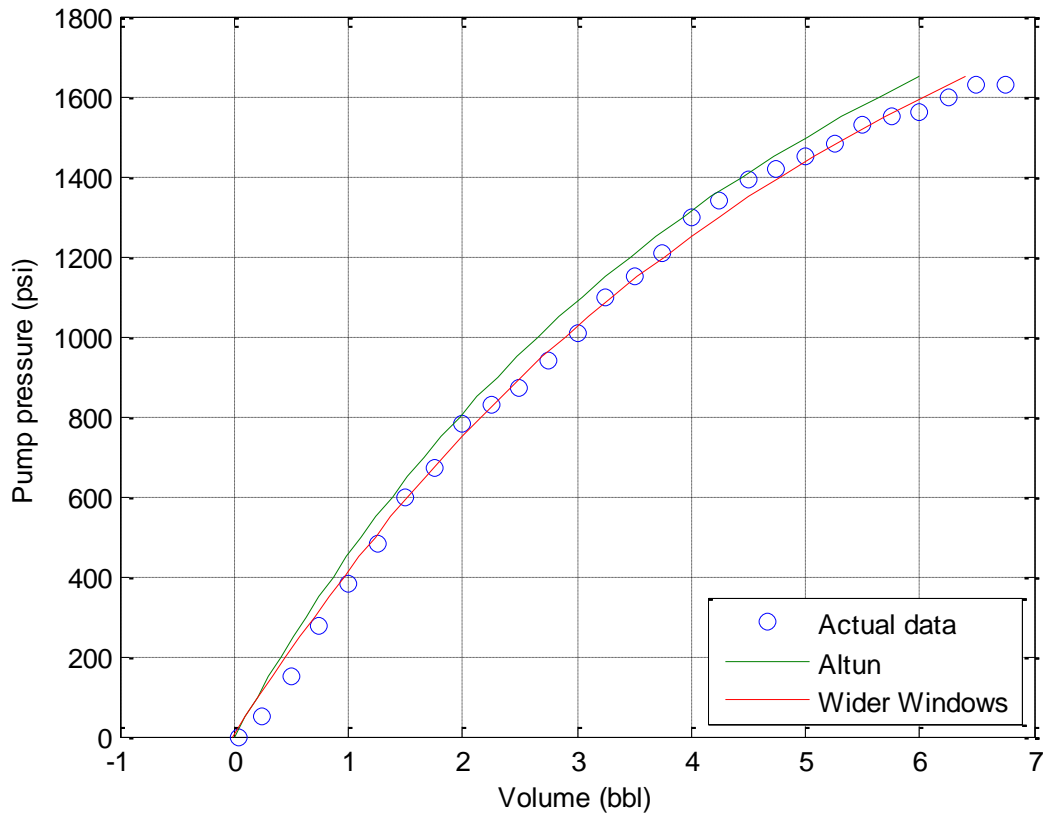


Figure 5.11: LOT prediction by Wider Windows and Altun models

Table 5.4 shows the comparison of the models based on quadratic fit generated by MATLAB. It can be seen that results from Wider Windows is closer to actual data fit compared to Altun's fit. It's is important to include thermal effects in the model because a more accurate results will be produced. Altun's model overestimates the curve since it doesn't include thermal effects. However, The Wider Windows model fits the data point better after correcting for thermal effect. The fit does not go over all the data point because 1.there are different assumptions associate with both models that introduce error. 2. The actual data may be reported with error.

## 5.2 THERMAL EFFECT ON DISPLACEMENT

It's is important to include thermal effects in the model for volume estimation because a more accurate results will be produced. Figure 5.12 shows this significance by comparing the slopes of the trends that were done on *case study I*. The *mechanical* line slope is  $\frac{dR}{dZ} = -\frac{1}{3} \times 10^{-6}$ , while mechanical and thermal is  $\frac{dR}{dZ} = \frac{1}{3.2} \times 10^{-5}$ .

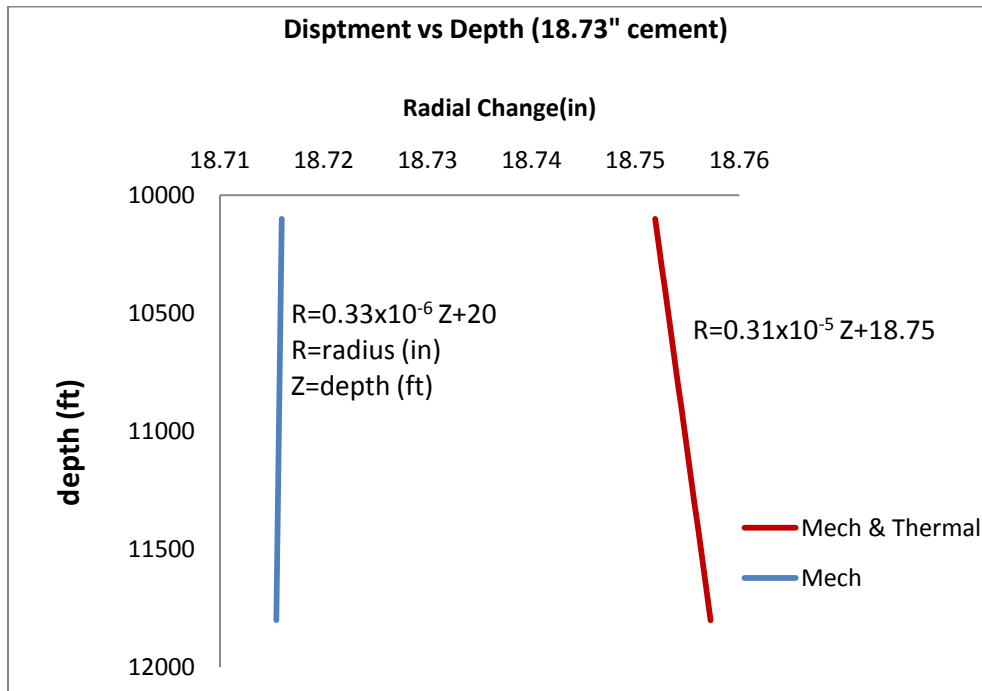


Figure 5.12: Radial change in cement in *case study I*

The model that only includes mechanical effects shows that thickness of the layer of cement has reduced due to the far field pressure. On the other hand, when the thermal effect is accounted into the model, the radial displacement is outward with increasing depth, meaning that the displacement due to thermal stresses has overcome mechanical displacement due to the horizontal far field stresses.

### 5.3 THERMAL EFFECT ON PRESSURE PROFILE

Another important effect of thermal behavior on the system is the additional pressure induced by the thermal stresses. Figure 5.13 shows the pressure profiles for the mechanical and thermo-mechanical effects for *case study I*. It can be seen how important the effect of thermal stress is around a wellbore. The pressure profile for the model that includes mechanical and thermal effects is 180 psi larger (on average) than the model that only takes mechanical effect into the account.

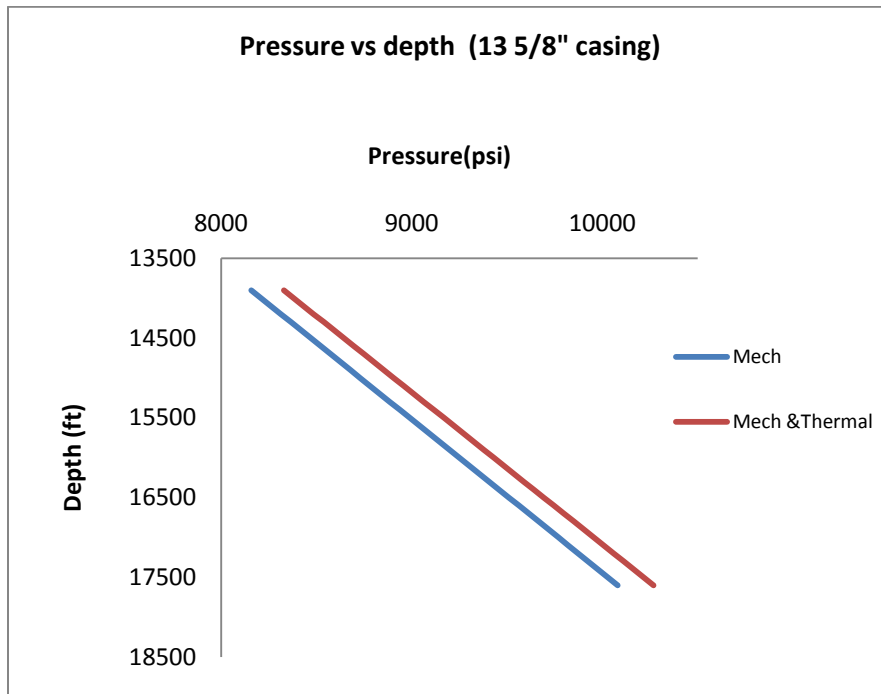


Figure 5.13: Pressure profile for 13 5/8" casing in *case study I*

It is very important to account for this pressure discrepancy because any mud weight window will be affected considerably by this difference.

## 5.4 ANALYTICAL THERMAL MODEL

This section will explain the model that was used to produce temperature profile inside the wellbore as discussed in previous sections.

An analytical model was formulated by Holmes and Swift (1970) based on a steady state and one dimension energy balance with no heat generation. The controlled volume used for energy balance is shown in Figure 5.14. Temperature in a wellbore changes with time, so a true steady state is never obtained. However, after one to two circulations the temperature doesn't vary very much (Raymond, 1969).

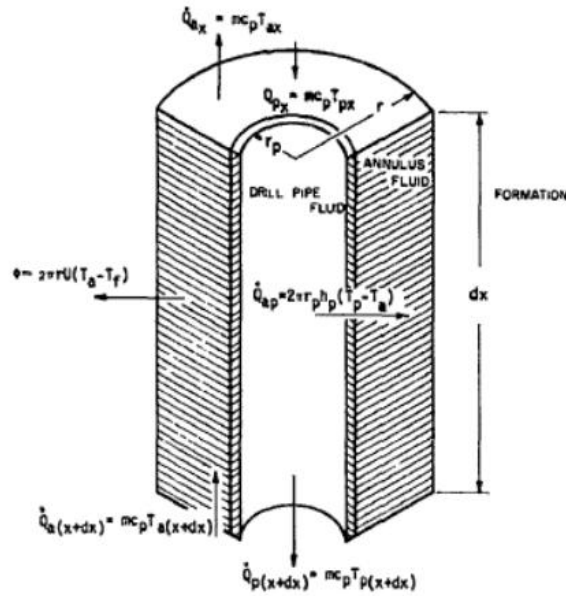


Figure 5.14: Controlled volume used for energy balance (Holmes and Swift, 1970)

The heat accumulation of the annular fluid between depth  $x$  to  $x+dx$  is given by

$$\dot{Q}_{ax} - \dot{Q}_{a(x+dx)} = mc_p [T_{ax} - T_{a(x+dx)}] \quad (5.1)$$

And the heat transferred between annular and the formation is given by

$$\Phi = 2\pi r U (T_a - T_f) dx \quad (5.2)$$



The heat balance across the drill pipe is as follow:

$$\dot{Q}_{ap} = 2\pi r_p h_p (T_p - T_a) dx \quad (5.3)$$

Combining Equation 5.1 to 5.3 yields

$$mc_p \frac{dT_a}{dx} + 2\pi r_p h_p (T_p - T_a) = 2\pi r U (T_a - T_f) \quad (5.4)$$

The formation temperature is approximated by

$$T_f = T_s + Gx \quad (5.5)$$

Substituting Equation 5.5 into 5.4 results into:

$$mc_p \frac{dT_a}{dx} + 2\pi r_p h_p (T_p - T_a) = 2\pi r U (T_a - T_s - Gx) \quad (5.6)$$

A similar approach for fluid in the drill pipe is given by

$$mc_p \frac{dT_p}{dx} = 2\pi r_p h_p (T_p - T_a) \quad (5.7)$$

All of the above equations are linear heat transfer equations. After integrating the above equation, temperature profile for mud in the system and annulus are found as shown in Equations 5.8 and 5.9.

$$T_p = K_1 e^{c_1 x} + K_2 e^{c_2 x} + Gx + T_s - GA \quad (5.8)$$

$$T_a = K_1 C_3 e^{c_1 x} + K_2 C_4 e^{c_2 x} + Gx + T_s \quad (5.9)$$

Two boundary conditions must be defined. One will be at surface where depth is zero. At this depth the mud temperature is known, and it is equal to the inlet mud temperature. The second boundary condition is at the bottom of the wellbore where annular temperature is equal to the drill pipe temperature.

Boundary condition 1 at  $x=0$ ;  $T_p=T_{pi}$

Boundary condition 2 at  $x=H$ ;  $T_{HP}=T_{Ha}$

With these boundary conditions, the following integration constants are obtained

$$K_1 = T_{pi} - K_2 - T_s + GA \quad (5.10)$$

$$K_2 = \frac{GA - [T_{pi} - T_s + GA]e^{C_2H} (1 - C_3)}{e^{C_2H} (1 - C_4) - e^{C_1H} (1 - C_3)} \quad (5.11)$$

Where,

$$C_1 = \left(\frac{B}{2A}\right) \left[1 + \left(1 + \frac{4}{B}\right)^{1/2}\right]$$

$$C_2 = \left(\frac{B}{2A}\right) \left[1 - \left(1 + \frac{4}{B}\right)^{1/2}\right]$$

$$C_3 = 1 + \left(\frac{B}{2}\right) \left[1 + \left(1 + \frac{4}{B}\right)^{1/2}\right]$$

$$C_4 = 1 + \left(\frac{B}{2}\right) \left[1 - \left(1 + \frac{4}{B}\right)^{1/2}\right]$$

$$A = \frac{mc_p}{2\pi r_p h_p}$$

$$B = \frac{rU}{r_p h_p}$$

$c_p$  = mud heat capacity, Btu/(lb-°F)

G = geothermal gradient, °F/ft

H = depth of the wellbore, ft

$h_p$  = overall heat transfer coefficient across drill pipe, Btu/(sq ft-°F-hour)

m = mass flow rate, lb/hour

$\overset{\circ}{Q}_a$  = heat flow in the annulus, Btu/hour

$\overset{\circ}{Q}_{ap}$  = heat flow across the drill pipe, Btu/hour

$\overset{\circ}{Q}_p$  = heat flow in the drill pipe, Btu/hour

r = wellbore radius, ft

$r_p$  = drill pipe radius, ft

$T_a$  = mud temperature in annulus, °F

$T_f$  = formation temperature, °F

$T_p$  = mud temperature in drill pipe, °F

$T_s$  = surface temperature, °F

$T_{Ha}$  = bottom-hole temperature of mud in annulus, °F

$T_{Hp}$  = bottom-hole temperature of mud in drill pipe, °F

$T_{pi}$  = inlet mud temperature on surface, °F

$\Phi$  = heat flux into formation, Btu/hour

$U$  = overall heat transfer coefficient across wellbore face, Btu/(sq ft-°F-hour)

$x$  = depth, ft

## Chapter 6: Thermal Effect on Fracture Gradient and Initiation

### 6.1 BACKGROUND

Lost circulation (LC) is an event when the fluid inside the wellbore escapes into the formation. LC has contributed the most to drilling operations' NPT. When the pressure inside the wellbore is higher than the fracture gradient of the formation, lost circulation happens. Table 6.1 shows different types of lost circulation along with their remedies.

Table 6.1: Lost circulation classification and remedies (Ghalambor et al. 2014)

Classification	Typical Loss Rate	Typical Formation Characteristics	Preventative Solutions	Mitigation Solutions
Seepage	<10 bbl/hr	<ul style="list-style-type: none"> <li>Sands</li> <li>Sandstones</li> <li>Silt</li> </ul>	<ul style="list-style-type: none"> <li>Particulate LCM</li> <li>Managed Pressure Drilling</li> <li>Drilling with Casing</li> </ul>	<ul style="list-style-type: none"> <li>Particulate LCM</li> </ul>
Partial	10-50 bbl/hr	<ul style="list-style-type: none"> <li>Unconsolidated sand or gravel</li> <li>Small natural fractures</li> <li>Small induced fractures</li> </ul>	<ul style="list-style-type: none"> <li>Particulate LCM</li> <li>Managed Pressure Drilling</li> <li>Drilling with Casing</li> <li>Solid Expandable Systems</li> </ul>	<ul style="list-style-type: none"> <li>Particulate/Fiber LCM</li> <li>Cross-linkable LCM</li> </ul>
Severe	>50 bbl/hr	<ul style="list-style-type: none"> <li>Unconsolidated sand or gravel</li> <li>Large natural fractures</li> <li>Large induced fractures</li> </ul>	<ul style="list-style-type: none"> <li>Managed Pressure Drilling</li> <li>Drilling with Casing</li> <li>Solid Expandable Systems</li> </ul>	<ul style="list-style-type: none"> <li>Particulate/Fiber LCM</li> <li>Cross-linkable LCM</li> </ul>
Total	No returns	<ul style="list-style-type: none"> <li>Cavernous formations</li> <li>Large, and/or numerous natural and/or induced fractures</li> </ul>	<ul style="list-style-type: none"> <li>Managed Pressure Drilling</li> <li>Drilling with Casing</li> <li>Solid Expandable Systems</li> </ul>	<ul style="list-style-type: none"> <li>Particulate/Fiber LCM</li> <li>Cross-linkable LCM</li> </ul>

Most widely used practice to battle LC is wellbore strengthening method (WSM) which involves pumping lost circulation materials (LCM) to bridge and close the fractures created near the wellbore. However, a robust guideline to select LCM properly

doesn't exist. When LC happens, since the exact size of the fractures are unknown, different sizes of LCM's are pumped down the wellbore in order to bridge or plug the fractures. Adding LCM pills may thicken the mud filter cake on the wellbore wall which may cause the drill string to differentially get stuck (Deeg and Wang, 2004).

Wellbore strengthening method (WSM) includes different techniques/approaches as shown in Table 6.2. All methods can only be applied in permeable formations where mud filtrate can be formed on the fracture walls in order to create an immobile mass inside the fracture (Salehi and Nygaard, 2010). The immobile mass inside the fracture hinders the fracture from further propagation and opening. One common factor that these methods haven't taken into account is the effect of temperature in fracture initiation/propagation during a LC event.

Table 6.2: Wellbore strengthening methods (Salehi and Nygaard, 2011)

Author	Materials	Material Size	Material Strength	Tip Isolation	Rock Stress	Method
Fuh et al., 1992	LPM	Important	Selected Strength	Required		Fracture Pressure Inhibitor
Alberty and McLean, 2004	Calcium Carbonate	Important	Important	Not Required	Changing	Stress Cage (SC)
Dupriest, 2008	DSF	Unimportant	Unimportant	Required	Changing	Fracture Closure Stress(FCS)
Wang et al., 2007a, 2007b	DVCS	Important	Important		Changing	Stress Cage (SC)
Van Oort et al., 2009		Important	Unimportant	Required	Not Changing	Fracture Propagation Resistance (FPR)
Aadnoy and Belayneh, 2008	High Strength Materials	Important	Very Important		Not Changing	Fracture Healing

## 6.2 OBJECTIVE

Most articles describe mechanical effect of mud additives, rock formations, but not the thermal effect during a LC event. Rock formations have very small thermal expansion coefficients, and a small temperature change can cause large changes in radial, tangential, and vertical stresses (Gray, 2013). Several case studies have been done to illustrate the importance of thermal behavior during drilling activities. Moreover, thermal behavior has not been fully studied in lost circulation scenarios. Wider Windows LC projects are intended to evaluate and explain thermal effect, along with rock properties such as porosity, permeability, and stress state during a lost circulation event. These thermal projects seek quantitative, thermo-poroelastic models for improving interpretation of routine leak-off tests and lost circulation events in order to reduce NPT.

An investigation of historical lost circulation events led to the consideration of thermal effects on formation stress as a possible cause. It was concluded that high differential temperatures between the drilling mud and the formations might be causing high thermally induced tensile stresses (Pepin et al., 2004). To support this claim, a field experiment in one of Chevron-Texaco well in South Texas was done. Three LOT's were done at different bottom-hole temperatures (BHT), to show the temperature effect on fracture gradient. Figure 6.1 shows the result of these LOT's. It can be seen that as the BHT increased the fracture gradient increased since the tensile stress of the rock has increased. By adding 34 deg C to the BHT, more than 1.5 ppg was added to the leak-off pressure (also known as FIP). This result shows the significance of thermal effect in drilling operations specifically lost circulation and LOT.

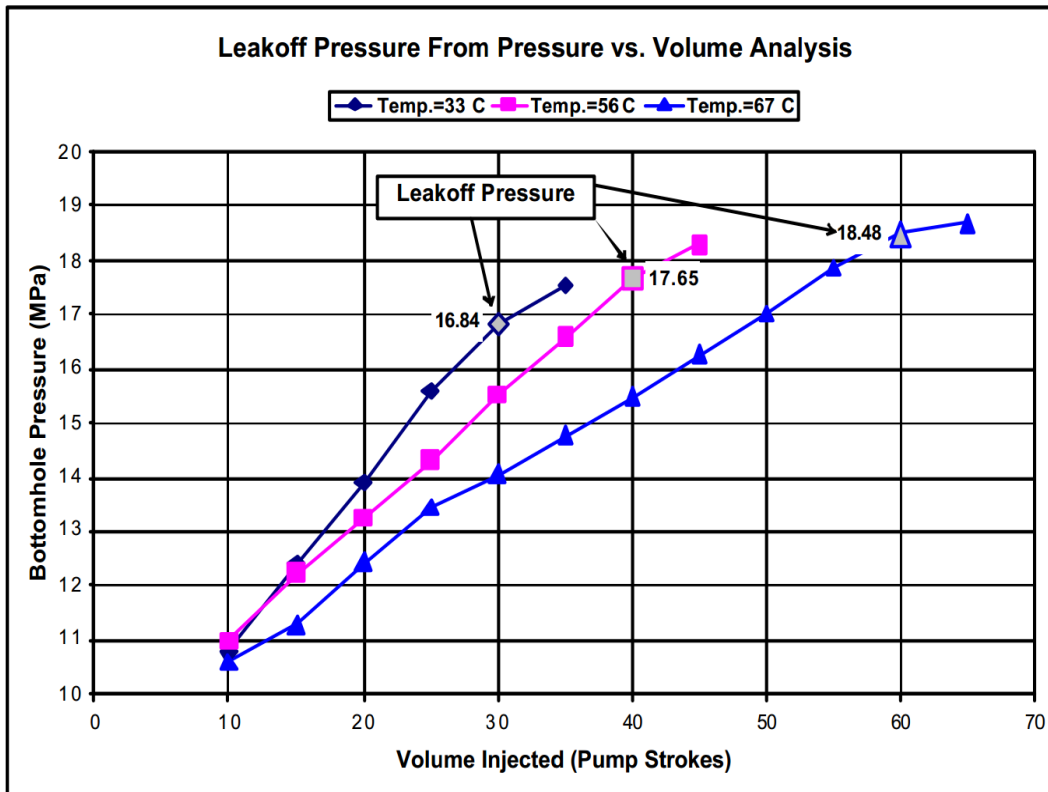


Figure 6.1: Leak of test at different bottom hole temperature (Pepin et. al. 2004)

### 6.3 MODEL

After reviewing the literature and concluding that the temperature has an important role in lost circulation, a thermo poro-elastic model was developed. Due to complexity of boundary conditions of rock formations and number of geological parameters, the finite element approach was used. ABAQUS is a powerful software that is used for this purpose. A three layer formation was selected for the study. The motivation was to estimate the tensile zones and fracture gradient in the model. Tensile zones are prone to lost circulation. As shown in Figure 6.2, a layer of sandstone is sandwiched between two shale layers. The sandstone layer is partially depleted compared to other layers. After defining all geological data and stresses on the block, the model was run in ABAQUS' "soil step". This step is very similar to geological modeling

since most geological parameters can be inputted. Also the near wellbore region is cooled down by 25 degrees to account for thermal effects.

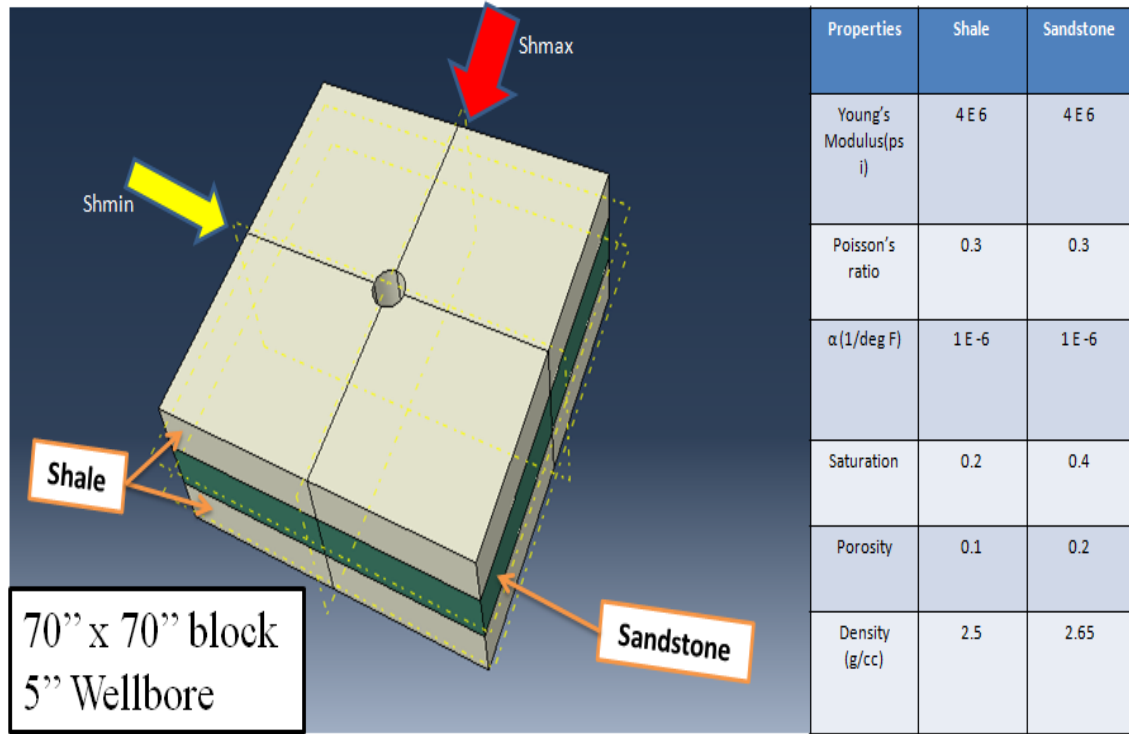


Figure 6.2: ABAQUS three layer model and formations properties

Vertical stress ( $S_v$ ),  $S_{hmax}$ , and  $S_{hmin}$  are taken to be 1100, 950, and 800 psi respectively. Pore pressure in sandstone is taken to be 250 psi, while in shale, it is 500 psi. Pressure inside the wellbore is 600 psi. It can be seen in Figure 6.3 that the most tensile zone is in the sandstone layer (dark red). Tensile zone is the place that lost circulation is more likely to occur. In this zone, rock doesn't have enough strength to prevent fracture initiation and propagation compared to other locations in the block. In ABAQUS positive value stands for tensile and negative value is for compression.



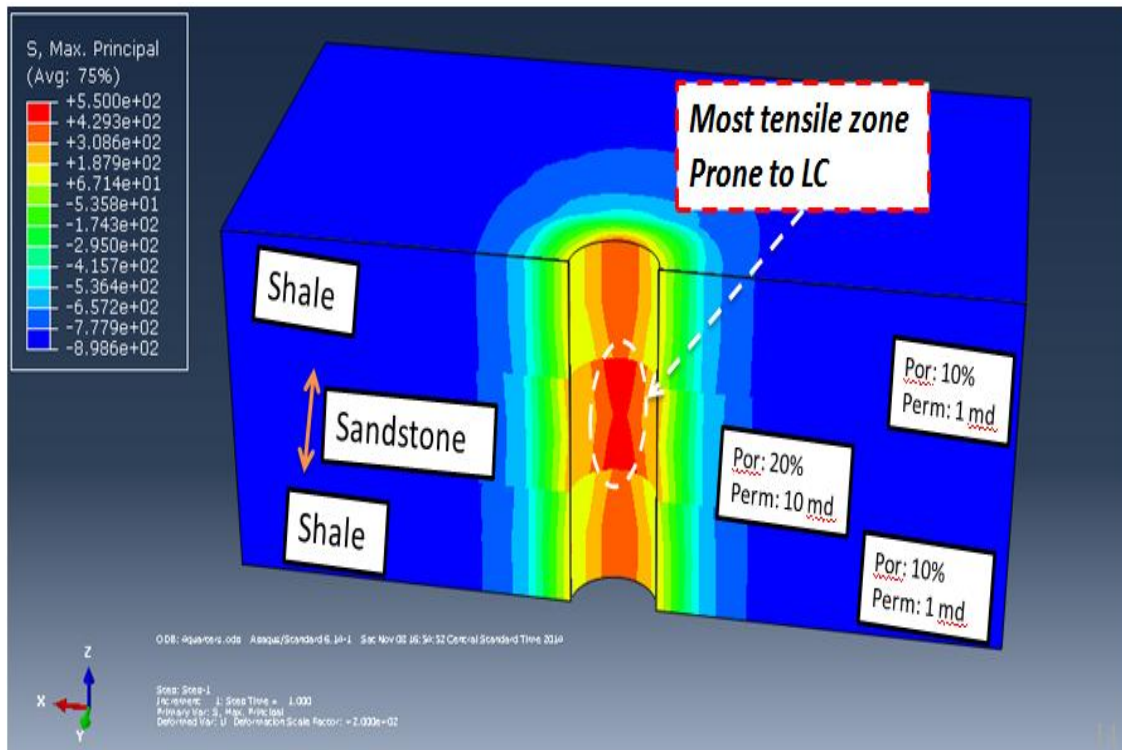


Figure 6.3: Result predictions of the block by ABAQUS

Since the temperature around the wellbore is changed only a short distance away from the wellbore, sub modeling was used to represent this situation. In the sub model, the cooling thermal effect on tensile stress distribution is studied. Figure 6.4 shows how the wellbore stresses are changed during a thermal cooling. It is shown that the magnitude of tensile stress around the wellbore is greatly changed. After ABAQUS has identified the location of highest tensile stresses prone to lost circulation, another package was used to study fracture initiation/propagation in these zones. Extended Finite Element Method (XFEM) was used for this purpose. In XFEM, a criterion is defined for initiation and propagation of the fractures. If the criterion is met then the fracture will be developed.

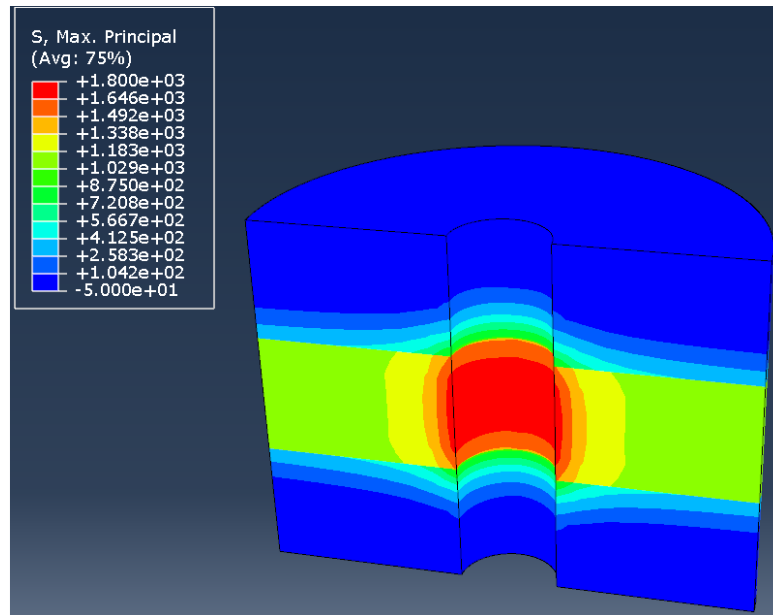


Figure 6.4: Stress distribution around the sub model after cooling the system by 25 degrees. Magnitude of tensile stress has increased around the wellbore compared to Figure 6.3, meaning fracture initiation and propagation are more likely to occur.

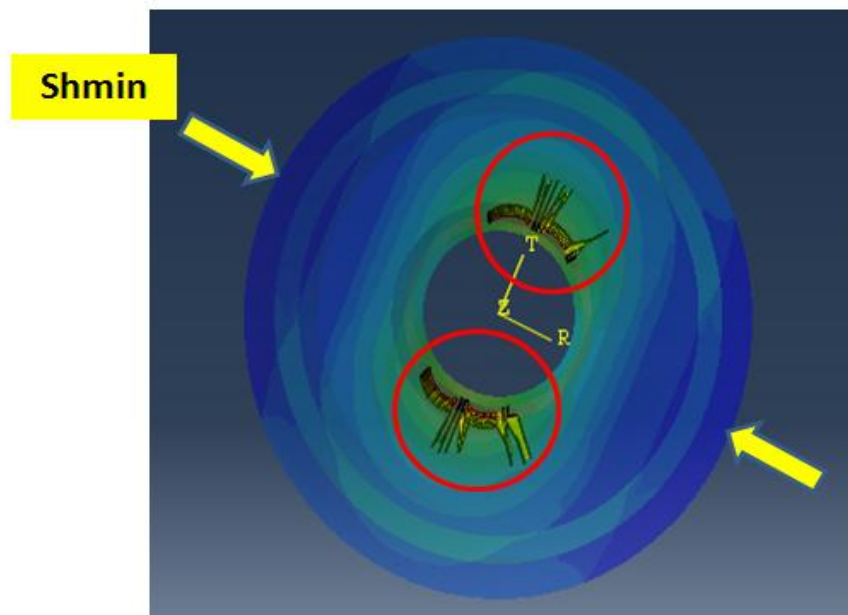


Figure 6.5: Fracture development using XFEM on the sub model analysis

Figure 6.5 shows the results after running XFEM on the block. It can be seen that fractures are developed in the tensile zone of the block as expected. Since the fractures are developed near the wellbore and will not likely extend all the way to the edge of the block, a sub-model was created to reduce computational time. As shown in Figure 6.5, the fractures are developed in direction of maximum horizontal stress ( $S_{hmax}$ ), while they open against the minimum horizontal stress ( $S_{hmin}$ ). The strong similarities between leak-off tests and fracture initiation and propagation could be utilized in modeling lost circulation and wellbore strengthening design, taking into account of bridging materials used in an LCM (Gray, 2011)

## Chapter 7: Compressibility

This chapter includes the effect of compressibility on leak-off test trend.

### 7.1 COMPRESSIBILITY EFFECT

Compressibility is the relative volume change of materials as a response to a pressure change. The higher the compressibility of a material is, the larger the volume change is. Geertsma (1957) suggests three different types of compressibility: 1. Rock matrix compressibility 2. Pore compressibility 3. Bulk compressibility.

#### 7.1.1 Rock Matrix Compressibility

Rock matrix compressibility is defined as the fractional change in volume of the solid rock material (rock grains) with a unit change in pressure (Ahmad, 2010). This can be expressed mathematically as follow:

$$C_r = -\frac{1}{V_r} \left( \frac{\partial V_r}{\partial P} \right)_T \quad (7.1)$$

Where,

$C_r$  = rock matrix compressibility (1/psi)

$V_r$  = volume of rock matrix (ft<sup>3</sup>)

$P$  = external pressure (psi)

The subscript T means that the change of volume respect to change in pressure is taken at constant temperature.  $C_r$  is always positive. Since the pressure change is positive and change in volume is negative, the negative sign in equation is introduced to force  $C_r$

to be positive. Volume is function of the pressure change only since temperature and amount of material are assumed to be constant.

### 7.1.2 Pore Compressibility

The pore compressibility is defined as the fractional change in pore volume of the rock with a unit change in pressure (Ahmad, 2003) and given by the following relationship:

$$C_p = C_f + S_w C_w \quad (7.2)$$

Where,

$C_p$  = pore compressibility (1/psi)

$V_p$  = pore volume (ft<sup>3</sup>)

$P$  = pore pressure (psi)

### 7.1.3 Bulk Compressibility

The bulk compressibility is defined as the fractional change in volume of the bulk volume of the rock with a unit change in pressure (Ahmad, 2010). It can be define as follow:

$$C_B = -\frac{1}{V_B} \left( \frac{\partial V_B}{\partial P} \right)_T \quad (7.3)$$

$C_B$  = bulk compressibility (1/psi)

$V_B$  = bulk volume of the rock (ft<sup>3</sup>)

$P$  = pore pressure (psi)

### 7.1.4 Compressibility Formulations

For most formations, the rock and bulk compressibilities are considered small in comparison with the pore compressibility (Ahmad, 2010). Therefore, the formation compressibility is set equal to pore compressibility as follow:

$$C_f = C_p = -\frac{1}{V_p} \left( \frac{\partial V_p}{\partial P} \right)_T \quad (7.4)$$

Where,

$C_f$  = formation compressibility (1/psi)

Typical values for formation compressibility range from  $3 \times 10^{-6}$  to  $25 \times 10^{-6}$  psi<sup>-1</sup> (Ahmed, 2013). The total compressibility of any formation is governed by its fluid compressibilities. For instance in a hydrocarbon reservoir the total compressibility is:

$$C_t = (1 - \phi)C_f + \phi(S_o C_o + S_w C_w + S_g C_g) \quad (7.5)$$

Where,

$C_t$  = total compressibility (1/psi)

$\phi$  = porosity (fraction)

$S_o, S_w,$  and  $S_g$  = oil, water, and gas saturations (unit less)

$C_o, C_w,$  and  $C_g$  = oil, water, and gas compressibility (1/psi)

Leak-off tests are all done in non-hydrocarbon bearing formations which are mostly saturated with water. Therefore, compressibility of oil and gas are not taken into account. So the Equation 7.5 becomes:

$$C_t = (1 - \phi)C_f + \phi S_w C_w \quad (7.6)$$

A non-porous solid model is assumed. Therefore, equation 7.6 is reduced to:

$$C_t = C_f \quad (7.7)$$

## 7.2 COMPRESSIBILITY OUTCOME

A wellbore at any depth could have different sequences such as mud inside the wellbore, casing, cement, and formation as shown in Figure 7.1. It is known that after 5 to 8 wellbore radii, the hoop stress dies out and stress become in-situ stress (Advanced Drilling and Completion course taught by Gray in Spring 2013). In Figure 7.1  $\sigma_{h_{min}}$  is the minimum effective in-situ horizontal stress. Each of these materials has different compressibility. During a leak-off test, wellbore is pressurized and pressure change is introduced. Along with this pressure change and compressibility of materials within vicinity of the wellbore, the volume can be changed. Therefore, this volume change can affect the volume recorded during the leak-off test.

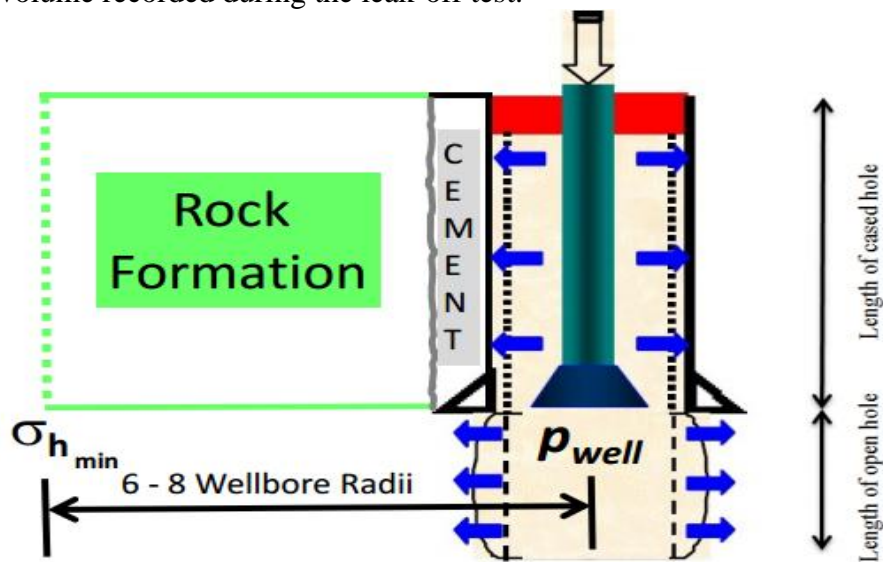


Figure 7.1: Approach adapting Altun's model to include cement and formation (Adapted from Altun, 2001) copied from (Gray, 2013)

### 7.2.1 Volume Change Due to Compressibility

The volume change of the formation due to compressibility effect is studied as shown in Figure 7.1. Figure 7.2 shows the schematic calculation.

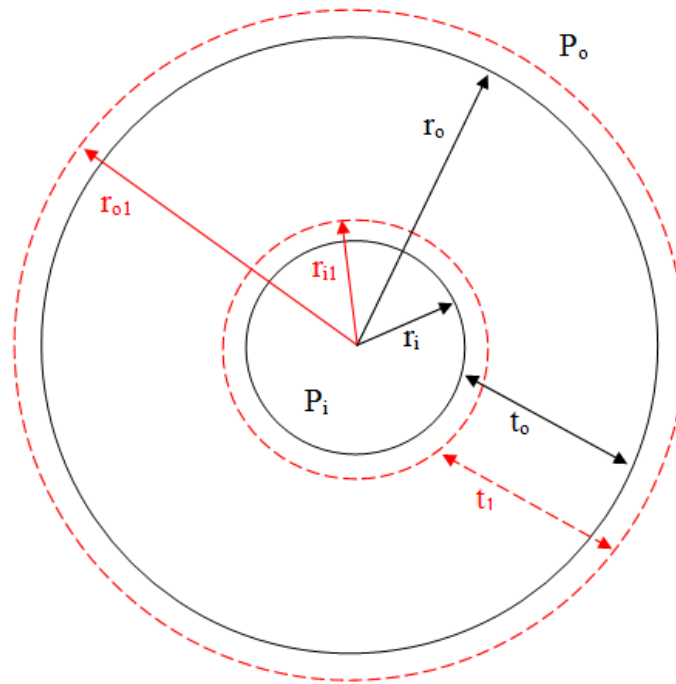


Figure 7.2: Volume calculation including compressibility effect (Gray, 2013)

$P_o$  and  $P_i$  are the outside and inside pressures applied on the wellbore respectively.  $P_i$  tries to push the wellbore out; while  $P_o$  is pushing the formation against the wellbore. At time zero, when there is no pressure change, the volume of the rock is calculated as follow:

$$A_o = \pi(r_o^2 - r_i^2) \quad (7.8)$$

$$Vol_o = A_o h \quad (7.9)$$

$$t_o = (r_o - r_i) \quad (7.10)$$



$$A_1 = \pi(r_{o1}^2 - r_{i1}^2) \quad (7.11)$$

$$Vol_1 = A_1 h \quad (7.12)$$

$$t_1 = (r_{o1} - r_{i1}) \quad (7.13)$$

Where,

$A_o$  = initial area of the formation

$A_1$  = area of the formation during pressure change

$r_o$  = outer formation radius

$r_{o1}$  = outer formation radius after volume change

$r_i$  = cement outer radius

$r_{i1}$  = cement outer radius after volume change

$h$  = height of the zone

$Vol_o$  = initial volume of the formation

$Vol_1$  = volume of the formation during pressure change

$t_o$  = thickness of the formation

$t_1$  = thickness of the formation after volume change

Formation compressibility equation is modified to a simple ratio of change in volume to pressure change as follow:

$$C_f = C_p = -\frac{1}{V_p} \left( \frac{\Delta V_p}{\Delta P} \right)_T \quad (7.14)$$

Rearrange for  $Vol_1$ :

$$Vol_1 - Vol_o = -Vol_o C_f \Delta P \quad (7.15)$$

$$Vol_1 = Vol_o(1 - C_f \Delta P) \quad (7.16)$$

There are three variables in Equation 7.15 that must be studied individually. A MATLAB program was developed to examine the effect of these parameters. In each example, one of the variables is changed versus outer radius ( $r_i$ ) while keeping the other two variables constant. Tests shown here were done for 5 to 8 times the wellbore radius. Figure 7.3 to 7.14 shows the results of these parameters. In this study, the formation and cement are taken as a single, non-porous solid region.

Results for 5 times the wellbore:

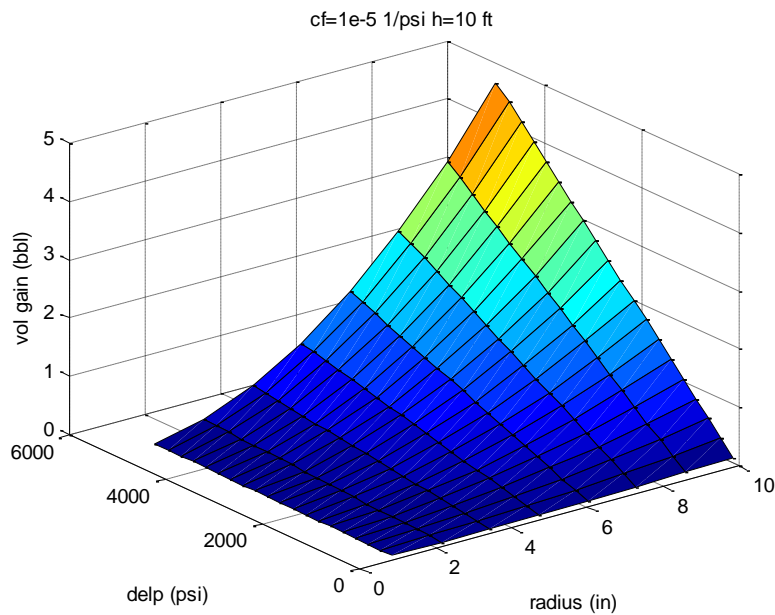


Figure 7.3: Volume change response to pressure change for 5 times the radius

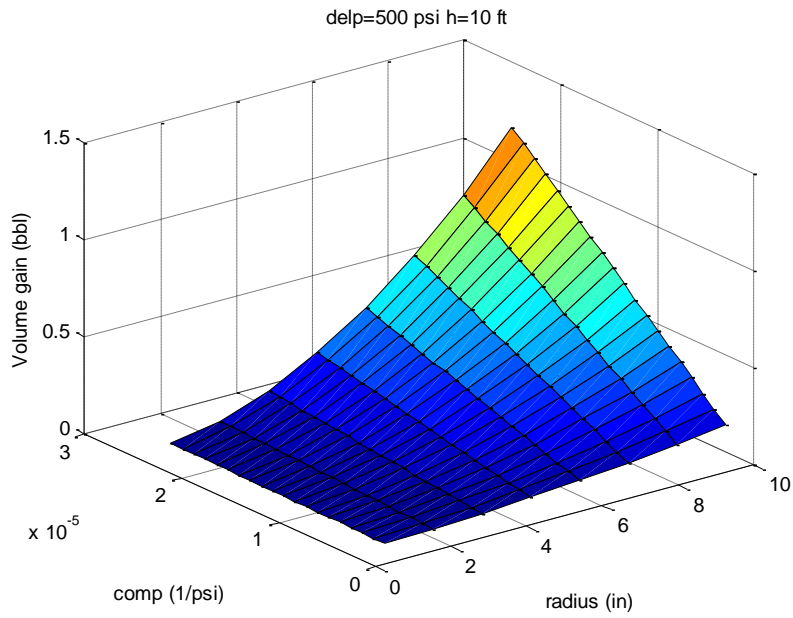


Figure 7.4: Volume change response to compressibility change for 5 times the radius

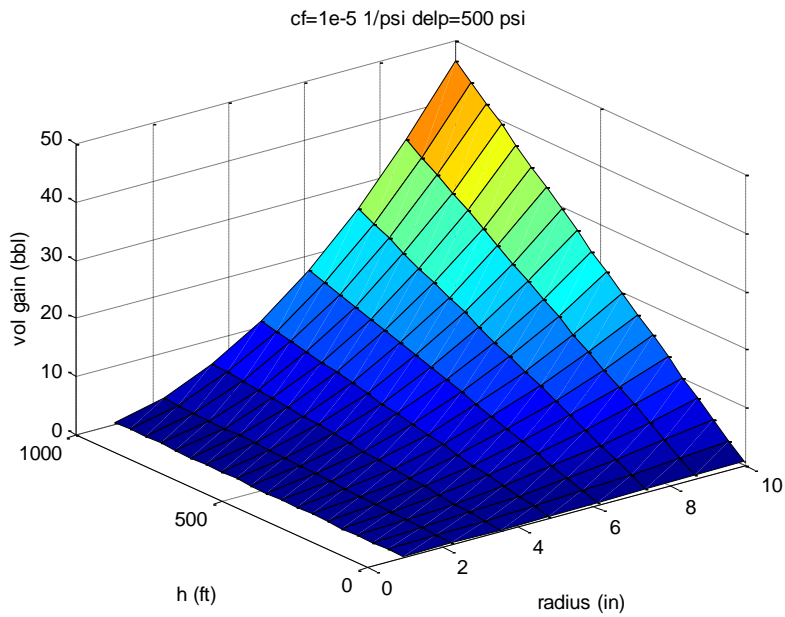


Figure 7.5: Volume change response to height change for 5 times the radius

Results for 6 times the wellbore radius:

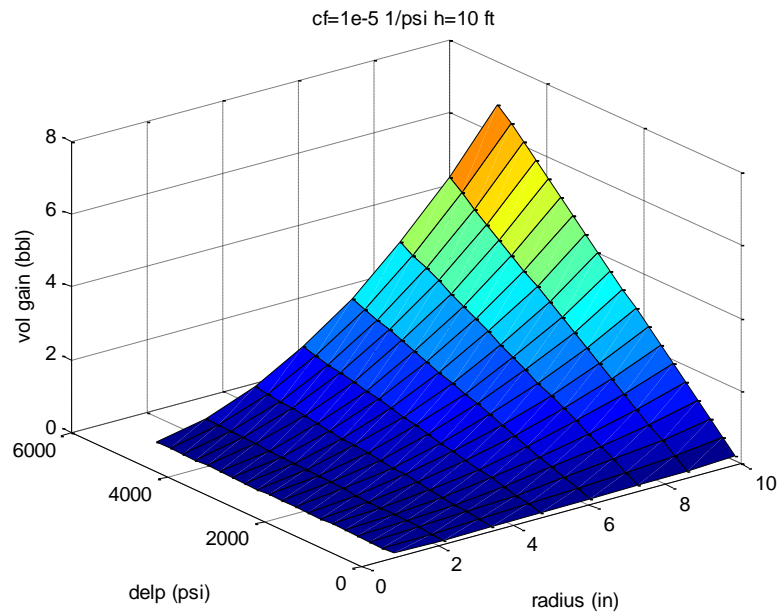


Figure 7.6: Volume change response to pressure change for 6 times the radius

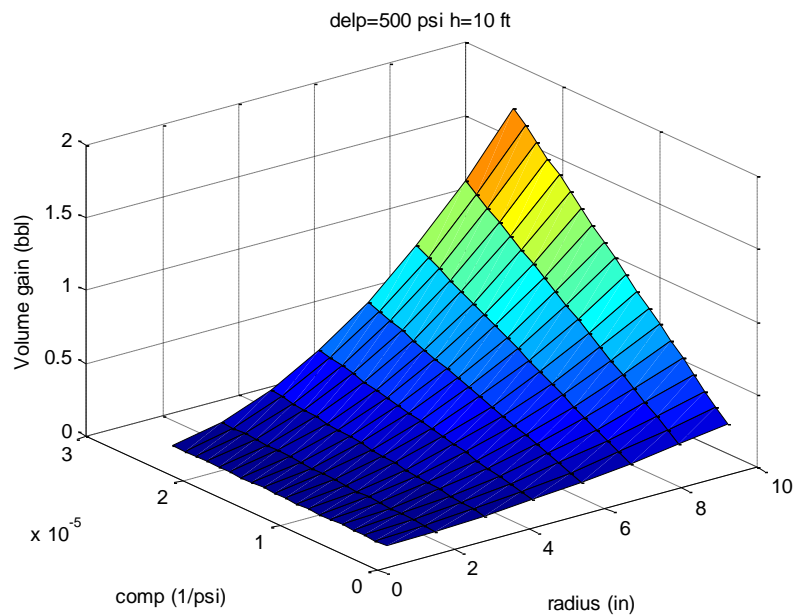


Figure 7.7: Volume change response to compressibility change for 6 times the radius

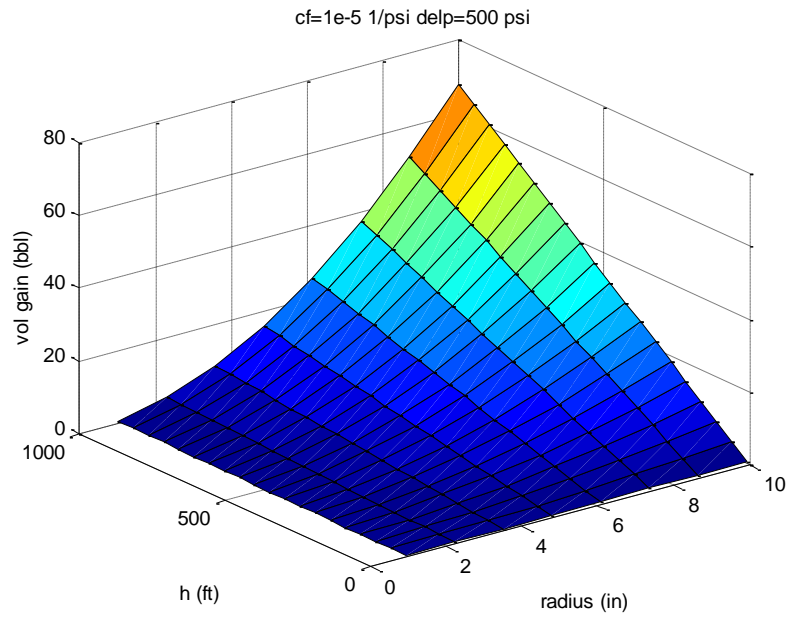


Figure 7.8: Volume change response to height change for 6 times the radius

Results for 7 times the wellbore:

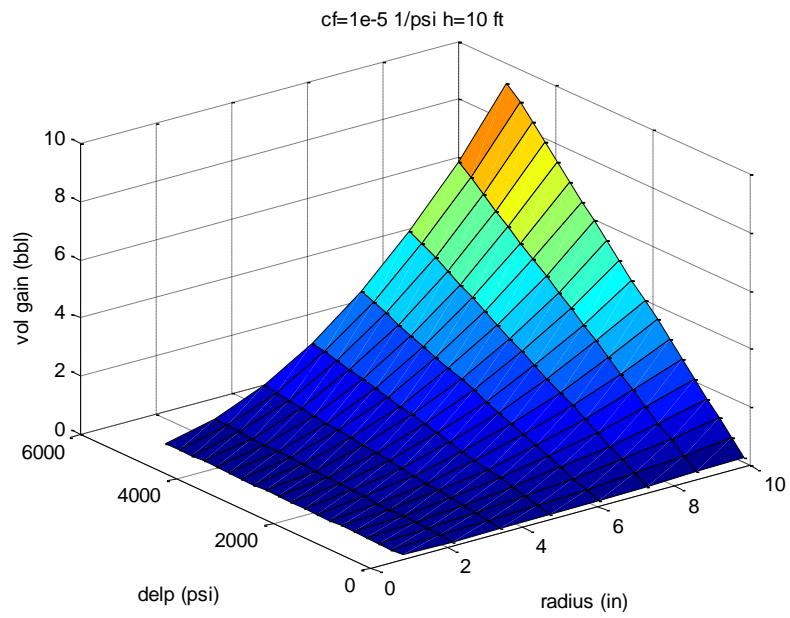


Figure 7.9: Volume change response to pressure change for 7 times the radius

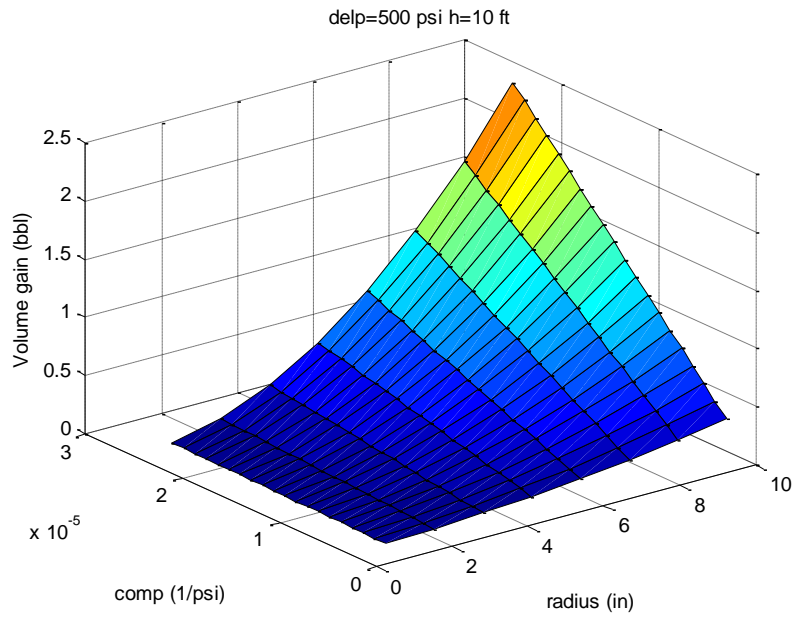


Figure 7.10: Volume change response to compressibility change for 7 times the radius

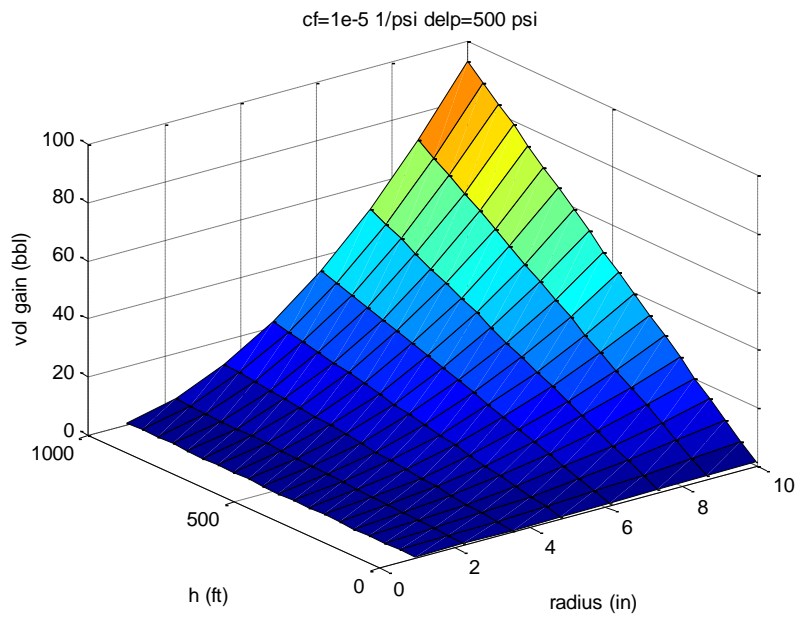


Figure 7.11: Volume change response to height change for 7 times the radius

Results for 8 times the wellbore:

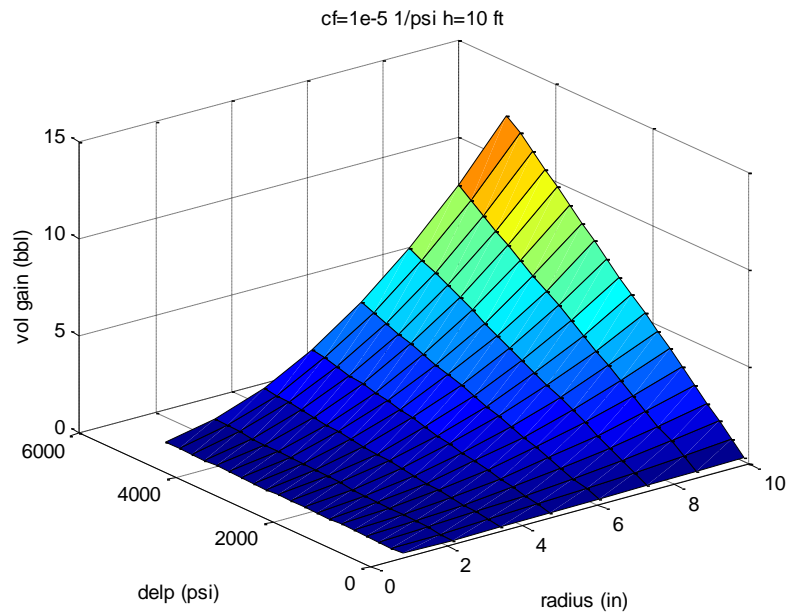


Figure 7.12: Volume change response to pressure change for 8 times the radius

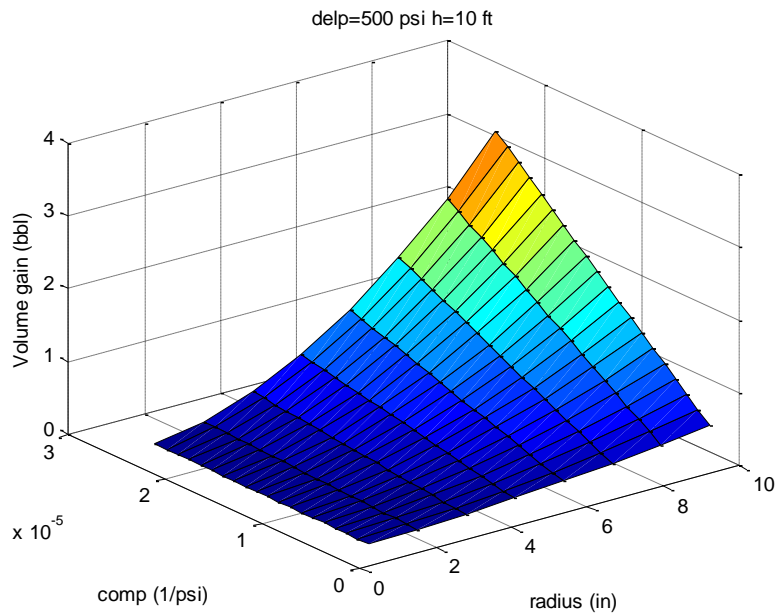


Figure 7.13: Volume change response to compressibility change for 8 times the radius

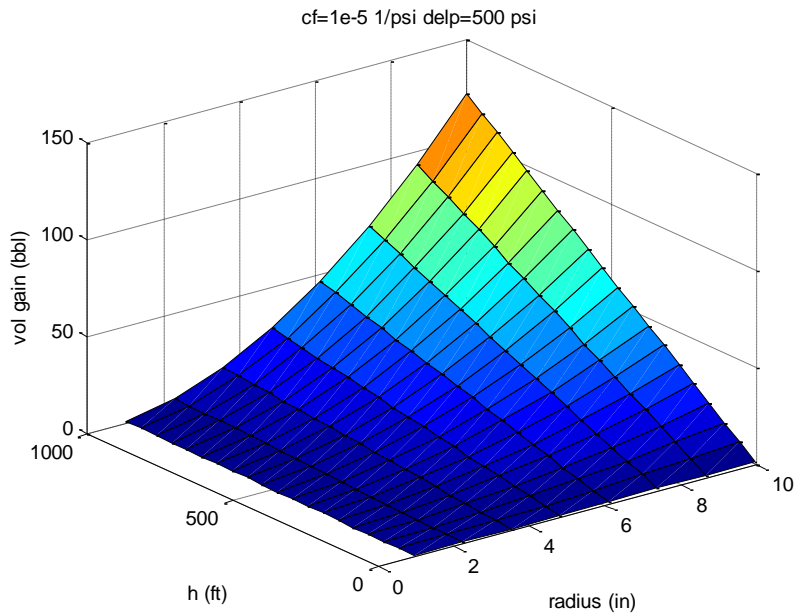


Figure 7.14: Volume change response to height change for 8 times the radius

As shown in Figure 7.3 to 7.14, pressure change, compressibility, and height of the formation have influenced the volume change during a leak-off test. However, their effects aren't identical. It is obvious that the height of the formation is a critical one since it has a very substantial effect on volume change. Of course, as the lateral investigation increases i.e. 5 to 8 times the wellbore, there is more formation volume. Therefore, the change in the volume gain increases substantially. Figure 7.15 shows the comparison of volume gain with respect to the lateral distance. A cement sheath's outer radius of 7 inches and pressure difference of 500 psi were assumed. The height of the zone was varied from 10 to 100 ft in this study.  $x$  tells how big is the lateral depth. For example,  $8x$  means 8 times the outer cement sheath radius.



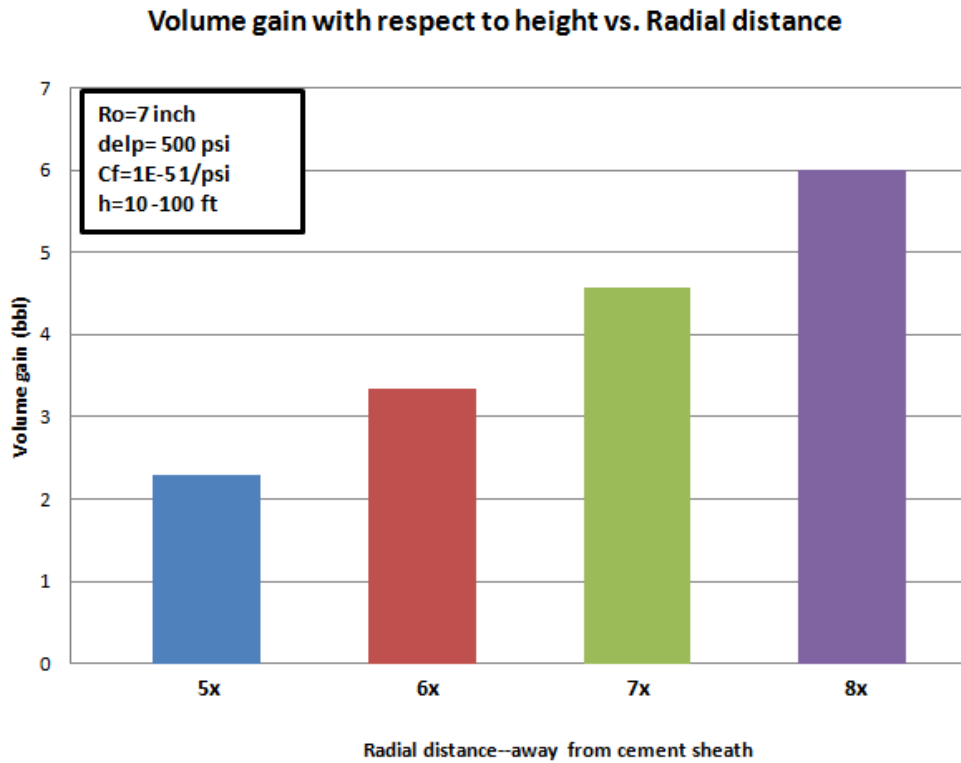


Figure 7.15: Lateral distance effect on volume gain with varying height for 10-100ft, and constant pressure difference and formation compressibility

In this study the effect of the porosity is neglected, as well that compressibility of the water that saturates the formation. The compressibility is ranges from  $3 \times 10^{-6}$  to  $25 \times 10^{-6}$   $\text{psi}^{-1}$  which is the typical value of rock formation's compressibility (Ahmad, 2010).

## Chapter 8: Software Development

### 8.1 HORIZONTAL STRESS ESTIMATION

During a leak-off test the wellbore pressure pushes out against the stresses around the wellbore, as shown in Figure 8.1. The hoop stress around the wellbore is determined by horizontal far-field stresses.

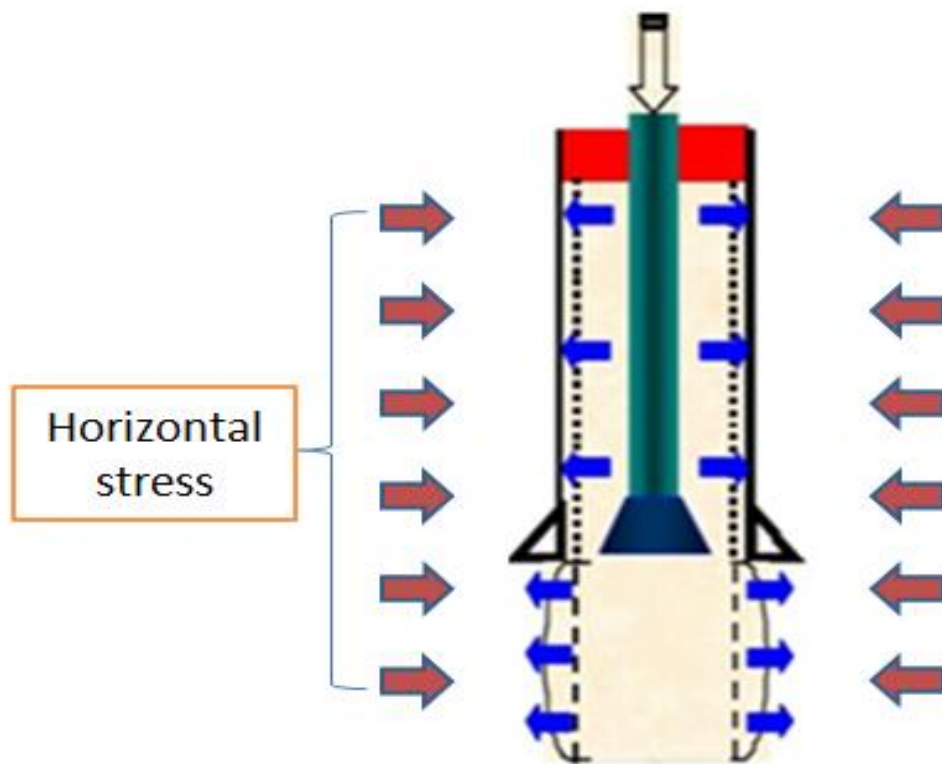


Figure 8.1: Horizontal stress schematic (Adapted from Altun, 2001)

If it is assumed that the wellbore is similar to Figure 4.2, then the horizontal stresses around the wellbore are isotropic, and  $S_{hmin}$  is equal to  $S_{hmax}$ . Since the pressure inside the wellbore is known, Norris' solution can be used to estimate the horizontal stress, with proper boundary conditions.

## **81.1 Procedures and Assumptions**

The procedures are as follows:

1. Relate the minimum horizontal stress to overburden stress using an estimate based on geological data.
2. Since Norris' solution assumes isotropic stresses, minimum and maximum horizontal stresses are equal.
3. There is no more volume change prior to leak-off test. Using this assumption, the line should start from the origin or at last very close to it. The initial volume gain is set to be zero or very close to zero.
4. The estimate is changed, and then iterated, until the previous step is met.

## **8.2 MATLAB SOFTWARE**

After incorporating the new sub-systems (cement and formation) into the model, a MATLAB Graphical User Interface (GUI) was developed to facilitate user data input with a graphical interface used to create different fields such as pull down tabs, text box, etc. Figure 8.2 illustrates the menu for creating a GUI. This tool box is accessed by typing "guide" in the command window of MATLAB. "Blank GUI" is used for this software.

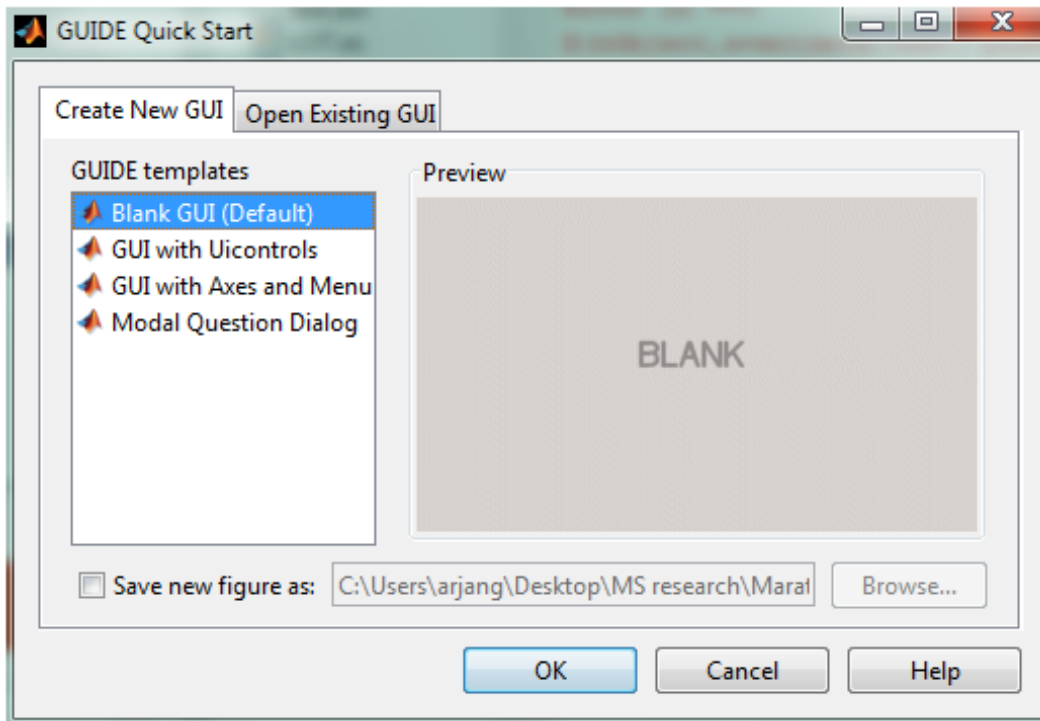


Figure 8.2: MATLAB GUI startup menu

Next step was to create tabs and field on a blank GUI page. These tabs and fields will be used for data input as shown in Figure 8.3. The user will define the function of these fields. For instance, a field can be a plain text box showing a phrase, or a drop down menu. In Figure 8.3, the “Browser” field is a popup tab that imports data from an Excel file. “Execute” tab run the model that is embedded in this GUI. The other fields are used to type in the value of the data by user. “axes 5” is the right bottom corner is used to show the logo. The positions of these fields can be modified by either dragging the field or by entering position points in their menus.

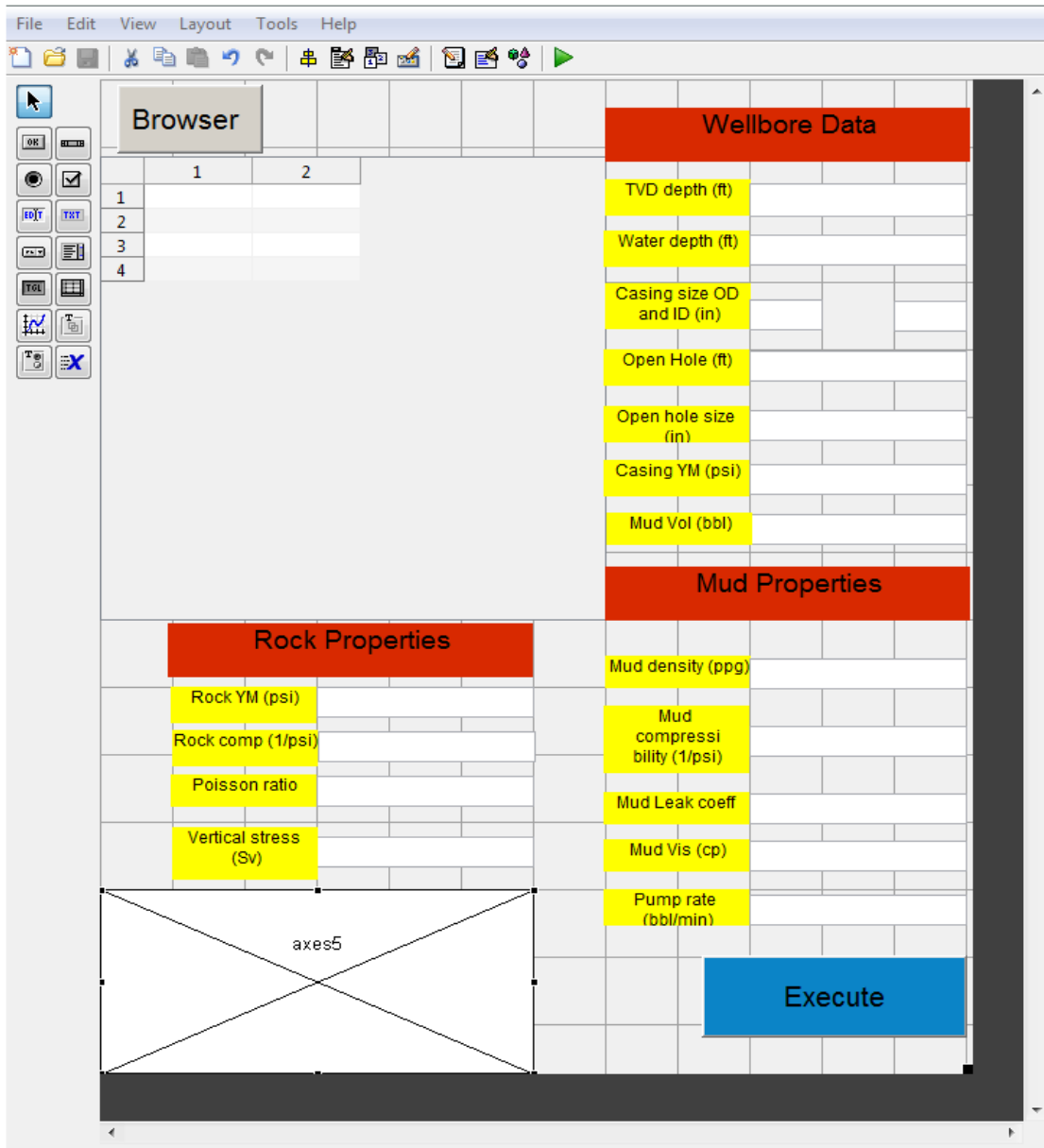


Figure 8.3: Wider Windows GUI layout

The final product of this MATLAB GUI is shown in Figure 8.4. Data can be exported and executed for results.

Browser	
	1      2
1	
2	
3	
4	


Wellbore Data	
TVD depth (ft)	<input type="text"/>
Water depth (ft)	<input type="text"/>
Casing size OD and ID (in)	<input type="text"/> <input type="text"/>
Open Hole (ft)	<input type="text"/>
Open hole size (in)	<input type="text"/>
Casing YM (psi)	<input type="text"/>
Mud Vol (bbl)	<input type="text"/>

Mud Properties	
Mud density (ppg)	<input type="text"/>
Mud compressibility (1/psi)	<input type="text"/>
Mud Leak coeff	<input type="text"/>
Mud Vis (cp)	<input type="text"/>
Pump rate (bbl/min)	<input type="text"/>

Rock Properties	
Rock YM (psi)	<input type="text"/>
Rock comp (1/psi)	<input type="text"/>
Poisson ratio	<input type="text"/>
Vertical stress (Sv)	<input type="text"/>

The diagram shows a wellbore cross-section with three pressure profiles:  $p_{pore}$  (pore pressure),  $p_{mud}$  (mud pressure), and  $p_{frac}$  (fracture pressure). The  $p_{pore}$  profile is shown as a dashed green line,  $p_{mud}$  as a solid black line, and  $p_{frac}$  as a dashed red line. A blue arrow points from the  $p_{pore}$  profile towards the wellbore wall.

Figure 8.4: Wider Windows LOT software menu

An advantage of MATLAB GUI is that this program can be easily converted into an .exe file or added to a Microsoft Excel file. It can also be converted to Android and iOS platform, so it can be run on mobile devices such as tablets or smart phones.

### 8.3 RESULTS

The program was tested with a set of field data provided by Marathon Oil Company (Wider Window's sponsor). The data are provided in Table 8.1. Also, Figure 8.5 shows additional data inputted in the software.

Tables 8.1: Wellbore data from program sponsor

Location	Gulf of Mexico (GOM)	
Water depth	80	ft
Mud type	Oil Based Mud (OBM)	
Young's Modulus (Rock)	$3 \times 10^6$	psi
Young's Modulus (Casing)	$30 \times 10^6$	psi
Poisson's Ratio	0.3	
TVD	15,832	ft

Browser		
	v	p
1	0	0
2	0.5000	130
3	1	215
4	1.5000	315
5	2	410
6	2.5000	500
7	3	590
8	3.5000	650
9	4	670

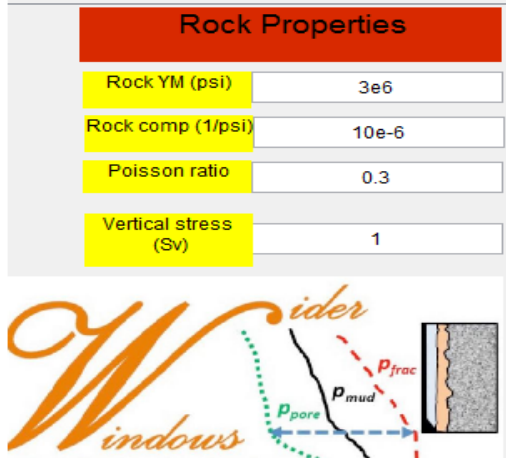
Wellbore Data

TVD depth (ft)	15832	
Water depth (ft)	80	
Casing size OD and ID (in)	8.417	7.5
Open Hole (ft)	1	
Open hole size (in)	9.5	
Casing YM (psi)	30e6	
Mud Vol (bbl)	930	

Mud Properties

Mud density (ppg)	18.1
Mud compressibility (1/psi)	3.6e-6
Mud Leak coeff	3.3e-4
Mud Vis (cp)	120
Pump rate (bbl/min)	0.5

Execute



The diagram shows a wellbore cross-section with a fracture. Labels include  $P_{pore}$  (pore pressure),  $P_{mud}$  (mud pressure), and  $P_{frac}$  (fracture pressure). The wellbore is labeled 'Wider' and 'Windows'.

Figure 8.5: LOT example

Due to lack of information, data were assumed for rock properties, mud compressibility and leak coefficient, casing' Young Modulus and inner radius, and open hole size. After executing the program, a series of graphs are shown. Figure 8.6 is the LOT curve history match.



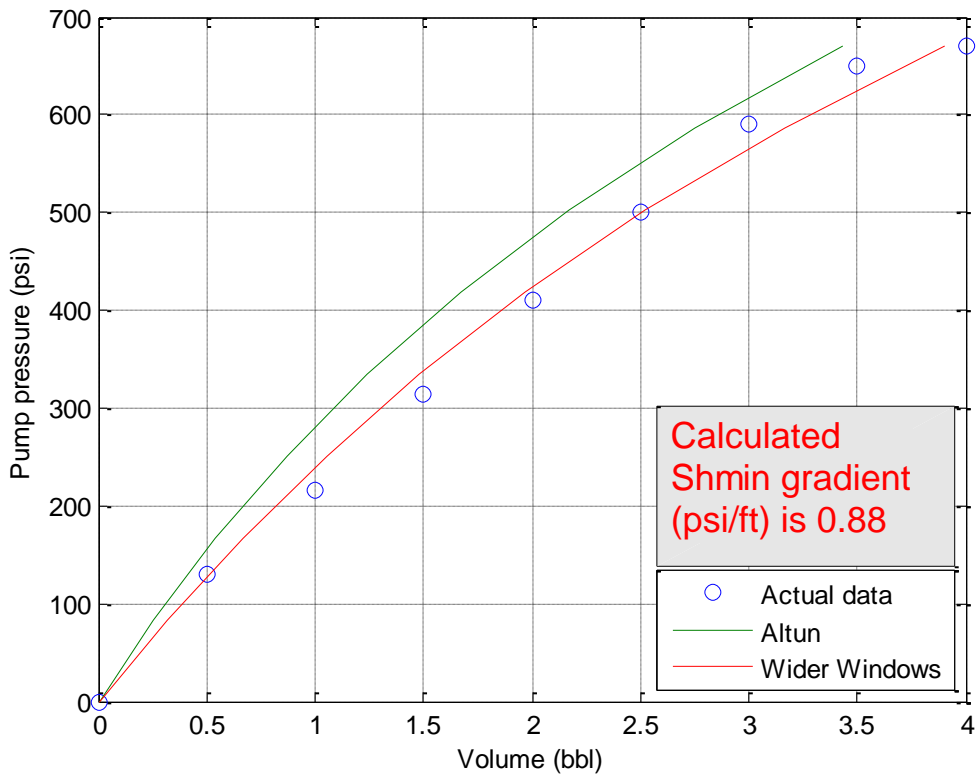


Figure 8.6: LOT curve match by Wider Windows and Altun models

As shown in Figure 8.6, a better match is predicted by Wider Windows model compared to Altun’s model. This improvement is due to the addition of formation compressibility effect on the entire system. Also, in Wider Windows, the user has the advantage to vary the leak coefficient for a better fit, while, Altun’s model predicts leak coefficient based on Poiseuille’s flow theorem. In this theorem, the user must define the fracture width and height which are not trivial to compute, so assumed values are used for them. Since horizontal far field stresses in the GOM are almost equal (low anisotropy) (Salehi and Nygaard 2012), the Wider Windows LOT model simulates leak-off volume, leak-off behaviors, and far field stress.

Figure 8.7 shows the minimum horizontal stress trend based on the predicted value from the program using Norris' solution.

Figure 8.8 shows fracture profile using the PKN model (Perkins and Kern 1961). The PKN model is suitable for a narrow/medium width fracture whose length is greater than its height. Height of the fracture is assumed to be the open hole interval used for the LOT. Note thermal effect is not included since field data were not available for it. However, Wider Windows model still produced a good result. This is because the total mud volume inside the system was reported before the LOT. This means that the reported volume already includes volume change due to thermal effect.

The fracture profile based on PKN model, in Figure 8.8, could be used as a guideline for LCM selection for the zone in which the LOT was conducted.

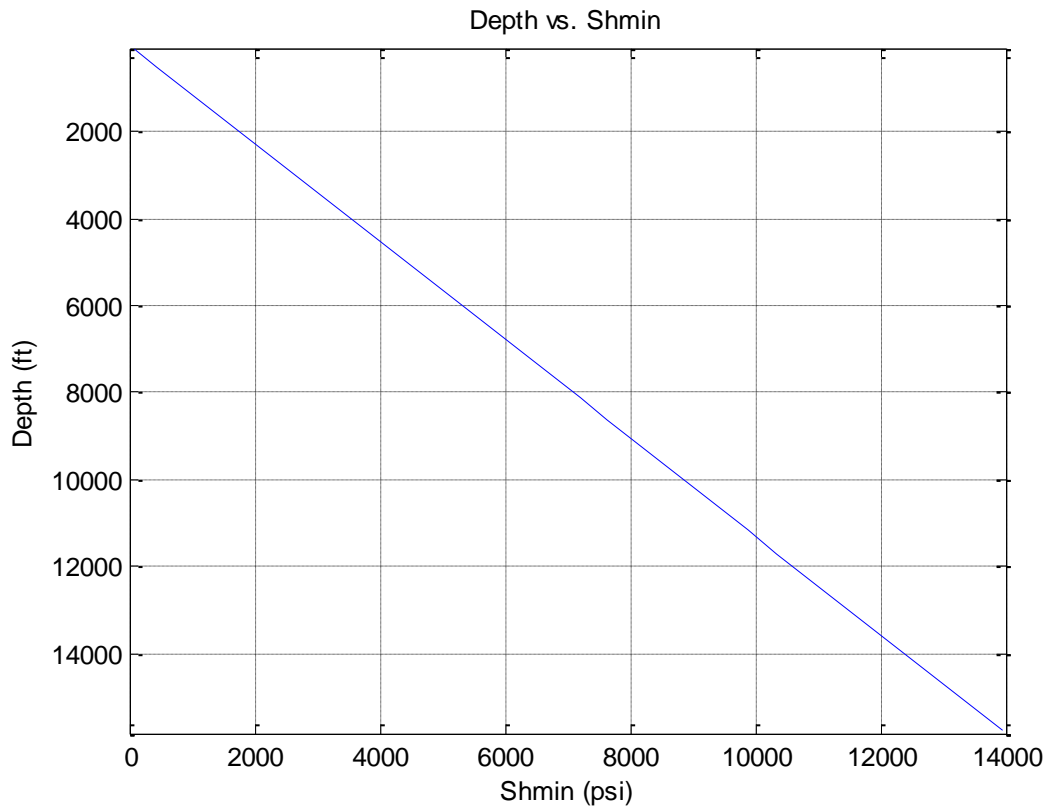


Figure 8.7: Shmin trend based on the Shmin gradient predicted by the software shown in Figure 8.6

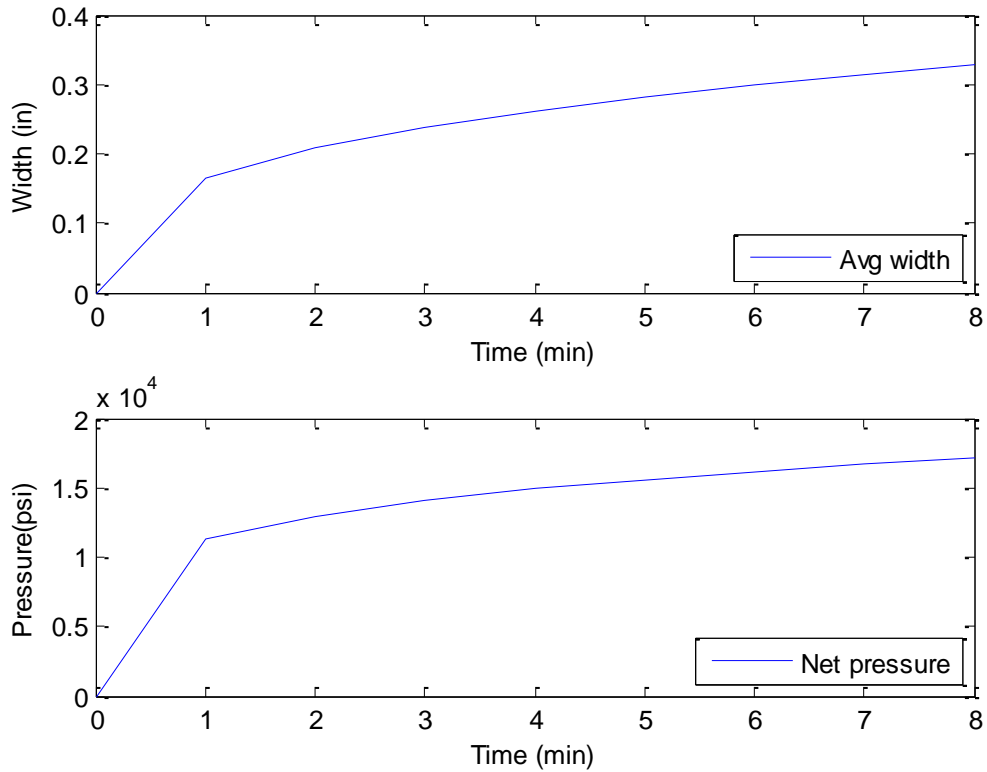


Figure 8.8: Fracture profile calculated based on PKN model

### 8.3.1. Model Advantages

The advantages of Wider Windows model are:

1. The model can estimate  $Sh_{min}$ , based on Norris' solution.
2. User can estimate a leak-off coefficient on a trial and error basis.
3. It can be used for both LOT and FIT (formation Integrity Test).
4. The user may find and correct erroneous reported data.

An example of the software's functionality is seen in Figure 8.9 which is a fit for an FIT test. The value for mud compressibility was used as  $8.2 \times 10^{-6}$  1/psi. However, OBM's compressibility is usually between  $3$  to  $4 \times 10^{-6}$  1/psi (Alberty and McLean 2014).

The indicated compressibility is higher than the usual OBM upper bound compressibility. The system likely has some trapped air or gas. After correcting the data, the model shows the new trend in Figure 8.10.

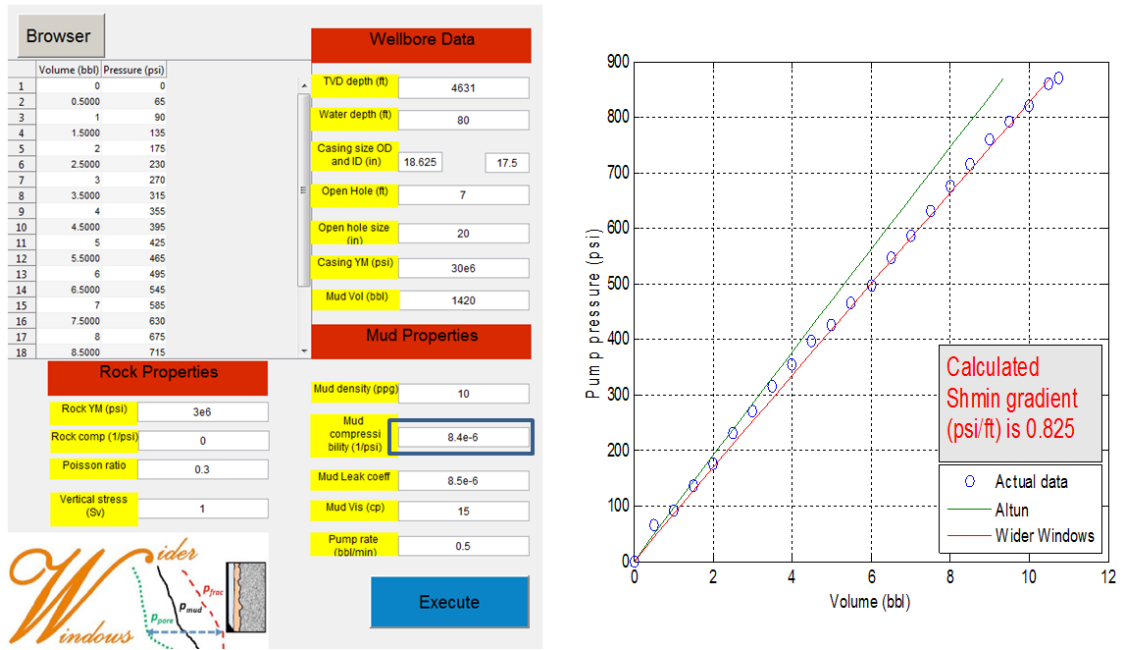


Figure 8.9: Erroneous FIT data due to trapped air or gas inside the wellbore

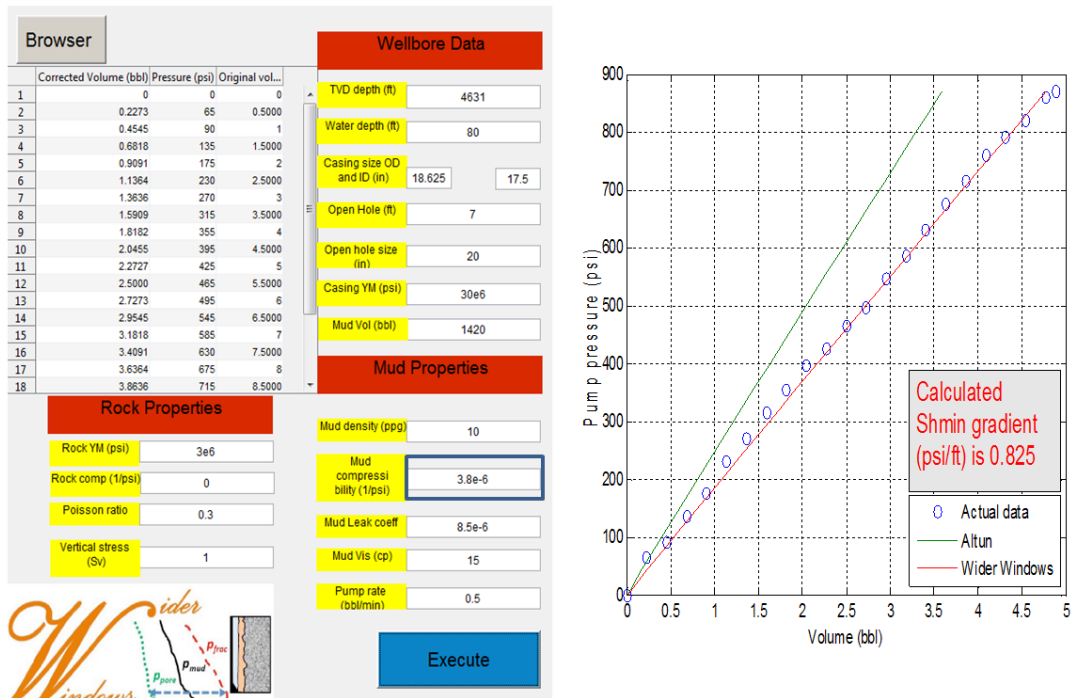


Figure 8.10: Corrected FIT data after subtracting the trapped air or gas from the system

## 8.2.2 Model Disadvantages

The disadvantages of the model are:

1. Linearly elastic, homogenous, and isotropic assumptions are limiting. Poro-elastic cement and formation behavior and compressibilities add to non-linear system behavior. However, for initial model simplicity, these assumptions are employed for comparison with existing models.
2. Minimum horizontal stress ( $S_{hmin}$ ) often is not equal to maximum horizontal stress ( $S_{hmax}$ ). The level of anisotropy depends on geological events as well as the location. For instance, in the GOM the anisotropy between  $S_{hmin}$  and  $S_{hmax}$  is very low (Salehi and Nygaard 2012). In this paper, they were assumed to be equal.

3. The PKN model is a one dimensional and asymptotic model. It may have limited utility in prediction of fracture profile.

#### 8.4 PKN MODEL FORMULATION

PKN is a classic model developed by Perkins, Kern, and Nordgren. Configuration of the model is shown in Figure 8.11. It is used when the fracture length is much greater than the fracture height. The model assumes: 1. that the fracture is confined by bounding layers of top and bottom formations, and 2. the fracture only grows in the lateral direction (Perkin and Kern, 1961 and Nordgren, 1972).

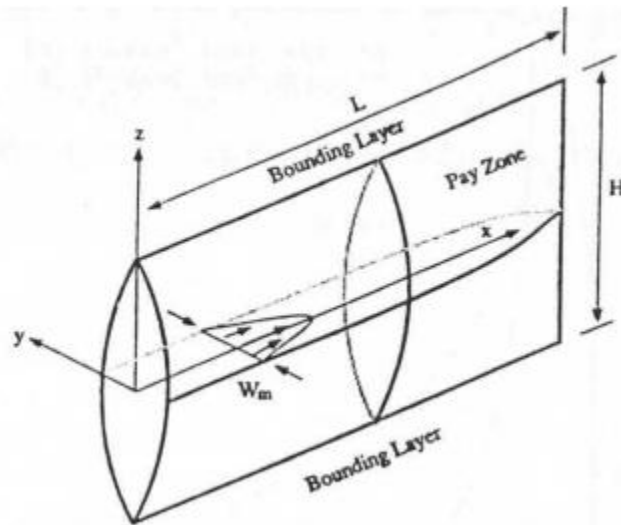


Figure 8.11: PKN fracture design (modified after Gidley et al., 1989, from Abousleiman et al., 1996)  $H$  is the height of the fracture and  $W$  stands for width of the fracture.

For convenience, equations for PKN model (John Olson's Hydraulic Fracturing course (PGE 383) at the University of Texas at Austin in Spring 2014) are used here.

$$x_f = 34.864 \left( \frac{q^3 E_p}{\mu h^4} \right)^{0.5} t^{\frac{4}{5}} \quad (8.1)$$

$$W_{avg} = 0.288 \left( \frac{q \mu x_f}{E_p} \right)^{0.25} \quad (8.2)$$

$$W_{max} = 0.4176 \left( \frac{q \mu x_f^2}{h E_p} \right)^{0.25} \quad (8.3)$$

$$P_{frac} = 0.0193 \left( \frac{q \mu x_f E_p^3}{h^4} \right)^{0.25} \quad (8.4)$$

Where,

$E_p = \frac{E_f}{1 - \nu^2}$  = effective Young's Modulus of formation (psi)

$E_f$  = formation Young's Modulus (psi)

$\nu$  = Poisson's ratio (unitless)

$x_f$  = fracture half length (ft)

$q$  = pump rate (bbl/min)

$t = \frac{\text{Volume}_{pumped}}{q}$  time (min)

$\text{Volume}_{pumped}$  = actual volume pumped during LOT

$h$  = formation height (ft)

$\mu$  = fluid viscosity (cp)

$W_{avg}$  = average fracture width (in)

$W_{max}$  = maximum fracture width (in)

$P_{frac}$  = pressure inside the fracture (psi)



## **Chapter 9: Conclusion and Recommendation**

### **9.1 WIDER WINDOWS MODEL**

Wider Windows model is based on Norris' solution (Norris, 2003) which is a concentric cylindrical model based on Lamé equations. With these solutions, the effects of other sub-systems that go beyond casing, such as cement and formation, are evaluated. Estimating horizontal stress based on this model was one of the advantages of Norris' solution. Altun's and previous LOT models only incorporated volume gain due to casing expansion, however, Wider Windows' Multi cylinders approach calculate displacements of casing, cement, and formation. Based on these displacements and volume changes, the volume of the system can be computed more accurately during a LOT test. The model improves interpretation of routine leak-off tests, especially non-linear trends and erroneously recorded data. Using Norris' solution, the estimation of minimum horizontal stress can be achieved with the pressure inside the wellbore and far-field stresses taken into account.

#### **9.1.1 Sub-Systems**

Additional sub-systems such as cement and formation were studied in this research. However, they both were incorporated as a single region for simplicity, since there were no data available for each. Cements can be designed to be very compressible or change characteristics with the temperature of the formation over time. Even though these two regions were treated as one, the improvement were significant compared to Altun's model as shown in Chapter 8.

## **9.2 NON-LINEARITY**

It has been assumed that the non-linear part of LOT trend is from mud leakage to the formation. However, when the compressibility of the formation is taken into account, it was shown that the changes are non-linear with change in pressure, height of the exposed formation, lateral distance, as well as the compressibility of the formation. As shown in Figures 7.5, 7.8, 7.11, and 7.14, the exposed interval of the formation has a major effect on volume change of the formation, a significant additional finding of this research.

## **9.3 FRACTURE PROFILE**

Fracture profile that is produced by this model is based on PKN model. This preliminary model is a guideline for LCM selection in a lost circulation event. Of course, PKN is a limited one dimensional and asymptotic model, but it still produces meaningful trends that could aid the user.

## **9.4 FUTURE WORK RECOMMENDATION**

Future models should be based on a conservative analytical model such as Bradley's equations that incorporate von Mises failure envelope and stress cloud using  $J_2^{1/2}$  function (Bradley 1979). Also, the future model should be extended to incorporate additional capabilities that allow selectable history matching of operational well construction scenarios, with particular application to lost circulation situations, fracture initiation, propagation, and closure, flow-back testing, wellbore ballooning and breathing, and others. Several additional capabilities the need to be incorporated into the future model are:

- Downhole fracture initiation, propagation and closure
- Fluid loss into fractures and into formation matrix through wellbore wall and fracture faces

- Effect of filter cakes on wellbore wall and fracture faces
- Effect of rock permeability and porosity
- unequal horizontal far-field stresses, superposed Lamé and Kirsch equations with and without pore pressure
- non-linear, elastic rock behavior
- non-elastic rock behavior
- operationally significant time-lapse studies
- Thermal effects in any of the above

Once the future model has been calibrated with field LOT data and its reliability established, then it could be used to investigate behavior of fractures as integral parts of an LOT.

## Nomenclature

BOP: Blow out preventer

FCP: Fracture closure pressure

FIP: Fracture initiation pressure

FIT: Formation integrity test

FPP: Fracture propagation pressure

FRP: Fracture reopening pressure

GOM: Gulf of Mexico

GUI: Graphical User Interface

ISIP: Instantaneous shut in pressure

LCM: Lost circulation material

LOT: Leak-off test

LP: Limit pressure

OBM: Oil based mud

PKN: Perkins, Kern, and Nordgern

ppg: pounds per gallon

SBM: Synthetic based mud

Shmax: Maximum horizontal stress

Shmin: Minimum horizontal stress

SMS: Shallow marine sediments

SPP: Stop pump pressure

TVD: True vertical depth

UFP: Unstable fracture pressure

WBM: Water based mud

XLOT: Extended leak-off test

## References

- Aadnoy, B.S., Mostafavi, V., and Hareland, G. 2009. Fracture Mechanics Interpretation of Leak-Off Tests. SPE 126452, presented at 2009 Kuwait International Petroleum Conference and Exhibition, Kuwait City, Kuwait, 14-16 December 2009.
- Abousleiman, Y. et al., 1996. Thermoporoelastic coupling in hydraulic fracturing. Rock Mechanics Institute, PP 1387-94, The University of Oklahoma, Norman, Oklahoma, USA. 1996.
- Addis, M.A., Hanssen, T.H., Yassir, N., Willoughby, D.R., and Enever, J. 1998. A Comparison of Leak-Off Test and Leak-Off Test Data for Stress Estimation. SPE 47235, presented at SPE/ISRM Eurock '98, Trondheim, Norway, 8-10 July 1998.
- Ahmad, T. 2010. *Reservoir Engineering Handbook, Fourth Edition*. Elsevier, MA, USA. PP 254-60.
- Alberty, M.W., Hafle, M.E., Mingle, J.C., and Byrd, T.M. 1999. Mechanisms of Shallow Waterflows and Drilling Practices for Intervention. SPE 56868, presented at Offshore Technology Conference, Houston, Texas, 5-8 May, 1997.
- Alberty, M.W., and McLean, M.R. 2014. The Use of Modeling To Enhance the Analysis of Formation-Pressure Integrity Tests. Paper SPE 167945, presented at SPE Drilling and Completion 2014.
- Allerstorfer, C. 2011. Investigation of the "Plastic-Behavior" Region in Leak-Off Tests. MS thesis, University of Leoben, Austria.
- Altun, G. 1999. Analysis of Non-linear Formation Fracture Resistance Tests Obtained During Oil Well Drilling Operations. PhD dissertation, Louisiana State University, Baton Rouge, Louisiana.
- Altun, G., Langlinais, J., and Bourgoyne Jr., A.T. 2001. Application of a New Model to Analyze Leak-Off Tests. SPE 72061, presented at SPE Annual Technical Conference and Exhibition, Houston, Texas, 3-6 October 1999.
- Bradley, W.B. 1979. Failure of Inclined Boreholes. ASME 78-Pet-44 presented at the Energy Technology Conference and Exhibition, Houston, TX, 5-9 November, 1978.

- Deeg, W.F.J. and Wang, H. 2004. "Changing Borehole Geometry and Lost-Circulation Control". ARMA/NARMS 04-577, presented at 6<sup>th</sup> North America Rock Mechanics Symposium (NARMS), Houston, TX, June 5-9, 2004.
- Edwards, S.T., Meredith, P.G., and Murrell, S.A.F. 1998. An Investigation of Leak-Off Test Data for Estimating In-situ Stress Magnitudes: Application to a Basin wide Study in the North Sea. SPE 47272, presented at SPE/ISRM Eurock '98, Trondheim, Norway, 5-10 July 1998.
- Fu, Y. 2014. Leak-Off Test (LOT) Models. MS thesis, University of Texas, Austin, Texas.
- Geertsma, J. 1957. "The Effect of Fluid Pressure Decline on Volumetric Changes of Porous Rock". SPE 728-G, presented at Petroleum Branch Fall Meeting, Los Angeles, October 14-17, 1956.
- Ghalambor, A., Salehi, S. et. al. 2014. "Integrated Workflow for Lost Circulation Prediction". SPE 168123, presented at SPE International Symposium and Exhibition on Formation Damage Control, Lafayette, LA, February 26-28, 2014.
- Gidley, J.L., et al. 1989. Two-Dimensional Fracture-Propagation Models. In Recent Advances in Hydraulic Fracturing, 12. Chap. 4, 81. Richardson, Texas: Monograph Series, SPE.
- Gonzalez, M.W. et al. 2004. Increasing Effective Fracture Gradients by Managing Wellbore Temperatures. SPE 87217, presented at the IDC/SPE Drilling Conference, Dallas, Texas March 2-4, 2004.
- Gray, K.E. 2013. Advanced Drilling and Well Completion course taught in Spring 2013. The University of Texas, Austin, Texas.
- Gray, K.E. 2013. Leak-Off Test Models Combining Wellbore and Near-Wellbore Fluid, Mechanical, and Thermal Behaviors. Wider Windows, July 7, 2013.
- Gray, K. E. 2011. Wider Windows Industrial Affiliate Program, 2011.
- Gray, K.E. and Fu, J. 2013. Leak-Off Test (LOT) Models. Wider Windows Report, May 29, 2013.
- Haimson, B., and Fairhurst, C. 1967. Initiation and Extension of Hydraulic Fractures in Rocks. Society of Petroleum Engineers. doi:10.2118/1710-PA.

- Holmes, C.S. and Swift, S.C. 1970. Calculation of Circulating Mud Temperatures. SPE. doi:10.2118/2318-PA.
- Ishijima, Y. and Roegiers, J.C. 1983. Fracture Initiation and Breakdown Pressure – Are they Similar? Proc. 24<sup>th</sup> U.S. Symposium on Rock Mechanics, pp. 761-772.
- Lee, D., Birchwood, R., and Braton, T. 2004. Leak-Off Test Interpretation and Modeling with Application to Geomechanics. ARMA 04-547, presented at Gulf Rocks 2004 the 6<sup>th</sup> North American Rock Mechanics Symposium, Houston, Texas, 5-9 June 2004.
- Nordgren, R. P. 1972. Propagation of a Vertical Hydraulic Fracture. Society of Petroleum Engineers. doi:10.2118/3009-PA.
- Norris, T. Algorithm Derivation. Toby Norris's website. [www.tobynorris.com/work/prog/cpp/mfc/concyl\\_hlp/algorithmderivation.htm](http://www.tobynorris.com/work/prog/cpp/mfc/concyl_hlp/algorithmderivation.htm). Downloaded 1 May 2013.
- Olson, J. 2014. Hydraulic Fracturing course taught in Spring 2014. The University of Texas, Austin, Texas.
- Paknejad, A., Schubert, J., and Amani, M. 2007. A New Method to Evaluate Leak-Off Tests in Shallow Marine Sediments (SMS). SPE 110953, presented at SPE Saudi Arabia Technical Symposium, Dhahran, Saudi Arabia, 7-8 May 2007.
- Pepin, G., Gonzalez, M., et. al. 2004. "Effect of Drilling Fluid Temperature on Fracture Gradient: Field Measurements and Model Predictions", ARMA/NARMS 04-527, presented at 6<sup>th</sup> North America Rock Mechanics Symposium (NARMS), Houston, TX, June 5-9, 2004.
- Perkins, T.K. and Kern, L.R. 1961. Widths of Hydraulic Fractures. Paper SPE-89-PA, presented at 36<sup>th</sup> Annual Fall Meeting of SPE, 8-11 October 1961, Dallas, Texas.
- Postler, D.P. 1997. Pressure Integrity Test Interpretation. SPE 37589, presented at 1997 SPE/IADC Drilling Conference, Amsterdam, The Netherlands, 4-6 March 1997.
- Raaen, A.M. and Brudy, M. 2001. Pump-in/Flowback Tests Reduce the Estimate of Horizontal in-Situ Stress Significantly. SPE 71367, presented at SPE Annual Technical Conference and Exhibition, New Orleans, Louisiana, 30 September-3 October 2001.
- Raymond, L.R. 1969. Temperature Distribution a Circulating Drilling Fluid. SPE, doi:10.2118/2320-PA.



- Rezmer-Cooper, I.M., Rambow, F.H.K., Arasteh, M., Hashem, M.N., Swanson, B., and Gzara, K. 2000. Real-Time Formation Integrity Tests Using Downhole Data. SPE 59123, presented at IADC/SPE Drilling Conference, New Orleans, Louisiana, 23-25 February 2000.
- Salehi, S. and Nygaard, R. 2012. Numerical Modeling of Induced Fracture Propagation. Paper SPE 135155, presented at SPE Annual Technical Conference and Exhibition, 8-10 October 2012, San Antonio, Texas.
- Salehi, S. and Nygaard, R. 2011. "Evaluation of New Drilling Approach for Widening Operational Window: Implications for Wellbore Strengthening", SPE 140753, presented at SPE Production and Operations Symposium, Oklahoma City, OK, March 27-29, 2011.
- Salehi, S. and Nygaard, R. 2010. "Finite-element analysis of deliberately increasing the wellbore fracture gradient", ARMA 10-202, presented at 44<sup>th</sup> US Rock Mechanics Symposium and 5<sup>th</sup> US-Canada Symposium, Salt Lake City, UT, June 27-30, 2010.
- van Oort, E. and Vargo, R. 2007. Improving Formation Strength Tests and Their Interpretation. SPE 105193, presented at 2007 SPE/IADC Drilling Conference, Amsterdam, The Netherlands, 20-22 February 2007.
- Wojtanowicz, A.K. and Zhou, D. 2001. Shallow Casing Shoe Integrity Interpretation Technique. SPE 67777, presented at SPE/IADC Drilling Conference, Amsterdam, The Netherlands, 27 February-1 March 2001.
- Zoback, M.D. 2007. Reservoir Geomechanics. New York, N.Y.: Cambridge University Press, 221.